⬥EPA United States
Environmental Protection
Agency

Atmospheric Light Detection and Ranging (LiDAR) Coupled With Point Measurement Air Quality Samplers to Measure Fine Particulate Matter (PM) Emissions From Agricultural Operations:

The Los Banos CA Fall 2007 Tillage Campaign

R E S E A R C H   A N D   D E V E L O P M E N T

Atmospheric Light Detection and Ranging (LiDAR) Coupled With Point Measurement Air Quality Samplers to Measure Fine Particulate Matter (PM) Emissions From Agricultural Operations:

The Los Banos CA Fall 2007 Tillage Campaign

David J. Williams[1], Sona Chilingaryan[2], and Dr. Jerry Hatfield[3]

[1] U.S. Environmental Protection Agency, Environmental Sciences Division,
National Research Laboratory, RTP, NC

[2] U.S. Environmental Protection Agency, Air Division, Region 9, San Francisco, CA

[3] U.S. Department of Agriculture, Agricultural Research Service, National Soil Tilth Laboratory, Ames, IA

Report Prepared By:

Dr. Gail Bingham[4], Jennifer Bowman[5], Dr. Christian Marchant[6],
Dr. Randal Martin[7], Kori Moore[8], Dr. Philip Silva[9], and Dr. Michael Wojcik[10]

[4]SDL Chief Scientist & Civil Space and Environment Division Leader,
Space Dynamics Laboratory, North Logan, UT

[5]Senior Manager, Internal Communications ATK Aerospace Systems, Magna, UT

[6]Imagery Scientist, National Geospatial-Intelligence Agency, Springfield, VA

[7]Research Associate Professor, Department of Civil and Environmental Engineering,
Utah State University, Logan, UT

[8]Environmental Engineer, Space Dynamics Laboratory, North Logan, UT

[9]Environmental Chemist, Animal Waste Management Research Unit,
USDA Agricultural Research Service, Bowling Green, KY

[10]Branch Chief for Environmental Measurement, Space Dynamics Laboratory, North Logan, UT

Atmospheric Light Detection and Ranging (LiDAR) coupled with point measurement air quality samplers to measure fine particulate matter (PM) emissions from agricultural operations: the Los Banos CA Fall 2007 tillage campaign.

Authors:

David Williams
Environmental Sciences Division
National Exposure Research Laboratory
U.S. Environmental Protection Agency
RTP, NC

Sona Chilingaryan
Air Division
Region 9
U.S. Environmental Protection Agency
San Francisco, CA

Dr. Jerry Hatfield
National Soil Tilth Laboratory
Agricultural Research Service
United States Department of Agriculture
Ames, Iowa

TABLE OF CONTENTS

LIST OF FIGURES

LIST OF TABLES

EXECUTIVE SUMMARY

Airborne particles, especially fine particulate matter 2.5 micrometers (µm) or less in aerodynamic diameter ($PM_{2.5}$), are microscopic solids or liquid droplets that can cause serious health problems, including increased respiratory symptoms such as coughing or difficulty breathing, decreased lung function, aggravated asthma, development of chronic bronchitis, irregular heartbeat, heart attacks, and premature death in people with heart or lung disease. Concern with these effects resulting from local operations in agricultural areas is drawing increased regulatory scrutiny and research. To investigate the control effectiveness of one of the current San Joaquin Valley Air Pollution Control District Conservation Management Practices (CMPs) listed for agricultural land preparation on the generation of particulate matter levels, the U.S. EPA Environmental Sciences Division, National Exposure Research Laboratory was awarded a Regional Applied Research Effort (RARE) project. The objectives of this study were to discover:

1) What are the magnitude, flux, and transport of PM emissions produced by agricultural practices for row crops where tillage CMPs are being implemented vs. the magnitude, flux, and transport of PM emissions produced by agricultural practices where CMPs are not being implemented?

2) What are the control efficiencies of equipment being used to implement the "combined operations" CMP? If resources allow assessing additional CMPs, what are the control efficiencies of the "equipment change/technological improvements" and "conservation tillage" CMPs?

3) Can these CMPs for a specific crop be quantitatively compared, controlling for soil type, soil moisture, and meteorological conditions?

This study used advanced measurement technologies such as atmospheric light detection and ranging (lidar) systems coupled with conventional point measurement air quality samplers to map PM emissions at high spatial and temporal resolutions, allowing for accurate comparisons of the CMP under test. The purpose of this field study was to determine whether and how much particulate emissions differ from the conventional method of agricultural fall tillage and a "Combined Operations" Conservation Management Practice.

The test location and CMP to be evaluated were chosen in discussion with stakeholders, regulatory agencies, and researchers. The RARE tillage experiment includes a fall tillage sequence following the harvest of a row crop (corn, cotton, tomatoes, etc.), followed by a repeat set of measurements at the spring harvest. The fall tillage site was near Los Banos, California and consisted of two adjacent fields that were cultivated in cotton for the 2007 growing season and were planned to grow similar crops in the 2008 growing season. The test fields were adjacent on a north/south orientation. Conventional tillage operations were applied to the north field, which contained 25.5 hectares. The combined operations tillage was applied to the south field, which contained 51.8 hectares. Soil type distribution for both fields are dominated by soil type 170 (Dos Palos clay loam, partially drained) and both contain small areas of soil type 103

(Alros clay loam, partially drained). Both fields contain another soil type, 139 (Bolfar clay loam, partially drained), isolated in the very corner of the north and on the eastern end the south field.

The conventional tillage method included two disc passes, separated by a chisel operation, followed by a land plane pass. A precipitation event occurred before the land plane event, which left the surface layer slightly moist reducing emissions for the land plane operation. The Combined Operation CMP chosen for examination was the Optimizer[1], which is designed to perform the work of several pieces of equipment in one pass, thereby reducing the number of passes and time spent on the tillage operation. The Optimizer was preceded by a chisel pass.

An extensive measurement system was applied during the study, which allowed two independent methods of emission analysis, one using conventional methods, and the other using the direct – near real-time measurements made with a lidar. Meteorological measurements included two 15.2 m towers instrumented at 5 heights with cup anemometers (2.5, 3.9, 6.2, 9.7 and 15.3 m) and relative humidity/temperature sensors (0.9, 2.4, 3.7, 6.1, and 8.2 m) to provide profiles of wind speed, temperature, and relative humidity. A wind vane was stationed at a height of 15.3 m on each tower. Four sonic anemometers surrounding the site provided atmospheric turbulence data, with two located at 11.3 m and two at 2.97 m elevations. Aerosol point samplers included both filter and optical measuring techniques, with the filter samplers utilizing impactor heads for aerodynamic separation. The filter-based samplers were arrayed in clusters to provide PM_1, $PM_{2.5}$, PM_{10} and TSP measurements at their various locations. The filter samplers ran for the entire time of each operation and provided one sample per operation for both mass and chemical analysis. The optical samplers were collocated with the filter-based samplers to provided aerosol size distribution integrated over the 20-second sample periods. Two additional aerosol chemical analysis systems were employed in a sampling trailer located on the downwind side of the field under test. Samples were collected using sample ports on the upwind side of the trailer just above and below the roof level. These samplers included an Organic Carbon/Elemental Carbon Analyzer (OC/EC) sampling the $PM_{2.5}$ size fraction, and an Aerosol Mass Spectrometer (AMS). The AMS provided chemical composition and particle size information for volatile and semi-volatile particle components in the 0.1 - 1.0 µm size ranges in vacuum aerodynamic diameter.

Two EPA-approved models were used to assess emission rates based on the particulate sampler data. They were the Industrial Source Complex Short-Term Model, version 3 (ISCST3) and the American Meteorological Society/Environmental Protection Agency Regulatory Model (AERMOD), which as of November 2005 is recommended for all regulatory applications [1][2]. Both models assume steady-state conditions, continuous emissions, and conservation of mass. ISCST3 assumes a Gaussian distribution of vertical and crosswind pollutant concentrations based on time averaged meteorological data. AERMOD uses continuous functions for atmospheric stability determinations, and based on stability determines the appropriate distribution: a Gaussian distribution for stable atmospheric conditions, and a non-Gaussian distribution for unstable, or turbulent conditions. Final emission rates were determined using inverse modeling coupled with observed facility-derived concentrations.

The Aglite lidar aerosol measurement and tracking system used for this experiment was a scanning monostatic unit that uses a three-wavelength, Nd:YAG laser, emitting at 1.064 (3W), 0.532 (2W) and 0.355 (1W) µm with a 10 kHz repetition rate. The lidar utilizes a turning mirror turret to direct the beam to collect vertical aerosol slices upwind and downwind of the field to

provide plume concentration images that are used to develop the 3D map of the source. This data, when combined with wind information, enables direct assessment of the transport of process generated aerosols off the field during the 1-minute scan time. A series of scans collected during the operation are used to provide the time integrated emission information for each operation. The lidar was calibrated against the point measurement systems (optical particle counter for volume concentration and filter data for mass conversion information) for each operation. The number of scans utilized to assess each operation varied from 47 to 122, with the sample number reduced during some operations by light and variable wind conditions. Emission values were determined by subtracting the upwind aerosol concentration from the downwind aerosol concentration measured by each scan and multiplying by the wind speed.

Chemical analyses of filter catch for $PM_{2.5}$, PM_{10}, and TSP showed that measured upwind (background) and downwind aerosols were composed of roughly the same concentrations of ionic species and organic and elemental carbon. For both upwind and downwind sample locations, all size fractions were dominated by an unknown mass fraction, which we attribute to crustal sources. The nature of the data collection and analysis does not allow for separation of local versus regional sources of collected crustal mass.

Emission data calculated for each measurement method for the conventional and conservation tillage operations are presented. The study showed that the conservation practice under study reduced the number of tillage passes by 50%, with similar reductions in fuel use and estimated tractor associated PM_{10} emissions.

The filter sampling/inverse model methods were severely challenged by the small fugitive dust emissions with spatial and temporal variations encountered in this study and differences (based on 67% confidence intervals not statistically significant) between average upwind and downwind concentrations for several of the operations. However, the scanning lidar provided highly significant emission measurements for all measurement periods.

Lidar-derived emission rates for $PM_{2.5}$, PM_{10}, and TSP by operation along with the average tillage rate in hours per hectare were summarized from the experiment. The Combined Operations tillage method reduced $PM_{2.5}$ emission by 29%, PM_{10} by 60%, and TSP by 25%. Differences in total emissions per tillage treatment were significant at the 95% confidence interval for $PM_{2.5}$, PM_{10}, and TSP. The time and fuel per hectare required to perform the conservation tillage was about 40% and 50% of the conventional method. The control efficiency of the Conservation Management Practice for particulate emissions was 0.289 ± 0.016, 0.604 ± 0.007, and 0.246 ± 0.013 for $PM_{2.5}$, PM_{10}, and TSP, respectively. The calculated tractor exhaust emission amount was smaller than the uncertainty in the measurements indicating that the tractor emissions were only a small part of the total aerosol emission from either operation. Tractor emissions from the combined operations method were reduced by 50%.

The report compares the results from this study with results from previous studies found in literature. The values from this experiment are in occasional agreement with those reported by Flocchini et al. (2001) and Madden et al. (2008), as well as the emission factors used by CARB to calculate area source PM_{10} contributions from agricultural tilling [3][4][13]. While the values from all three published studies are generally not in close agreement, they are well within the range of the variability expected from measurements made under different meteorological and

soil conditions, as demonstrated by the wide range of values in the literature. The largest difference between the emission rates herein derived and those found in literature is that the PM emission rates in literature for a land plane operation are much higher, up to 10 times greater, than most other tillage operations, whereas the opposite was found in this study - the lowest emission rates were calculated for the land plane operation. This is likely due to the presence of residual moisture in the soil surface from a precipitation event that occurred 2 days earlier. Therefore, the control efficiency of the Combined Operations tillage method is likely greater under normal conditions.

1.   BACKGROUND

Airborne particles, especially fine particulate matter 2.5 micrometers (µm) or less in aerodynamic diameter ($PM_{2.5}$), are microscopic solids or liquid droplets that can cause serious health problems, including increased respiratory symptoms such as coughing or difficulty breathing, decreased lung function, aggravated asthma, development of chronic bronchitis, irregular heartbeat, heart attacks, and premature death in people with heart or lung disease [5]. Larger particles tend to be removed from the air stream by the nose and throat before entering the lungs [6]. The U.S. Environmental Protection Agency (U.S. EPA) has established limits for $PM_{2.5}$ and PM_{10} (particles less than or equal to an aerodynamic diameter of 10 µm) levels in order to protect public health as part of the National Ambient Air Quality Standards (NAAQS) [7][8]. The U.S. EPA requires state air quality management agencies to monitor ambient $PM_{2.5}$ and PM_{10} concentrations for conditions hazardous to the population, report areas that exceed the NAAQS beyond the allowed number of times, and establish procedures to reduce particulate concentrations to meet the standards.

To address the problems associated with exposure to high particulate matter levels, the U.S. EPA Environmental Sciences Division, National Exposure Research Laboratory was awarded a Regional Applied Research Effort (RARE) project to determine the control effectiveness of Conservation Management Practices (CMPs) for agricultural tillage using advanced measurement technologies such as atmospheric light detection and ranging (lidar) systems. These systems, when coupled with point measurement air quality samplers, can map PM emissions at high spatial and temporal resolutions, allowing for accurate comparisons of various CMPs for a variety of agricultural practices [9]. The purpose of this RARE project was to deploy an elastic lidar system, together with a network of air samplers, to measure PM emissions from agricultural operations in order to answer the following research questions:

1.   What are the magnitude, flux, and transport of PM emissions produced by agricultural practices for row crops where tillage CMPs are being implemented vs. the magnitude, flux, and transport of PM emissions produced by agricultural practices where CMPs are not being implemented?

2.   What are the control efficiencies of equipment being used to implement the "combined operations" CMP? If resources allow assessing additional CMPs, what are the control efficiencies of the "equipment change/technological improvements" and "conservation tillage" CMPs?

3.   Can these CMPs for a specific crop be quantitatively compared, controlling for soil type, soil moisture, and meteorological conditions?

The San Joaquin Valley was selected as the research site because it is one of five high priority geographic areas for air quality identified in Region IX's Strategic Plan because of its size, population, and extensive air pollution problems. In November 2008, EPA redesignated the San Joaquin Valley to attainment for the PM_{10} NAAQS, but sources in the Valley must continue to implement measures that helped the District attain the PM_{10} standard, including CMPs. The Valley continues to violate the $PM_{2.5}$ NAAQS. The CMP chosen for comparison against the

conventional tillage method was the Combined Operations CMP, which is defined as a process that combines equipment to perform several tillage operations in one pass [10]. Data collected October 12-29, 2007 at a site near Los Banos, California are included in this report.

1.1 LITERATURE REVIEW

There are a handful of published articles pertaining to particulate matter emissions from agricultural tilling, with the majority of the studies being performed in the state of California. There are also several papers that collectively examine impacts of a variety of conservation tillage practices with respect to soil characteristics, fuel consumption, cost of production, and air emissions.

The use of an elastic lidar system by the University of California at Davis (UC Davis) to examine dust plumes resulting from tillage activities was presented by Holmen el al.[9]. Qualitatively, the constructed system was able to track the plume emitted from the moving source and provide a 2-D vertical, downwind map of the plume. It was observed that the plume heights were often above the point samplers located at 10 m along the downwind plane. The authors suggested that the best fugitive dust sampling procedures would include a combination of elastic lidar and strategically placed point samplers.

Two papers by Holmen et al., presented in series in 2001, further discuss tillage PM_{10} emission rate investigations by UC Davis using filter-based mass concentration samplers and qualitative measurements from the previously mentioned elastic lidar system [11][12]. The 24 samples listed within the articles as being valid were collected from Fall 1996 to Winter 1998 in the San Joaquin Valley during a wide range of environmental (temperature = 7-35 °C, relative humidity = 20-90%, and from prior to the season's first precipitation to periods between winter storms) and soil moisture conditions (1.5-20%). Tillage operations examined were discing, listing, root cutting, and ripping. Calculated PM_{10} emission rates ranged from 0 to 800 mg/m^2 (0 to 6.9 lb/acre), the mean ± one standard deviation was $152 ± 240$ mg/m^2 ($1.4 ± 2.1$ lb/acre), and the median was 43 mg/m^2 (0.4 lb/acre). One point made by Holmen et al. [12] is that several environmental conditions (temperature profile, relative humidity, soil moisture, etc.) can have very significant effects on PM emissions and should be monitored and accounted for in emission rate measurement and reporting. As a result, the reliability of direct comparisons of emission rates measured under different environmental conditions must be carefully examined.

The studies published by researchers at UC Davis and herein previously discussed were part of a much larger investigation of agricultural PM_{10} emission rates in the San Joaquin Valley as funded by the U.S. Department of Agriculture Special Research Grant Program. Findings of this broad study are published in Flocchini et al. (2001) [3]. Table 1 presents emission factors published in this study for different types of agricultural tillage along with the crop and time of year. As seen in results measured by Holmen et al. [12], the emission factors reported by Flocchini et al. for agricultural tillage were significantly influenced by environmental conditions, such as the near-ground temperature profile, relative humidity, and soil moisture. The potential variability with the same implement under opposing extreme environmental conditions may be larger than the variation from the type of crop or equipment used for tilling.

Table 1. Emission factors and uncertainties for land preparation as reported by Flocchini et al. (2001) [3].

Date	Emission Factor (mg/m^2)	Uncertainty		Date	Emission Factor (mg/m^2)	Uncertainty
Stubble Disc						
10/27/1995	257.7	NC		11/6/1998	50.0	146%
11/3/1995	49.3	9%		11/6/1998	28.4	145%
11/3/1995	27.4	470%		11/6/1998	35.0	NC
11/3/1995	231.0	4%		11/6/1998	28.0	10%
11/3/1995	136.7	7%		11/6/1998	117.0	18%
11/3/1995	140.8	6%		11/6/1998	32.4	9%
11/3/1995	286.1	5%		11/6/1998	58.9	8%
11/15/1995	537.9	9%		11/6/1998	93.5	9%
11/15/1995	542.2	125%		11/6/1998	74.2	8%
6/24/1997	430.0	17%				
Finish disc						
11/26/1996	124.3	3%		12/4/1996	9.2	NC
11/26/1996	142.4	4%		12/4/1996	0.6	NC
11/26/1996	97.5	5%		12/4/1996	3.5	NC
12/2/1996	91.0	9%		12/5/1996	-0.5	NC
Ripping/chisel						
6/24/1997	765.0	5%		6/25/1997	331.0	5%
6/26/1997	112.0	5%		6/25/1997	577.0	6%
6/26/1997	776.0	3%				
Root cutting						
11/16/1996	30.0	12%		11/16/1996	36.0	8%

The California Air Resources Board (CARB) developed their area source emission inventory calculation methodologies for agricultural tillage and harvesting operations based on the report by Flocchini et al. [3][13][14]. A summary of the resulting emission factors appears in Table 2. The given unit for the emission factor can be explained as the mass of PM_{10} particles released per acre for each operation, or pass. Specific tillage operations were assigned to one of these five categories and the displayed emission factor was used for all operations in each category.

Table 2. Emission factors used by the California Air Resources Board in estimating agricultural tilling PM_{10} emissions [13].

Agricultural Tilling Operation	Emission Factor	
	(lb PM_{10}/acre-pass)	(mg PM_{10}/m^2-pass)
Root cutting	0.3	33.6
Discing, Tilling, Chiseling	1.2	134.5
Ripping, Subsoiling	4.6	515.6
Land Planing & Floating	12.5	1401.0
Weeding	0.8	89.7

The U.S. EPA (2001) uses the empirically derived equation shown below to estimate the quantity of particulate matter emitted from all agricultural tilling processes [15].

$$E = c \times k \times s^{0.6} \times p \times a \tag{1}$$

where E = PM emission in lbs, c = constant 4.8 lb/acre-pass, k = dimensionless particle size multiplier (TSP = 1.0, PM_{10} = 0.21, $PM_{2.5}$ = 0.042), s = silt content of surface soil (%), p =

number of passes or tillings in a year, and *a* = acres of land tilled. The above equation was developed to estimate TSP emissions (k = 1.0) and has since been scaled to estimate PM_{10} and $PM_{2.5}$ emissions by using the respective k value. Average values of s are tabulated in Table 4.8-6, U.S. EPA (2001) as a function of soil type on the soil texture classification triangle [15].

A comparison between standard tilling practices and conservation tilling (strip-till) in dairy forage production on two farms in the San Joaquin Valley is given by Madden et al. (2008) [4]. Both strip-till and standard till operations were monitored for PM_{10} emissions over two tillage cycles at both farms. Results show that conservation tillage practices reduce PM_{10} emissions from one farm by 86% and 52% for 2004 and 2005, respectively. At the second farm, conservation tillage emissions were reduced by 85% and 93% for 2004 and 2005, respectively. Derived emission rates are presented in Table 3. Madden et al. attribute these reductions, in part, to a reduced total number of passes (from 3-6 passes in standard tillage to 1 pass in conservation tillage) and the ability for conservation tillage operations to be done under a higher soil moisture content than standard operations.

Table 3. Conventional and conservation tillage emission rates reported by Madden et al. (2008) for tillage in a dairy forage crop rotation [4]. ST= standard tillage method, CT = conservation tillage method.

Season/Year	Sweet Haven Dairy		Barcellos Farms	
	Operation	Avg Emission Factor (mg/m^2)	Operation	Avg Emission Factor (mg/m^2)
Spring 2004	ST: 1st discing	198	ST: 1st discing	259
	ST: 2nd discing (w/ roller)	1035	ST: 2nd discing	917
	ST: 3rd discing (w/roller)	114	ST: Listing	615
	ST: Planting	103	ST: Bed discing	25
	CT: Strip-tilling	181	ST: Bed mulching	89
	CT: Planting	26	ST: Ring roller	566
			ST: Planting	96
			ST: Ring roller	104
			CT: Planting	394
Spring 2005	ST: 1st discing	139	ST: 1st discing	51
	ST: 2nd discing (w/ roller)	375	ST: 2nd discing	123
	ST: 3rd discing (w/roller)	404	ST: Circle harrow	337
	ST: Planting	263	ST: Listing	466
	CT: Strip-tilling	180	ST: Bed discing	109
	CT: Planting	385	ST: Bed mulching	384
			ST: Planting	481
			CT: Planting	130

Dust concentrations produced by agricultural implements used at a University of California Davis research farm west of Davis, California were reported by Clausnitzer and Singer (1996) [16]. Personal exposure samplers measuring respirable dust (RD) concentrations, particles that may reach the alveolar region of the lungs when breathed in (with a 50% cut-point diameter of 4 µm), were mounted on implements in 22 different operations over 7 month period in 1994; only the 18 operations with replicate samples were reported. Average RD concentrations measured on the implement ranged from 0.33 mg/m^3 for discing corn stubble to 10.3 mg/m^3 for both land planing and ripping operations. While RD concentration was heavily influenced by operation,

other factors determined to be significant in dust production were relative humidity, air temperature, soil moisture, wind speed, and tractor speed.

Further investigation of the data set presented by Clausnitzer and Singer (1996) [16] and of another data set collected on a different University of California Davis research farm was reported by Clausnitzer and Singer (2000) [17]. Both sets of data focus on RD concentrations as measured on the agricultural implement and the analysis examined environmental influences on the measured concentration. Again, soil moisture and air temperature were found to be significant factors in RD production. The RD production with respect to soil moisture was well fit by a power function, with the curve predicting RD concentrations becoming significantly steeper below 5%. Air temperature was hypothesized to be significant in that it was a surrogate measurement of atmospheric instability – as temperature increases near the surface, the atmosphere becomes less stable and may carry greater quantities of dust upwards.

Baker et al. (2005) examined differences between dust concentrations resulting from standard and conservation tillage practices in the San Joaquin Valley over a two year cotton-tomato crop rotation, each under two different cover crop scenarios: 1) no cover crop and 2) a cover crop forage mixture [18]. Total dust (TD), particles < 100 µm in aerodynamic diameter, and RD samplers were stationed on the implements to collect samples in the plume. For both TD and RD, the presence or lack of a cover crop in the standard till treatment did not seem to affect concentrations. Summed concentrations for conservation tillage without a cover crop were about one third of standard tillage and for conservation tillage with a cover crop they were about two thirds for both dust fractions measured. Reductions in summed concentrations with conservation tillage were attributed to fewer operations, including the elimination of the dustiest (discing and power incorporation). When comparing operations common to all four treatments, tomato planting and harvesting in conservation till produced higher concentrations than standard till (thought to be due to increased organic matter on the surface) and concentrations during cotton harvesting, which does not disturb the soil, were equivalent for all treatments. This study was part of a larger effort to quantify the effects of conservation tillage in California on crop production, soil quality, and time and resources dedicated to production as outlined by Mitchell et al. (2008) and Veenstra et al. (2006) [19][20].

Upadhyaya et al. (2001) compared the Incorpramaster, a one-pass tillage instrument against a conventional combination of discing twice and land planing twice based on fuel consumption, timeliness, and effect on soil [21]. Studies on four experimental fields at UC Davis showed no statistical difference between resulting soil conditions (bulk density changes, soil moisture changes, and aggregate size), but the Incorpramaster used between 19 and 81% less fuel with a mean of 50%. The time savings ranged from 67 to 83% with a mean of 72%. In most cases, two passes with the Incorpramaster were required to achieve the same soil conditions as the four passes in the conventional till.

Three conservation tillage methods were compared against the standard tillage method in cotton production and reported in Mitchell et al. (2006) in terms of yield, yield quality, tractor passes, fuel, and production costs [22]. A single field near Fresno, CA was divided in area among seven tillage treatments: 1) standard, 2) no till/chop, 3) no till, 4) ridge till/chop, 5) ridge till, 6) strip till/chop, and 7) strip till. Prior to both cotton growing seasons examined, a small grain wheat was planted in the field to enhance soil properties; this crop was sprayed with herbicide, and in

treatments 2, 4, and 6 it was chopped with a mower prior to tillage activities. In the other treatments (1, 3, 5, and 7), the dead wheat was either incorporated by the tilling or left standing. Yield and yield quality were statistically the same for both years for all treatments, though the standard treatment was numerically higher the 2nd year. Conservation tillage treatments reduced tractor passes by 41% to 53% over the standard method and estimated fuel reduction was 48% to 62% for the conservation practices. The estimated overall production costs of the conservation tillage systems were 14% to 18% lower than the conventional system. Mitchell et al. estimated, by extrapolation from other work, that whole-tillage process particulate matter emissions would also be decreased.

Particulate matter is released during agricultural tillage activities from both the operational activity of the tillage implement, as well as the tractor in use. Emissions from the tractor mainly originate from the tires in contact with the soil and the combustion engine. Attempts to quantify the PM emitted in agricultural tractor exhaust have been made by the U.S. EPA and the California Air Resources Board in software designed to estimate off-road engine emissions on a county or regional scale. The U.S. EPA developed the NONROAD software program, with the latest version distributed in 2005 [23]. Emission factors from compression ignition (diesel) engines used in the NONROAD model are calculated by adjusting a zero-hour, steady state measured emission factor (EF_{ss}) for engine deterioration with operation time (DF) and a transient adjustment factor (TAF) that accounts for variations from steady state engine loading and speed, as shown in the following equation [24].

$$EF_{adj(PM)} = EF_{ss} \times TAF \times DF - S_{PMadj} \qquad (2)$$

where $EF_{adj(PM)}$ is the adjusted PM emission factor and S_{PMadj} is the emission factor adjustment accounting for the use of a diesel fuel with a sulfur content different than the default concentrations, as fuel sulfur level is known to affect PM emissions. The units for $EF_{adj(PM)}$, EF_{ss}, and S_{PMadj} are g/hp-hr, where hp stands for horsepower, and TAF and DF are both unitless. All four variables on the right side of Eq. 2 vary with model year and engine size, expressed in horsepower (hp), according to measured values and/or the emission standards each model year and engine size was designed to meet. The selection of values for steady state emission factors and all the adjustment variables given in U.S. EPA (2004) [24] was performed using a variety of tests and resources, including the Nonroad Engine and Vehicle Emission Study (NEVES) Report [25], or by setting the values such that the adjusted PM emissions were equal to model year-specific emission standards.

The California Air Resources Board (CARB) has also developed a model to forecast and backcast daily exhaust emissions from off-road engines, including agricultural tractors, called OFFROAD. Similarly to the U.S. EPA's NONROAD model, emission factors (EF) for each engine size and model year are calculated based on a zero-hour emission rate (ZH) with a deterioration factor (DF) applied to account for engine wear with use, as in Eq. 3. The derived emission factor is then multiplied by the load factor (LF), the maximum rated average horsepower (HP), and the amount of time the engine is active through the year (Activity) in hr/yr.

$$EF = ZH + DR * CHrs \qquad (3)$$

$$P = EF * HP * LF * Activity * CF \qquad\qquad (4)$$

where CHrs is the cumulative engine operation hours, P is the amount of pollutant released in tons/day, and CF is the conversion factor from units of grams per year to tons per day. The values for the EF and DR are derived from measured values or they are calculated based on requirements to meet the proposed emissions limits for future years [26].

Kean et al. (2000) estimated off-road diesel engine, locomotive, and marine vehicle emissions of NO_x and PM_{10} for 1996 based on fuel sales [27]. Diesel engine exhaust emission factors were developed based on information provided in the development of the U.S. EPA NONROAD off-road vehicle emissions model with supplemental information in order to calculate emissions based on fuel consumption. A fleet-wide average PM_{10} emission factor was determined for farm diesel equipment to be 3.8 g/kg of fuel used, at an average mass per volume of 0.85 kg/L of diesel fuel. Fuel sales surveys from 1996 were used to calculate regional and national emissions. In the off-road category, which includes farm equipment, the U.S. EPA NONROAD model calculated on average 2.3 times higher emissions, which was attributed to higher engine activity assumed in the EPA model than represented in the reported fuel sales data.

2. EXPERIMENT DESIGN

2.1 SITE DESCRIPTION

After discussion among stakeholders, regulatory agencies, and researchers, it was collectively determined that the appropriate type of tillage for this experiment would be the fall tillage sequence following the harvest of a row crop (corn, cotton, tomatoes, etc.). Fall tillage activities prepare the ground for planting the next season's crop. An appropriate site was identified near Los Banos, California (see Figure 1) and consisted of two adjacent fields. Both fields were cultivated in cotton for the 2007 growing season, and plans indicated that both would receive similar crops in the 2008 growing season. Upon arrival at the site, immediately prior to the study, both fields had been harvested and the cotton stalks had been shredded and left on the ground.

An aerial photo and soil classification map of the experimental site is shown in Figure 2. This photo was extracted from the Merced County Soil Survey that was completed by the U.S. Natural Resources Conservation Service (NRCS). The two fields are delineated in the photo by red outlines. The field to the north, labeled Field A, is 254,600 m^2 (62.9 acres) in area. The field to the south, labeled Field B, is 518,400 m^2 (128.1 acres). Soil type distribution is also indicated in Figure 2 by orange lines separating different soil classifications. Both fields are dominated by soil type 170 (Dos Palos clay loam, partially drained) and both contain small areas of soil type 103 (Alros clay loam, partially drained). Both fields contain another soil, soil type 139 (Bolfar clay loam, partially drained) but it is isolated in the very corner of Field A and on the eastern end of Field B [28].

The experiment fields were surrounded on all sides by other cultivated fields, dirt access roads, irrigation ditches, and drainage ditches. The majority of the land in the surrounding area is used for agricultural purposes. The crops grown in the surrounding fields were cotton, tomatoes, and alfalfa hay. Tomatoes had already been harvested and the ground had been tilled. The cotton

Figure 1. Shaded relief map of the State of California, USA, with the location of the selected sample site shown by the white star. Image from geology.com [29].

fields were in various stages of harvest with some fields already harvested and tilled in preparation for the next crop. Fields already harvested were bare of most standing vegetation. Alfalfa hay was still being grown in some fields to the southeast of the site. The dirt roads were mainly used for access to the fields and were only occasionally traveled by farm vehicles. The ditches did not appear to be at operational flows and some appeared to contain little or no water.

The terrain surrounding the fields was relatively flat for many miles in all directions. The main form of topographical relief was provided by the drainage and irrigation ditches, with banks of varying elevations higher than the fields and channel bottoms which were all lower than the agricultural fields. Several hundred meters to the north of field A was a long row of trees that ran
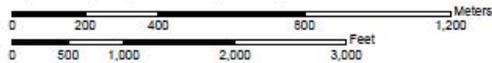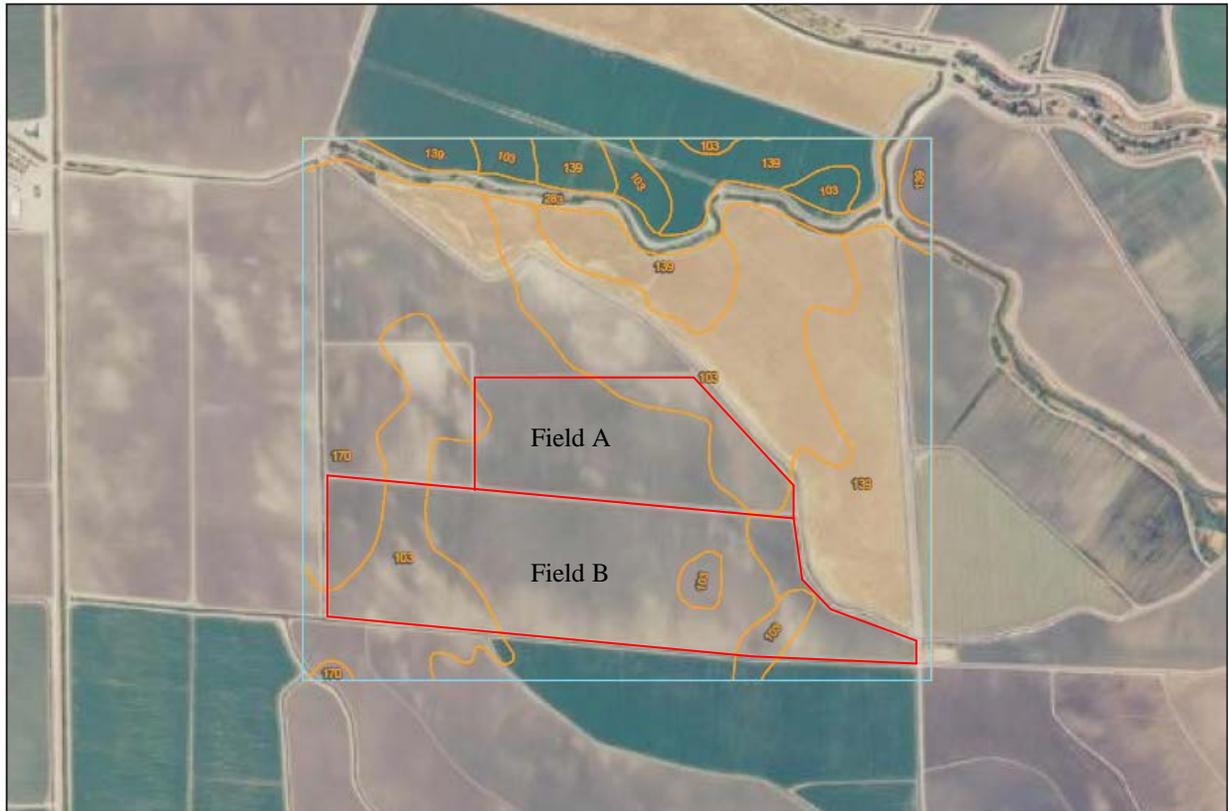
Figure 2. Soil type overlay on an aerial photo of the fields of interest (Field A and Field B) with field boundaries in red. Soil classifications include: 103 – Alros clay loam, partially drained; 139 – Bolfar clay loam, partially drained; 170 – Dos Palos clay loam, partially drained; and 283 – Xerofluvents, channeled [28].

in a roughly east-west line along a waterway. This band of trees is visible along the skyline in Figure 3. Also shown is an approximately 9 m wide border that had been disced around each field.

Figure 3. Photo taken on October 19, 2007 standing near the southern edge of Field B looking north across fields B and A during the chisel pass of the combined operations tillage method.

2.2 OPERATION DESCRIPTION

The purpose of this field study was to determine if and how much particulate emissions differ between the conventional method of agricultural fall tillage and a "Combined Operations" Conservation Management Practice. The Combined Operation CMP chosen for examination was the Optimizer[1], which is designed to perform the work of several pieces of equipment in one pass, thereby reducing the number of passes and time spent on the tillage operation. The farm on which the study was performed has been using the Optimizer for all of its fall tillage for several years, including on both fields herein studied. Prior to that, all fields were tilled using the conventional method [30].

The conventional tillage method was employed in field Field A and the combined tillage operations were used in Field B. The operations performed in each method are shown in order in

---

[1] Mention of a specific tradename or manufacturer does not imply endorsement or preferential treatment by the USDA-ARS or Space Dynamics Laboratory or Utah State University.

Table 4, with their corresponding dates. It should be noted that in the conventional tillage method, the second pass with the disc (Disc 2) was monitored twice due to tillage equipment malfunctions on the first day (Disc 2A), causing long periods of inactivity during the sampling period. On the second day, Disc 2B, the rest of the field not tilled during Disc 2A was finished; there was minimal overlap of the two areas tilled between Disc 2A and 2B. However, it should be noted that a third disc pass between the second disc pass and the land plane pass may be performed, depending on the resulting soil conditions from the previous passes.

Table 4. Tillage operations and dates performed for the comparison study.

Sequence	Operation	Date
Combined Operations Tillage (Field B)		
1	Chisel	10/19/2007
2	Optimizer	10/20/2007
Conventional Tillage (Field A)		
1	Disc 1	10/23/2007
2	Chisel	10/25/2007
3	Disc 2A	10/26/2007
4	Disc 2B	10/27/2007
5	Land Plane	10/29/2007

In this study, the use of the Optimizer reduced the number of passes by two, not counting the extra day in the conventional tillage due to equipment malfunctions. However, it is possible in some circumstances, based on field conditions, to eliminate the chisel pass before the Optimizer and further reduce the number of tillage passes. Therefore, the Optimizer may potentially reduce tillage passes by 2-4 in comparison with conventional practices.

The tractors and implements used during all the tillage operations are listed in Table 5 by date and operation. During all but the land plane operation, two tractors were pulling identical implements, with one usually providing a straight line based on an on-board global positioning system (GPS) unit for the second operator. Both tractors pulling the Optimizer implement, studied on 10/20, were equipped with on-board GPS units. A separate handheld GPS unit was placed on the tractor designated as Tractor 1 for each day and actively logged the tractor's position over time. It should be noted that on 10/23, 10/25, and 10/26 there were mechanical problems with one or both of the tractors that resulted in periods during each of those sample runs where there was only one or no tractors operating. On 10/23, another tractor, Tractor 3, was used to replace Tractor 2 after mechanical problems required it to stop operating for the duration of the experiment.

Table 5. Equipment used on the fields to perform the tillage operations.

Operation	Date	Tractor	Implement (1 per tractor)
Chisel	10/19/2007	1)John Deere 9520 w/ rubber track	Schmeiser Chisel, 5 shank, 26" depth, 16' wide pulling a 16' wide spiked ring roller
		2)John Deere 9400 w/ rubber track	
Optimizer	10/20/2007	1)John Deere 9620 w/ rubber track	Optimizer 5000
		2)John Deere 9620 w/ rubber track	
Disc 1 *	10/23/2007	1John Deere 9520 w/ rubber track	Rome Full Stubble Disc, 32" blade, 16' wide
		2John Deere 9400 w/ rubber track	
		3John Deere 9320 1/ 8 tires	
Chisel	10/25/2007	1John Deere 9520 w/ rubber track	Schmeiser Chisel, 5 shank, 26" depth, 16' wide pulling a 16' wide spiked ring roller
		2John Deere 9400 w/ rubber track	
Disc 2A	10/26/2007	1John Deere 9520 w/ rubber track	Rome Full Stubble Disc, 32" blade, 16' wide
		2John Deere 9400 w/ rubber track	
Disc 2B	10/27/2007	1John Deere 9520 w/ rubber track	Rome Full Stubble Disc, 32" blade, 16' wide
		2John Deere 9400 w/ rubber track	
Land Plane	10/29/2007	1John Deere 7920	Schmeiser Tri-Plane, 24' long, 16' wide

* Note: the 9400 ran for ~ 15 minutes, then the 9320 came to replace it using the same disc set

The Optimizer, manufactured by Tillage International (Turlock, CA), is an agricultural tillage implement that incorporates all forms of conventional tillage in a single pass. It combines multiple soil preparation processes into one. It uses the following tools in order from front to back: 1) two rows of inline disc units, 2) two rows of flow control reels or coulters, one after each row of disc units, 3) optional third row of reels, rollers, or coulters 4) axle assembly with off-set walking beam assembly, 5) three rows of off-set chisel shank and/or spring tooth assemblies, 6) two rows of flow control baskets, 7) optional roller assemblies for light or heavy soil, 8) optional planting unit for forage crops, and 9) optional unit for injection or application of fertilizer or herbicide. The flow control reels perform chopping, shattering clods, and incorporating activities. Also, attached to the axle assembly is a leveling system for consistent function of components, which helps the Optimizer to also perform the function of a land plane in leveling the field. Two models are available, depending on crop and horsepower requirements. Figure 4 shows an Optimizer Model 5000 unit, the larger of the two models, with the optional roller assemblies attached as utilized in this experiment, and Figure 5 shows one of the two identical units in operation [31].

Figure 4. Photograph of a stationary Optimizer Model 5000 with attached roller assemblies.

Figure 5. An Optimizer Model 5000 in operation during this field experiment, with an instrumented tower in the background.

Field personnel observed operations continually and recorded notes on tractor operation times, potential contamination issues due to traffic on surrounding dirt roads, general meteorological observations, etc.

The cooperating farming company recorded fuel usage and tractor run time, as shown in Table 4, throughout the field study time period in order to examine tractor time and fuel consumption differences between the conventional and combined operations methods [31]. Tractor run times were recorded by SDL employees and included periods of time during which the tractors were not moving for servicing, break downs, or operator break times. Fuel usage was measured by a volume-calibrated meter on the service truck and recorded in the service log by the attending employee. The service log and fuel meter were verified monthly for accuracy.

Table 6. Tractor run time and fuel usage as recorded by the farming company.

Operation	Date	Total tractor time (hr)	Total fuel used	
			(gallons)	(liters)
Combined Operation Tillage				
Chisel	10/19	8.5	90.0	340.7
Optimizer	10/20	4.36	46.2	174.9
	Sum	**12.76**	**136.2**	**438.2**
Conventional Tillage				
Disc 1	10/23	11.0	104.6	396.0
Chisel	10/25	6.5	58.5	188.2
Disc 2	10/26-27	9.16	82.5	265.5
Land Plane	10/29	3.33	26.6	85.6
	Sum	**29.99**	**272.2**	**875.8**

2.3   TILLAGE OPERATION DATA

Based on field notes and GPS data points, the total tractor run time in tractor hours ($hr_{tractor}$), or the sum of individual tractor operation times, and the area tilled per day were calculated. This tractor run time is smaller than that reported by the cooperating farming company because it only includes times when the tractor was moving and performing the specified operation in the field. The tractor hours reported therefore do not include the time the tractor spent motionless with an idling engine. From these two numbers, the tillage rate (hectares/$hr_{tractor}$) and the operation rate of the tractors ($hr_{tractor}$/hectares) were calculated. Tractor operation rates were summed to provide the total amount of time per hectare spent preparing the ground for the next season's crops (Table 7). In this study, the tillage rate of the combined operations was 0.59 $hr_{tractor}$/hectare and the conventional tillage rate was about 2.5 times that amount at 1.56 $hr_{tractor}$/hectare. It should be noted that these numbers only include times when the tractors and implements were tilling, and that the downtimes mentioned earlier due to mechanical failures are not included.

Table 7. Operation data for both the conventional and combined operation tillage studies as recorded by field personnel.

Operation	Date	Total Tractor Time $(hr_{tractor})$	Area tilled (hectares)	Tillage Rate $(hectare/hr_{tractor})$	Tractor Rate $(hr_{tractor}/hectare)$	Fuel-use Rate (liter/hectare)
Combined Operation Tillage						
Chisel	10/19	8.5	22.0	2.6	0.38	15.5
Optimizer	10/20	4.25	20.0	4.7	0.21	8.7
			Sum		0.59	24.2
			Average	3.7		
Conventional Tillage						
Disc 1	10/23	11.0	24.8	2.3	0.44	16.0
Chisel	10/25	6.5	19.5	3.0	0.33	9.7
Disc 2A	*10/26*	*3.4*	*10.5*			
Disc 2B	*10/27*	*5.75*	*14.2*			
Disc 2	10/26-27	9.16	24.7	2.7	0.37	10.7
Land Plane	10/29	3.33	8.0	2.4	0.42	10.7
			Sum		1.56	47.1
			Average	2.6		

Due to the breaks in tractor run time and the presence of multiple tractors in most cases and single tractors in others, the ratio of the sample period length and total tractor operation time was slightly different for each day, as shown in Table 8 below. The tractor problems on 10/26 caused an unusually high sample time to tractor operation time ratio. The difference between total tractor operation time and sample period time is important because the source strength will also vary based on how many tractors, if any, are operating at a given time. All calculations of emission rates herein undertaken have accounted for this difference in source strength with time, with final emission rates based on time being reported as the emission rate of a single tractor.

Table 8. Sample period, total tractor operation time, and the sample period-to-tractor operation ratio for all sample periods.

Date	Sample Time (hr)	Total Tractor Time (hr)	Sample time/Tractor time
10/19	5.33	8.50	0.63
10/20	2.85	4.25	0.67
10/23	7.27	11.00	0.66
10/25	4.24	6.50	0.65
10/26	5.52	3.41	1.62
10/27	4.09	5.75	0.71
10/29	3.49	3.33	1.05

3. MEASUREMENTS AND METHODS

3.1 OVERVIEW

A wide variety of air quality and meteorological sampling equipment was employed during this field study to meet the experiment objectives. These instruments are described in the following sections along with their functions, data analysis procedures, and calibration verification procedures which were performed before, during, and after the campaign to ensure the accuracy of data collected.

As wind direction and wind speed are important factors in obtaining accurate and representative data from the sampling systems to meet the project objectives, it was necessary to determine the dominant wind direction for this period of year in the Los Banos area. Meteorological data from the California Irrigation Management Information System (CIMIS) database were downloaded for October of 2004 through 2006 for the Los Banos station (#56) [33]. Based on these data the dominant wind direction was determined to be from the west to the northwest, as shown in Figure 6.

Figure 6. Wind rose for September and October of 2004 - 2006 as recorded by the CIMIS Station # 56 (Los Banos).

Due to the orientation of the fields, the preferred dominant wind direction for sampling purposes was from the northwest. Based on a northwest wind, instrument deployment was such that samplers meant to measure background aerosol parameters were to the north and northwest of the fields of interest and samplers meant to measure background plus plume parameters were to the south and east. Due to the large size of each field, one sample layout per field was utilized during the study. The first layout, shown in Figure 7, accommodated the sampling that took place during the combined operations tillage in Field B on October 19th and 20th. Tillage in Field B was completed prior to tillage being performed in Field A, the northern field. The flags indicate instrumentation locations with location names as labeled. Table 9 summarizes the type of instruments that were located at each site.

Figure 7. Sample layout used for Field B, with the area tilled shown by the shaded polygon. Created using Google Earth software.

Table 9. Summary of instruments located at each site for the combined operations tillage study of Field B. All height given as above ground level (agl).

Instrument Location	Description
S1	1 - 10 m tower 2 - OPCs @ 2 and 9 m 4 - MiniVols: PM_{10} and $PM_{2.5}$ @ 2 and 9 m
S Met 1	1 - 15 m tower 5 - cup anemometers (2.5, 3.9, 6.2, 9.7 and 15.3 m) 1 - wind vane @ 15.3 m 5 - temp/RH sensors (0.9, 2.4, 3.7, 6.1, and 8.2 m) 2 - Campbell Scientific dataloggers 1 - sonic anemometer @ 11.3 m 1 - energy balance system @ 2 m
S2	1 - 10 m tower 2 - OPCs @ 2 and 9 m 6 - MiniVols: TSP, PM_{10}, $PM_{2.5}$, and PM_1 @ 9 m; PM_{10} and $PM_{2.5}$ @ 2 m
S3	1 - 10 m tower 1 - OPC @ 9 m 4 - MiniVols: PM_{10} and $PM_{2.5}$ @ 9 m; PM_{10} and $PM_{2.5}$ @ 2 m
E1	1 - 10 m tower 1 - OPC @ 9 m 2 - MiniVols: PM_{10} and $PM_{2.5}$ @ 9 m 1 - sonic anemometer @ 2.7 m 1 - Campbell Scientific datalogger
N1	1 - 10 m tower 2 - OPCs @ 2 and 9 m 6 - MiniVols: TSP, PM_{10}, $PM_{2.5}$, and PM_1 @ 9 m; PM_{10} and $PM_{2.5}$ @ 2 m
N2	1 - 2 m tripod 2 - MiniVols: PM_{10} and $PM_{2.5}$ @ 2 m
NMet	1 - 15 m tower 5 - cup anemometers (2.5, 3.9, 6.2, 9.7 and 15.3 m) 1 - wind vane @ 15.3 m 5 - temp/RH sensors (0.9, 2.4, 3.7, 6.1, and 8.2 m) 2 - Campbell Scientific dataloggers 1 - sonic anemometer @ 11.3 m
U1	1 - 10 m tower 1 - OPC @ 9 m 2 - MiniVols: PM_{10} and $PM_{2.5}$ @ 9 m
W1	1 - 10 m tower 2 - MiniVols: PM_{10} and $PM_{2.5}$ @ 9 m ($PM_{2.5}$ stopped working on 10/20/2007) 1 - sonic anemometer @ 2.97 m 1 - Campbell Scientific datalogger
Tethersonde	1 - tethersonde data collection package with a MadgeTech PRHT sensor
Lidar 1	1 - Lidar data collection system 1 - Davis met station for lidar operator's reference
AQ1	1 - OPC @ 5 m 2 - MiniVols: PM_{10} and $PM_{2.5}$ @ 5 m 1 - Davis met station @ 5 m 1 - OC/EC Analyzer (inlet @ 4.5 m) 1 - AMS (inlet @ 4 m) 1 - radio and laptop for OPC Data collection

For the first portion of the study, while monitoring the combined operations method of tillage, the AgLite lidar was located at position lidar 1 and used the tower U1 as the upwind reference point. Downwind scans were made along the line of sampling towers S1, S2, and S3 and the trailer housing other air quality sampling instruments, AQ1.

To capture the particulate emitted by various tillage operations, the scanning lidar sampled vertical profiles from the upwind (entering aerosol mass) and downwind (exiting particulate/aerosol mass) sides of the tillage field in combination with horizontal scans from up-to down-wind position. These fast horizontal scans were used to monitor the height of the flux box to make sure that no source-emitted particulate transport passes through the top of the 'staple'. However, the scanning ability of the lidar system during this field study was limited according to U.S. Federal Aviation Administration (FAA) requirements communicated to SDL through a letter in response to our request for permission to operate a laser at this location. This letter permitted the use of a laser beam near ground level only at 0° N and 90° E and that all horizontal scans had to be made at > 13° from horizontal. In accordance with these requirements, the scanning 'staple' used throughout all the tillage operation sample periods consisted of an upwind vertical scan at 0° N lasting 73 seconds, an elevated horizontal scan to move to the downwind side (19 sec), two downwind vertical scans (2x73 sec = 146 sec) at about 90° E, and another elevated horizontal scan (19 sec) to return to the upwind location to return to the start of the sequence. The total time per 'staple' scan was 257 seconds.

To assure the quality of PM mass concentration retrievals from lidar observations, routine 'stare' modes were programmed into the lidar measurement profile. This quality assurance step was repeated every three 'staple' scans and held stationary for 60 sec each time.

After completing the tillage in Field B, the sampling equipment along the south, east, and west sides of Field B were moved to equivalent locations surrounding Field A to the north in order to monitor air quality during the conventional tillage method (samples taken from October 23-29, 2007). This second sample array is shown in Figure 8, with the flags again indicating sample locations and the location names as labels. Table 10 summarizes the type of instruments that were located at each site.

Figure 8. Layout used during tillage of Field A, with the area tilled shown by the shaded polygon. Created using the Google Earth software.

Table 10. Summary of instruments located at each site for tillage study of Field A. All heights given as agl.

Instrument Location	Description
S4	1 - 10 m tower 2 - OPCs @ 2 and 9 m 4 - MiniVols: PM_{10} and $PM_{2.5}$ @ 2 and 9 m
S Met 2	1 - 15 m tower 5 - cup anemometers (2.5, 3.9, 6.2, 9.7 and 15.3 m) 1 - wind vane @ 15 m 5 - temp/RH sensors (0.9, 2.4, 3.7, 6.1, and 8.2 m) 2 - Campbell Scientific dataloggers 1 - sonic anemometer @ 11.3 m 1 - energy balance system @ 2 m
S5	1 - 10 m tower 2 - OPCs @ 2 and 9 m 6 - MiniVols: TSP, PM_{10}, $PM_{2.5}$, and PM_1 @ 9 m; PM_{10} and $PM_{2.5}$ @ 2 m
S6	1 - 10 m tower 1 - OPC @ 9 m 4 - MiniVols: PM_{10} and $PM_{2.5}$ @ 9 m; PM_{10} and $PM_{2.5}$ @ 2 m

Instrument Location	Description
E2	1 - 10 m tower 1 - OPC @ 9 m 2 - MiniVols: PM_{10} and $PM_{2.5}$ @ 9 m 1 - sonic anemometer @ 2.7 m 1 - Campbell Scientific datalogger
N1	1 - 10 m tower 2 - OPCs @ 2 and 9 m 6 - MiniVols: TSP, PM_{10}, $PM_{2.5}$, and PM_1 @ 9 m; PM_{10} and $PM_{2.5}$ @ 2 m
N2	1 - 2 m tripod 2 - MiniVols: PM_{10} and $PM_{2.5}$ @ 2 m
NMet	1 - 15 m tower 5 - cup anemometers (2.5, 3.9, 6.2, 9.7 and 15.3 m) 1 - wind vane @ 15.3 m 5 - temp/RH sensors (0.9, 2.4, 3.7, 6.1, and 8.2 m) 2 - Campbell Scientific dataloggers 1 - sonic anemometer @ 11.3 m
U2	1 - 10 m tower 1 - OPC @ 9 m 2 - MiniVols: PM_{10} and $PM_{2.5}$ @ 9 m
W2	1 - 10 m tower 2 - MiniVols: PM_{10} and $PM_{2.5}$ @ 9 m ($PM_{2.5}$ stopped working on 10/20/2007) 1 - sonic anemometer @ 2.97 m 1 - Campbell Scientific datalogger
Tethersonde	1 - tethersonde data collection package with a MadgeTech PRHT sensor
Lidar 2	1 - Lidar data collection system 1 - Davis met station for lidar operator's reference
AQ2	1 - OPC @ 5 m 2 - MiniVols: PM_{10} and $PM_{2.5}$ @ 5 m 1 - Davis met station @ 5 m 1 - OC/EC Analyzer (inlet @ 4.5 m) 1 - AMS (inlet @ 4 m) 1 - radio and laptop for OPC Data collection
Tr1*	2 - MiniVols: PM_{10} and $PM_{2.5}$ @ 2 m (* temporary location for sampling on 10/27 due to the area of the field being worked being largely to the west of most downwind towers)

The lidar was located at position lidar 2 for this second portion while the conventional tillage method was being monitored. From this location, the upwind reference tower was U2 and the lidar was again able to scan along the downwind side in line with the towers S4, S5, and S6 and the air quality sampling trailer at AQ2. The same lidar 'staple' and 'stare' sequences were used at the first location, lidar 1.

3.1.1 Meteorological Measurements

A tethersonde system from Atmospheric Instrumentation Research, Inc. (Boulder, CO) was employed to provide vertical wind speed, wind direction, temperature, humidity, and pressure profiles. The tethersonde meteorological package was a Model TS-3A-SP, which transmits 10 second averaged data to a receiver package (Atmospheric Data Acquisition System Model AIR-3A) at ground level. Data were collected and stored on a laptop computer connected to the receiver. Due to malfunctioning temperature and pressure sensors, the tethersonde package was retrofitted with a sensor/datalogger from MadgeTech (model PRHTemp 101, Contoocook, NH). The PRHTemp 101 averages pressure, temperature, and relative humidity at a user specified

interval and logs the data. For this experiment, the data averaging interval was 10 seconds to match the tethersonde averaging time. The PRHTemp 101 was launched and data were downloaded at the end of each run on the same computer that stored the tethersonde data to ensure that the time stamps would be synchronized. A helium filled balloon tethered to a manually operated winch lifted the tethersonde package to heights of about 460 m above ground level.

A Vantage Pro2 Plus weather station from Davis Instruments, Inc. (Hayward, CA) was used to monitor wind speed, wind direction, temperature, humidity, precipitation, barometric pressure, and solar radiation. It was located on top of the Air Quality sampling trailer, at an approximate height of 5 m above ground level. It was wired to a datalogger and display panel inside the trailer, which was connected to a computer for data storage.

Two 15.2 m towers were instrumented with 3-cup anemometers (model 12102) at 5 heights (2.5, 3.9, 6.2, 9.7 and 15.3 m) to provide the vertical wind speed profiles. Relative humidity/temperature sensors (Vaisala HMP45C) from Campbell Scientific, Inc. (Logan, UT) were also stationed at 5 heights (0.9, 2.4, 3.7, 6.1, and 8.2 m) to provide profiles of temperature and relative humidity. A Met One Instruments, Inc. (model 024A, Grants Pass, OR) Wind Vane was stationed at a height of 15.3 m on each tower. Data from each tower were stored as one minute averages on Campbell Scientific, Inc. (Logan, UT) CR23X dataloggers and were downloaded daily.

3.1.1.1   Eddy Covariance Measurements

The transport of mass, energy and scalars between a surface and the overlying layer of the lowest part of the atmosphere (boundary layer) overwhelmingly are dominated by turbulence as opposed to diffusion. Appropriate characterization of the turbulence transport of any mass/scalar requires high frequency response sensors that measure the 3-dimensional components of the wind field and measurements of mass/scalar of interest. In this study eddy covariance (EC) systems were mounted on 4 towers surrounding the field of interest to measure components of the turbulent flow field in conjunction with the particulate concentration measurements. EC systems were mounted on the following towers and at the specified height above ground level, as presented in Tables 6 and 7: W1 and W2 = 2.97 m agl, E1 and E2 = 2.7 m agl, and NMet, SMet1, and SMet2 = 11.3 m agl. As can be seen two heights were near the surface (E and W towers) and two were substantially higher (N and S meteorology towers). This was done to capture a quasi-vertical profile of the turbulence characteristics for this particular flow field, one near the surface and the other higher above.

The EC instrumentation was comprised of four Campbell Scientific Inc. (Logan, UT) 3-dimensional sonic anemometers (CSAT) and four LiCOR 7500 infrared gas analyzers (IRGA). The sensor separation for all four EC systems was 10 cm. Sampling rate was 20 Hz, all data were stored on to a Campbell Scientific data logger (CR5000). Together the CSAT and LiCOR measure water vapor (q), carbon dioxide (c) concentrations and velocity components of the wind flow in three spatial dimensions x, y, and z. In meteorology wind components in the x, y and z directions are defined as streamwise direction u, lateral direction v and in the vertical w respectively. These measurements were made at a scan rate of 20 Hz, 20 measurements per second for u, v, w, q and c. All of the high frequency data were preserved for subsequent post

processing of fluxes of latent heat (LE, evaporation), sensible heat (H), carbon dioxide (c) and momentum ($\overline{u'w'}$ and $\overline{v'w'}$). Each tower was visited daily between 06:00-07:00 hours for maintenance. The maintenance visit included exchanging compact flash cards for data storage on the CR5000, sensor interrogation at the data logger screen to evaluate measurement status, cleaning dust from the surface of the IRGA lens with de-ionized water and removing cob weds from the transducer arms.

The term "flux" used herein follows the definition in physics as the number of changes in mass/energy flow across a given surface per unit area per unit time. As represented here uw and vw are covariances of the streamwise (u) and lateral (v) velocities with the vertical (w) velocities which is a momentum flux. The term covariance is a statistical measure of the variance of any two random variables observed or measured in the same mean time period. This measure is equal to the product of the deviations of corresponding values of the two variables from their respective means. The superscript ($'$) represents the instantaneous velocity departures (which are the turbulence) from the mean velocity of each of the components. The over bar ($\overline{}$)is a time averaged operator and can in theory represent any time averaged period. The more common averaging period is typically about 30 minutes. In this study we evaluate multiple time averaging periods ranging from 1- 30 minutes. In addition to the fluxes there are a large number of statistical parameters that provide important insights to the governing processes of particulate transport to the boundary layer which is the key issue in this study.

Specifically we focus on friction velocity (u_*), the standard deviation of the vertical wind velocity (σ_w), mean wind speed and direction. Collectively these parameters are used to develop an understanding of how spatial and temporal changes of the turbulent flow field can affect the particulate emissions from agricultural production activities. Through this understanding improved model algorithm development can proceed by incorporating parameters that are directly relevant to the turbulent transport of particulates during tillage operations. The critical component is to develop a defensible approach to compute emission loading into the boundary layer and to this end must include an operational parameterization for turbulence.

Additionally, the flux of water vapor (E) from the fields of interest was estimated using Eq. 5 in order to determine if and how much water contributed by precipitation events was present in the top layer of soil at the time of the tillage activity following the precipitation.

$$E = \overline{w'\rho_v'} \tag{5}$$

where the units for the flux of water vapor are in kg m^{-2} s^{-1}, w is the vertical wind, and ρ_v is water vapor density. Again, the superscripts ($'$) represent the instantaneous deviation from the average and the overbar ($\overline{}$) denotes a time average. This expression is identical to the covariance of these two properties. The raw fluxes were determined for 30 minute averages. Various corrections were made to the initial values. A traditional coordinate rotation (Tanner and Thurtell, 1969; and Lee et al., 2004) was performed to account for tilt errors of the anemometer, and align the x-axis with the mean wind direction [34][35]. Then the correction reported by Webb et al. (1980) was made for effects of density fluctuations caused by water vapor and heat transport [36].

3.1.2 Wind Profile Calculations

Wind profiles near the surface were calculated based on one minute averaged wind speed data from the logarithmically spaced cup anemometers on the 15 m meteorological towers located at N Met, the meteorological tower located upwind of both tillage sites. Due to malfunctions with the meteorological package, the wind speed data collected by the tethersonde system was not used in the wind profile estimation above the highest cup anemometer. Instead, the logarithmic wind speed profile fit to the tower data was extrapolated up to 250 m to estimate the wind speed at higher elevations. An error in the code used to calculate the one minute average wind directions from the wind vane at the top of the meteorological towers (15.3 m) was discovered in post processing. Instead, one minute averaged horizontal wind directions calculated from the sonic anemometer data were used in subsequent analyses. Therefore, the wind direction measured by the sonic anemometer was applied to the entire wind speed profile. For most sample periods, wind profiles above 150 m were not required for the lidar emission rate calculations. An example of a calculated wind speed profile based on tower-mounted cup anemometer data is presented in Figure 9. Averaged horizontal wind speed data from the sonic anemometer (11.3 m agl) on N Met were compared with the nearest cup anemometer (9.7 m agl) wind speed measurements as a quality check. Both data sets showed the same patterns and recorded wind speeds were close (< 0.25 m/s difference), with the observed difference likely due to a combination of vertically separated sample heights and instrument error.
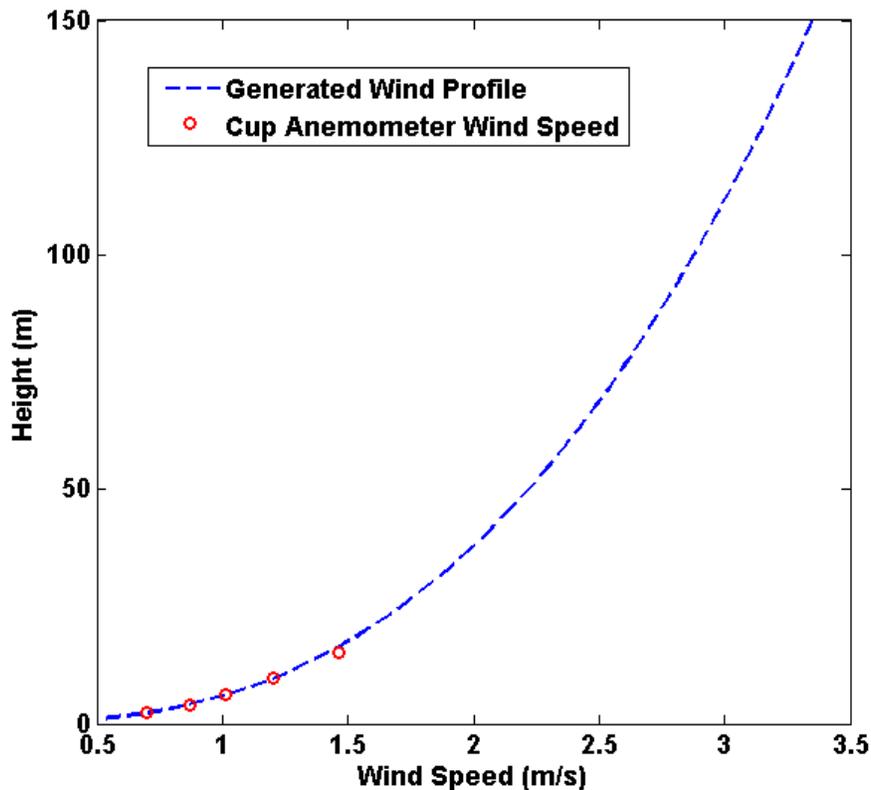
Figure 9. A wind profile calculated for the Disc 2B pass on 10/27/2007.

3.1.3 Soil Sampling

Soil characterization involved collecting soil samples for analysis of bulk density, soil moisture, and sand/silt/clay content. Bulk Density samples were collected prior to tillage operations along two transects, one across each field, in both the furrow and on the ridge at each sample location. A manual device consisting of a 7.6 cm in diameter and 7.6 cm deep cylinder was hand driven into the soil until the top of the cylinder was level with the soil surface. Samples were removed and placed into pre-weighed cans. Post-weights were performed in the field for determination of wet weight. All weights were determined using a Mettler balance (Columbus, OH), Model PM2000.

Samples for soil moisture were taken for each day of operation at random locations in the field and collected in pre-weighed cans 7 cm in diameter and 4 cm deep. Samples were collected immediately prior to the tillage period or shortly after commencement in areas that had not been tilled. The can was pushed into the soil approximately 3cm and removed. The can was closed and weighed in the field for determination of wet weight.

All soil samples were dried at the Agricultural Research Service (ARS) National Soil Tilth Laboratory (NSTL) in Ames, IA at a temperature of 105 °C until a constant weight was achieved (~60 hours). Samples were then weighed to determine dry weight. Calculations for soil moisture and bulk density were performed according to the following equations as found in Doran and Jones 1996 [34].

$$\text{field water content (\%)} = \frac{\text{weight of moist soil} - \text{weight of oven dried soil}}{\text{weight of oven dried soil}} \times 100 \qquad (6)$$

$$\text{\% moisture} = \frac{\text{weight of moist soil} - \text{weight of oven dried soil}}{\text{weight of moist soil}} \times 100 \qquad (7)$$

$$\text{bulk density} = \frac{\text{weight of moist soil} \times (1 - \text{field water content})}{\text{volume of soil collected}} \qquad (8)$$

where "volume of soil collected" = π x radius^2 x length of cylinder = π x 3.81^2 x 7.62 = 347.3 cm^3 and "field water content" is the value given by Eq. 6 expressed as a fraction.

A composite of all the samples collected was made. It was analyzed for the percent of sand, silt, and clay according to the Hygrometer Procedure, as given in Soil Sampling and Methods of Analysis (1993) [38]. The percent of stable aggregates was also determined from the composite sample according to the Dry-Sieve Method, as given in the Soil Sampling and Methods of Analysis (1993) [39].

3.1.4 Air Quality Point Samplers

The suite of point air quality samplers deployed around the tillage plots to quantify both the ambient and ambient plus operations emissions values were summarized in Table 9 and Table 10. Details of each of these sensors and their data processing methods are presented below.

3.1.4.1   MiniVol Portable Air Sampler

Thirty MiniVol Portable Air Samplers (Airmetrics, Eugene, OR) were distributed to gravimetrically measure the time-averaged mass concentrations of aerosols at multiple locations surrounding the fields of interest. The MiniVol is a battery operated, ambient air sampler that gives results that closely approximate air quality data collected by a Federal Reference Method (FRM) sampler [40][41]. The sampler draws air through a particle size separator, or impactor head, and then through a filter medium [42]. The photos in Figure 10 show a closeup of a MiniVol mounted on a rechargeable battery pack with attached impactor filter heads, and an example of how these PM samplers were deployed for the fall tillage field experiment.

Figure 10. Airmetrics MiniVol Portable Air Sampler, a closeup view and an example of field deployment.

Particulate concentrations in the PM_{10}, $PM_{2.5}$, and PM_1 size fractions were measured using impactor heads for size separation based on aerodynamic diameter, while Total Suspended Particulate (TSP) was measured by not using an impactor head. Each PM sampler was assigned to sample a specific size fraction at a specific location throughout the study, with location changes made as deemed necessary. Clusters of four PM samplers were assigned to two locations, one upwind and one downwind, in order to provide size fractionated, mass-based particle loading distributions. One instrument malfunctioned on October 20, 2007 and was unable to be used for further sample collection.

Filters used in the PM samplers were pre-conditioned according to the protocols outlined in 40 CFR 50 Appendix J before obtaining pre- and post-sample filter weights. Final average weights were found using a Type MT5 Microbalance (Mettler-Toledo, Inc., Columbus, OH) located at the Utah Water Research Laboratory (UWRL) in Logan, UT to determine three stable weights within ± 5 µg, measured on different days. Filters were transported to and from the site and stored on-site in dessicators to maintain filter conditioning. Flow calibrations on each MiniVol were performed using a slant manometer prior to the study and the actual sample flow was

adjusted daily on each instrument in order to maintain the required 5.0 L/min for accurate particle size separation.

3.1.4.2   Optical Particle Counter

Nine Optical Particle Counters (OPCs), Model 9722 from Met One Instruments, Inc. (Grants Pass, OR), were deployed around the study area collocated with MiniVols in order to describe the particle count and size distribution at locations measuring background and those measuring background plus plume aerosols. Figure 11 shows an OPC deployed for the tillage campaign, collocated with MiniVols, with an accompanying rechargeable battery pack and solar panel.

Figure 11. Met One Instruments Optical Particle Counter (OPC) Model 9722, indicated by arrow, setup for field deployment on a tower base with an accompanying rechargeable battery pack and solar panel.

The 9722 particle counter uses scattered light to size and count airborne particles. Particle counts are reported in eight, user-defined channels over the user-defined sample time. For this study, the OPCs collected samples continuously at a sample time of 20 seconds with the following channel sizes, in units of µm: (1) 0.3-0.5, (2) 0.51-0.6, (3) 0.61-1.0, (4) 1.01-2.0, (5) 2.01-2.5, (6) 2.51-5.0, (7) 5.01-10.0, and (8) >10.0. The data from each OPC were relayed to a single computer over a custom radio network for storage. Inlet flows for individual OPCs were measured on-site before and after the experiment using a Gilian Gilibrator2 Calibration System, a volumetric flow meter. The average of the averages from each flow measurement period was used as the sample flow throughout the field study.

Calibration of OPC particle counts was performed for each sample day in post-campaign analysis. For this calibration, careful examination of the number concentration (number of particles/m^3) time series yielded a time period prior to or after the tillage operation during which no apparent plumes were detected. Number concentration was chosen as the calibration point, as

opposed to the raw particle count data, because it normalizes the raw particle counts by sample flow (see Eq. 10); sample flow varies up to 20% between OPCs. The average number concentration (N_{ij}) per bin (i) for the designated calibration time for each OPC (j) was calculated, and the mean of the averages ($\breve{N}_i$) was used as the calibration concentration. A Counting Correction Factor (CCF_{ij}) for each bin of each OPC was calculated for each collocated run based on the calibration concentration for that bin according to the following equation:

$$CCF_{ij} = \frac{\breve{N}_i}{N_{ij}} \qquad (9)$$

Due to nearby agricultural activity contaminating the sample, the average number concentration for the OPC located at site E2 on sample dates 10/25/2007 and 10/26/2007 was not included in the mean $\breve{N}_i$, and counting correction factors were not calculated for this OPC on these days. In addition, contamination of multiple OPCs during available non-operation times on 10/20/2007 prevented an adequate calibration based on the data collected that day. In place of a daily CCF_{ij} specific for 10/20, the average for each bin of each OPC from the other six sample days was used.

Number concentration (N) is a function of raw particle counts (p), the measured average flow rate (q), the sample time (t), and the CCF_{ij}, as shown in Eq. 10.

$$N_i = \frac{p_i \times CCF_i}{q \times t} \qquad (10)$$

where the units for each variable are N = number per liter ($\#/cm^3$), p = number ($\#$), q = cubic centimeters per minute (cm^3/min), t = minutes, and CCF is unitless. As in Eq. 9, the subscript i represents a specified bin.

The volume concentration of aerosols based on a number concentration N is calculated based on the following assumptions: 1) the particles are spheres, 2) the maximum particle diameter measured is 20 µm, and 3) the geometric mean particle diameter per bin (GMD_i) is representative of the particles in a given bin i with the assumption of a log-normal distribution of particle numbers. The GMD_i is calculated by Eq. 11.

$$GMD_i = \sqrt{d_{i,upper} \times d_{i,lower}} \qquad (11)$$

where $d_{i,upper}$ and $d_{i,lower}$ are the diameters of the upper and lower ranges for bin i. The assumption of a maximum measured particle diameter must be made in order to calculate the GMD for channel 8, which counts particles > 10 µm.

The cumulative volume concentration of aerosols (V_k) up to a particle diameter k may be calculated using the following equation:

$$V_k = \frac{\pi}{6} \int_0^{d_k} n(d) d^3 dd \qquad (12)$$

where n(d) is the number concentration at diameter d. For application to the OPC data, Eq. 12 is expressed in the following terms that have been previously defined:

$$V_k = \frac{\pi}{6} \sum_{i=1}^{GMD_i \leq d_k} GMD_i^3 N_i \tag{13}$$

where GMD_i is expressed in μm, N_i is in #/cm^3, V_k is in units of μm^3/cm^3, and i represents the bin number. In this case, the V_k definition is similar to PM$_k$ concentrations: the fraction of the total volume of particles whose diameter, in μm, is $\leq k = 1, 2.5, 10$, and ∞ for TSP.

By collocating PM samplers and OPCs, the data provide information about the relationship between optical and aerodynamic measurements and allow direct calibration of optical instruments (both OPC and lidar) to mass concentration instruments by estimation of the mass conversion factor (MCF) for each PM$_k$ fraction. Theoretically the conversion from particulate volume concentration to mass concentration is complex and several simplifying assumptions have to be made. These include a spherical particle shape approximation, *a priori* assumption of the refractive index, and neglecting multiple scattering effects. The time-resolved V_k data from each OPC as calculated in Eq. 13 are then averaged over the corresponding PM sampler sample time. The MCFs, in units of density (g/cm^3), for each PM size fraction k are calculated by dividing the mass concentrations measured by the PM samplers (PM$_k$) by the time-averaged V_k. These data are averaged over several locations or instrument clusters i, where $\Sigma i = N$, and both a daily mean value and an overall mean value of the MCF$_k$ is calculated for each PM$_k$ fraction separately.

$$MCF_k = \frac{1}{N} \sum_{i=1}^{N} \frac{PM_{i,k}}{V_{i,k}} \tag{14}$$

The aerosol size distribution ($dN/d(ln(d))$) is calculated as outlined in Hinds [6] and expressed mathematically in Eq. 15.

$$dN/d(\ln(d)) = \frac{N_i}{\ln(d_{i,upper}) - \ln(d_{i,lower})} \tag{15}$$

where $d_{i,upper}$ and $d_{i,lower}$ are the diameters of the upper and lower ranges of bin i.

3.1.4.3 Organic Carbon/Elemental Carbon Analyzer

An Organic Carbon/Elemental Carbon Analyzer (OC/EC), Model 5400 from Rupprecht and Patashnick Co., Inc. (Albany, NY), was located in the sampling trailer on the downwind borders of the study areas. This instrument provides sample-averaged organic carbon and elemental carbon mass concentrations over a user-defined sample time, which was set at one hour for this study. The system alternately collects particulate matter onto one of two ceramic filters which, after the desired collection period, are heated within a closed-loop system to determine carbon content via direct thermal desorption and pyrolysis techniques developed and validated by Rupprecht and Patashnick [43]. As recommended by the manufacturer, during the analysis phases, an initial temperature plateau of 250°C for 600 seconds was used for determination of the organic carbon (OC) fraction and a final temperature plateau of 750°C was used for

quantification of the elemental carbon (EC) fraction. To account for non-carbon components of the organic compounds' mass, the OC concentrations reported by the 5400 were increased by the recommended multiplier of 1.7 [44]. A sharp-cut $PM_{2.5}$ cyclonic separator was placed at the inlet, which was located directly above the instrument on top of the trailer. A nominal flow rate of 16.7 Lpm was maintained through the system by on-board mass flow controllers and integral temperature and pressure sensors.

Flow checks, leak checks, and CO_2 audits, as per the instrument manual, were performed and passed at the UWRL during the week prior to departure for the field campaign and upon setup of the instrument on October 13, 2007 [43]. Additionally, CO_2 audits in the field were administered according to the instrument manual instructions and passed on October 20 and 29 of 2007.

3.1.4.4   Ion Chromatographic (IC) Analysis

In an attempt to more fully chemically characterize the nature of the upwind and downwind particulate matter, ion chromatographic analysis was performed on selected filters collected via the MiniVol systems at the air quality trailer (downwind), a second downwind location (S5 at 9 m) and a presumed upwind location (N1 at 9 m). The selected filters were from the October 23rd, 25th, and 26th observations of the conventional tillage practices (refer back to Table 8). After final post-test weights were determined from the filters ($PM_{2.5}$, PM_{10}, and TSP) at the UWRL, the chosen filters were sonicated with triplicate rinses in 10 mL double-distilled, de-ionized water (DDI) and split into two aliquots of approximately 15 mL each for separate anion and cation analysis. The anion analysis occurred within 48 hours of sonication and the cation aliquots were stabilized with 10 µL of 0.5 M HCl acid and analyzed within 28 days of sonication. The base IC system (Dionex Corporation) utilized an AS 40 Automated Sampler, CD 20 Conductivity Detector, GP 40 Gradient Pump, and membrane suppressor.   Cation quantification was accomplished using an IonPac® CS12A cation column, a CG12A cation guard column, and a 500 µL sample loop. The system eluent was 0.15 M H_2SO_4 with a 1.0 mL/min flow.   Anion concentrations were determined using an IonPac® AS11HC anion column, a AG11HC anion guard column, and a 188 µL sample loop. For anions, the system eluent was 30 mM NaOH with a 1.0 mL/min flow. ACS regent grade materials were used to prepare a stock standard solutions for each of the target ions, from which concentrations of 0.5, 1.0, and 5.0 mg/L (ppm) were mixed to make IC calibration curves. The ions quantified were fluoride (F^-), chloride (Cl^-), nitrite (NO_2^-), sulfate (SO_4^{-2}), nitrate (NO_3^-), sodium (Na^+), ammonium (NH_4^+), potassium (K^+), magnesium (Mg^{+2}), and calcium (Ca^{+2}). Verifications of the system calibrations were performed prior to each analysis run and roughly every 10 samples blank (DDI water) and continuing calibration verification standards (CCV) were tested. Peak identification and data processing were executed using Dionex PeakNet Data Chromatography software (Version 2.0).

3.1.4.5   Aerosol Mass Spectrometer
An Aerosol Mass Spectrometer (AMS) from Aerodyne Research, Inc. (Billerica, MA) was located in the sampling trailer, with a sample port on the upwind side of the trailer just below the roof level. The AMS provides chemical composition and particle size information for volatile and semi-volatile particle components in the 0.1 - 1.0 µm size ranges in vacuum aerodynamic diameter. AMS size and mass calibrations were conducted the first day of arrival at the site (10/13/2007) using polystyrene latex spheres (PSLs) and ammonium nitrate respectively. The AMS vaporizer was operated at higher than normal temperature (~800 ºC vs. ~600 ºC) to attempt

to detect some of the inorganic components in dust particles. During sampling, the AMS integrated and saved particle composition and size data every 10 minutes.

3.1.5 Lidar Aerosol Measurement and Tracking System

The Aglite lidar system is a monostatic laser transmitter and 28-cm receiver telescope (Figure 12). The laser is a three-wavelength, 6W, Nd:YAG laser, emitting at 1.064 (3W), 0.532 (2W) and 0.355 (1W) μm with a 10 kHz repetition rate. The lidar utilizes a turning mirror turret mounted on the top of a small trailer to direct the beam -10 to + 45° vertically and ± 140° horizontally. Lidar scan rates from 0.5 – 1°/s are used to develop the 3D map of the source(s), dependent on range and concentration of the aerosol.

Figure 12. The three wavelength Aglite lidar at dusk, scanning a harvested wheat field.

The process used to retrieve aerosol mass concentration from lidar data is illustrated in Figure 13. The details of Aglite lidar calibration and aerosol retrieval process are discussed by Marchant [45] and Zavyalov [46]. The retrieval is as follows. First, preprocessing on the lidar data is performed. The relationships between backscatter, extinction, volume concentration, and mass concentration of the aerosol components are established using *in-situ* data measured by OPCs and clusters of PM samplers with different separation heads (PM$_k$). Then, the inversion of the lidar data is performed using a form of Klett's solution [47] for two scatterers where extinction is proportional to backscatter. Finally, a least-squares method is used to convert backscatter values to aerosol mass concentration using the previously established relationships.
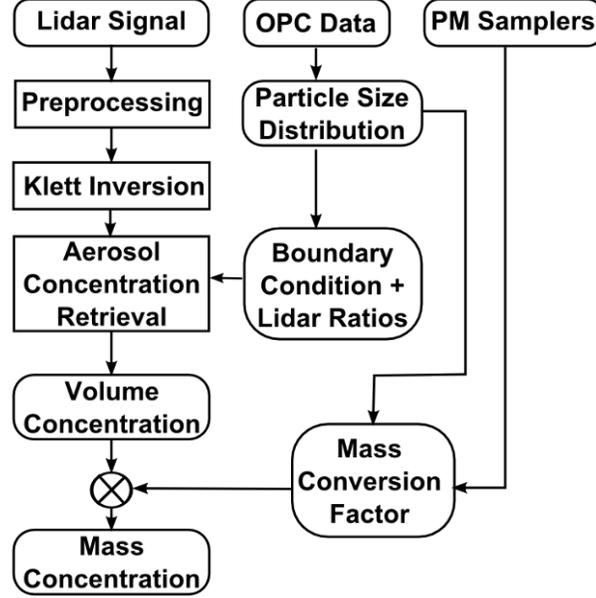
Figure 13. The Aglite lidar retrieval algorithm flow chart, showing the input locations for the in situ data.

From the OPC channel counts, the particle size distribution at a single point as a function of time may be calculated according to Eq. 15. The backscatter and extinction coefficients necessary for solving the lidar equation are then calculated at the OPC reference point as a function of time.

Klett's inversion is used to convert the lidar signal to the optical parameters (backscatter values in particular) of particulate emitted by the operation [47]. Having recovered backscatter values as a function of range and wavelength using the Klett inversion, these must be converted to the aerosol cumulative volume concentration. Expressing the particle normalized backscatter values from the OPC (β_v) and the lidar measured backscatter values (β_E) in a vector form, and applying the Moore-Penrose weighted minimum least-squares solution results in the value for particle concentration $n(z)$ at range z

$$n(z) = \frac{\tilde{\boldsymbol{\beta}}_v^T \mathbf{W} \boldsymbol{\beta}_E(z)}{\tilde{\boldsymbol{\beta}}_v^T \mathbf{W} \tilde{\boldsymbol{\beta}}_E} \tag{16}$$

which can be multiplied by the particle normalized volume concentration vector, resulting in the $V_k(z)$:

$$\mathbf{V}_K(z) = \tilde{\mathbf{V}}_E n(z) \tag{17}$$

The term $\mathbf{W}$ is a diagonal weighting matrix, whose diagonal elements are the expected variance of the emission backscatter for the corresponding channel.

The retrieved aerosol volume concentration from the lidar return signal is multiplied by the MCF_k, which was previously calculated using *in-situ* data (Eq. 14). At this point, the *k*th fraction of the aerosol mass concentration of the emission component is known as a function of distance.

$$PM_K(z) = MCF_K \cdot V_K(z) \qquad (18)$$

The concept behind our flux measurement approach is shown in Figure 14A, where the facility is treated as one would calculate the source strength in a bioreactor. In this simplified approach, the source strength is determined using the mean flow rate through the reactor and the difference in reactive species concentration entering and leaving the vessel. The scanning lidar samples the mass concentration fields entering and leaving the facility, while standard cup anemometers provide the mean wind speed profile. If we define our box large enough so that none of the emitted material escapes through the top or sides of the box, and the downwind side is far enough from the facility to minimize high frequency fluctuations, the same simple relationship found in a bioreactor applies. An example of our lidar derived concentration data is shown in Figure 14B. The concentration plot pattern from scanning up one side, across the top, and down the other looks like the common office staple (the paper fastener), and will be referred to as a "staple" scan. The data from the top of the box is regularly examined to be sure that no significant particulate transport is passing through the top. The data for the left side panel of the staple provides the background concentration entering the box, while that on the right provides the background plus facility concentrations leaving the box. The integrated mass concentration difference multiplied by the wind speed during the scan completes the flux emission calculation by yielding a mass per unit time emission from the facility.
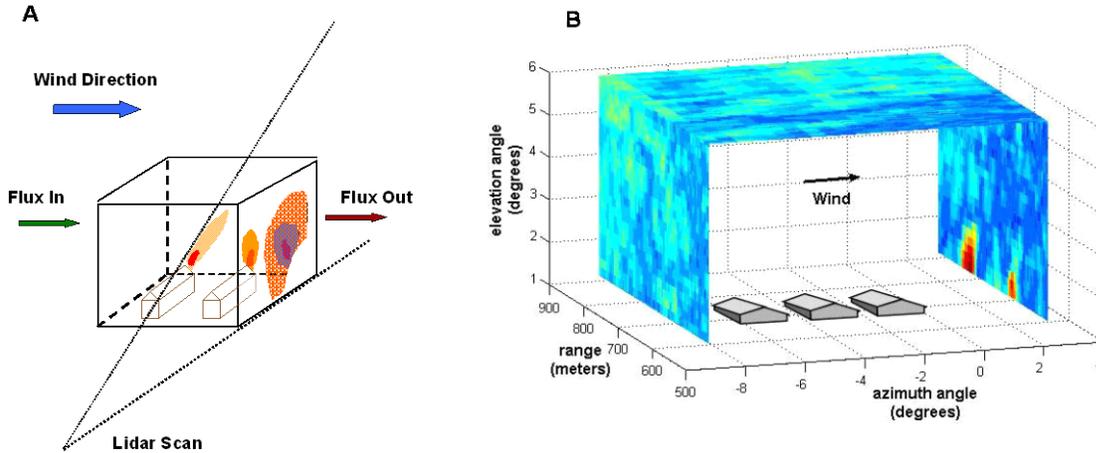
Figure 14. (A) Conceptual illustration of the method for using lidar to generate time resolved local area particulate fluxes. (B) An example of a "staple" lidar scan over the facility showing aerosol concentration on the three sides of the box.

The flux calculation in the integral form can be expressed as following:

$$F = \iint_{r,h} \overline{v}_\parallel(r,h) \cdot \left(\cos\theta_D C_D(r,h) - \cos\theta_U C_U(r,h) \right) dr dh \qquad (19)$$

where $\overline{v}_\parallel$ is the average wind speed component, defined as parallel to the long axis of the staple box, $\cos\theta_D C_D(r,h)$ and $\cos\theta_U C_U(r,h)$ are downwind and upwind, respectively, particle concentration corrections for wind direction for each data point at range r and height h, and C_D –

C_U form the mass concentration difference upwind and downwind, integrated over the range (width) and height of the sides of the staple. In our routine, Eq. 19 is discretized as:

$$F = \sum_{i=R_0}^{R} \sum_{j=H_0}^{H} \overline{v}_{\|ij} \left(\cos\theta_D C_{Dij} - \cos\theta_U C_{Uij} \right) \cdot \Delta r \cdot \Delta h \qquad (20)$$

where R_0 and R are the near and far along beam edges of the box and H_0 and H form the top and bottom of the box. (In many cases, H_0 is set above eye level and concentration is extrapolated to the ground to avoid illuminating personnel and animals.) The $\Delta r \cdot \Delta h$ term is the individual area element for which each flux component as calculated by each step in the double summation.

Figure 14B shows an example of single scan staple faces for the C_U and C_D mass concentration values for PM_{10} between the distances of 600 and 900 m from the lidar. Single scan differences, of course, do not account for accumulation or depletion in the box due to wind speed variation during a scan, or from high or low concentration pulses that may still exist in the downwind sample. For a meaningful estimate of the facility emission, many scans are combined to achieve a time averaged emission rate.

To perform the lidar calibration using the *in-situ* instruments, collocated samples are needed for the PM sampler, OPC, and lidar. In other words, the lidar beam must be directed past an OPC/PM sampler location and held in place for the duration of at least one OPC sample collection time. Holding the beam stationary, usually directed next to a sample tower, is referred to as the 'stare' mode. The 'stare' sample mode provides not only calibration, but quality assurance of the data set as well. After data processing and PM concentrations along the beam have been calculated, successive 'stare' data are compared against data from the reference OPC and PM samplers to verify that the concentrations calculated from both instruments are similar within measurement errors.

All lidar scans were quality checked to prevent the use of data that was contaminated or that was collected during times when the tractors were not actively tilling. All scans collected during times when no tillage activity was occurring were removed from further calculations. Upwind scans were checked for contamination from traffic on dirt access roads or agricultural activity to the north of the study site; upwind scans containing such contamination, as well as the corresponding downwind scans, were removed from further emission rate calculations. Downwind scans were not considered valid, and therefore not used in further calculations, if:

1) The corresponding wind direction was outside of ± 80° from North (0 or 360°)

2) The lidar scan contained apparent plumes from an outside source (such as from dirt road traffic which stretches across the length of the scan at a time when the wind was blowing perpendicular to the scan)

3) No plumes were detected

4) The tillage plume had a potentially significant portion crossing the lidar beam closer than 500 meters to the lidar trailer.

As the upwind scans are used as background references for specific downwind scans, only the upwind scans that corresponded with valid downwind scans were used. Table 11 presents the number of both total and valid upwind and downwind scans collected per day. In many cases two or more downwind scans use the same upwind scan as a reference because multiple downwind scans were made for each upwind scan, resulting in a little over half as many upwind scans as there are downwind scans.

Table 11. Number of upwind and downwind lidar scans determined to be valid for emission rate calculations.

Date	Upwind scans		Downwind scans		
	Total	Valid	Total	Valid	% Valid
10/19/2007	68	23	140	47	33.6
10/20/2007	46	42	95	78	82.1
10/23/2007	123	69	246	122	49.6
10/25/2007	70	38	141	70	49.6
10/26/2007	90	37	180	70	38.9
10/27/2007	76	42	155	77	49.7
10/29/2007	65	28	131	50	38.2

3.2   MODELING SOFTWARE

Air dispersion modeling and the prediction of plume centerline position along the southern boundary of the field were performed during the data analysis. The techniques for these steps are explained in detail in the following sections.

3.2.1   Dispersion model software

The U. S. EPA has approved a number of air dispersion models for use in regulatory applications. These are listed in Appendix W of 40 CFR Part 51 [48]; included are the Industrial Source Complex Short-Term Model, version 3 (ISCST3) and the American Meteorological Society/Environmental Protection Agency Regulatory Model (AERMOD), which as of November 2005 is recommended for all regulatory applications [1][2]. Both models assume steady-state conditions, continuous emissions, and conservation of mass. The default, and minimum, time step available for both models is one hour. Therefore, all meteorological input data represent one hour averages.

ISCST3 assumes a Gaussian distribution of vertical and crosswind pollutant concentrations [49]. The Gaussian plume equation uses the Pasquill-Gifford horizontal and vertical plume spread parameters, σ_y and σ_z, respectively, shown in Eq. 21.

$$C_{10} = \frac{Q}{2u\pi\sigma_y\sigma_z}\exp\left(-\frac{1}{2}\frac{y^2}{\sigma_y^2}\right)\left\{\exp\left(-\frac{1}{2}\frac{(z-H)^2}{\sigma_z^2}\right)+\exp\left(-\frac{1}{2}\frac{(z+H)^2}{\sigma_z^2}\right)\right\} \qquad (21)$$

C_{10} is the 10 minute average concentration ($\mu g/m^3$), Q is the emission rate ($\mu g/s$), u is the average wind speed at release height (m/s), y is the horizontal distance of the chosen receptor from the centerline of the plume (m), z is the height of the receptor above ground level (m) and H is the effective stack height (m), which includes estimates of plume rise due to buoyancy and/or momentum [49].

ISCST3 assumes a Gaussian distribution of pollutants based on time-averaged meteorological data. It also uses stability classes to address pollution dispersion due to atmospheric mixing. Stability classes are typically determined by a combination of vertical temperature lapse rates and incoming solar radiation or methods using vertical or horizontal wind variance [50]. AERMOD requires more detailed meteorological and surface characteristic information. Because of the additional input requirements for AERMOD and the lack of an established database for these inputs, many regulatory agencies continue to use ISCST3. The suite of meteorological instruments employed during this field study allowed us to use both models in this study. AERMOD uses continuous functions for atmospheric stability determinations, and based on stability determines the appropriate distribution, a Gaussian distribution for stable atmospheric conditions, and a non-Gaussian distribution for unstable, or turbulent conditions. AERMOD is also better at accounting for terrain features and building downwash phenomena than ISCST3 [51]. The interface used to run the models was the commercially available ISC-AERMOD View packaged by Lakes Environmental, Inc (Waterloo, Ontario, Canada).

Final emission rates were determined using inverse modeling coupled with observed facility-derived pollutant concentrations. In inverse modeling, the downwind impact on pollutant concentrations by a source is known while the emission rate is unknown. To solve for the source emission rate, a model such as ISCST3 or AERMOD is run with the following inputs: on-site collected meteorological data, the facility layout, the locations of pollutant sources and receptors (samplers), and an estimated or "seed" emission rate, which can be obtained from literature. Observed facility-derived concentrations are calculated by subtracting measured background levels from concentrations measured at locations impacted by the source plume. Modeled concentrations are then compared to the facility-derived concentrations at each sampler location. The location specific ratio of the measured concentration ($C_{measured}$) to the modeled concentration ($C_{modeled}$) is multiplied by the seed emission rate (E_{seed}) and an average across all valid locations is calculated to yield the source emission rate corresponding to the measured facility-derived concentrations ($E_{estimated}$) as shown in Eq. 22.

$$E_{estimated} = E_{seed}\left(\frac{C_{measured}}{C_{modeled}}\right) \tag{22}$$

A seed emission rate of 50 μg/s-m^2 was calculated using the AP-42 4th Edition emission factor estimate for agricultural tillage operations, Chapter 9.1 [52], assuming soil with 50% silt content. The equation is given as follows:

$$E = k(5.38)s^{0.6} \tag{23}$$

where E is the emissions in units of kg/ha, k is a cumulative particle size multiplier (TSP = 1.0, PM_{10} = 0.21, $PM_{2.5}$ = 0.042), and s is the silt content of the surface soil. A run time of 2 hours was assumed to provide a seed emission rate based on time and the same emission rate was used for all PM size fractions. The current edition of AP-42 (i.e. 5th Edition) does not include a method for estimating PM emissions from agricultural tillage [53].

It should be noted that evaluations of air dispersion model accuracy have shown that models are better at predicting concentrations over longer averaging times than shorter time periods at a

specific location; such models were developed and optimized to predict longer term averages and do not incorporate all of the many temporally and spatially variable factors that may affect dispersion in the atmosphere. Models can predict the magnitude of the highest concentration reasonably well, with a typical range of errors of $\pm$10-40%, but do not predict the exact location and time of the highest value well. Paired measured and modeled concentrations at a specific location throughout the modeling domain are usually poorly correlated, which is likely due to a combination of uncertainties in the input data that potentially may be reduced and unquantifiable uncertainties within the model itself.

An example of errors due to uncertainty in the input parameters is that concentration errors between 20 and 70% can result from an uncertainty of five to 10 degrees in the wind direction that directly affects plume location, depending on atmospheric stability and the sampler/receptor location. Uncertainty within air dispersion models, called "inherent uncertainty", is mostly due to the simplification of complex and highly variable processes affecting dispersion in the atmosphere. If atmospheric conditions that are used as inputs into the model (wind speed, wind direction, mixing height, etc.) are consistent across multiple sample periods, the model would predict the same concentration while measured concentrations could vary significantly due to variability in the complex processes that are not accounted for in the model. These inherent uncertainties can produce predicted ground level concentration errors of up to 50%. A more detailed discussion of air dispersion model uncertainty and accuracy is presented in Appendix W to Part 51 of Section 40 of the Code of Federal Regulations [48]. The report "Air Emissions from Animal Feeding Operations: Current Knowledge, Future Needs" by the National Research Council of the National Academies states that due to the assumptions required with Gaussian dispersion models, the uncertainty associated with predicted concentrations are not smaller than $\pm$50%. Additional uncertainty is introduced by stability classification and sample instruments [54]. However, the placement of near ground-level receptors along the dominantly downwind side of large ground level area sources, such as those used in this study, potentially may reduce the inherent uncertainty of the predicted concentrations due to both the vertical and horizontal proximity of the receptor to the source. Unfortunately, no discussion of inherent uncertainty in dispersion models under such conditions is available.

Based on the issue of potentially reducible uncertainty, all of the input data for both models were very carefully screened to reduce uncertainty in the output to the maximum extent possible, as is subsequently described. Even with such efforts, the error in the model predicted concentrations for this study is expected to be $\pm$50% according to the above sources, which, when combined with a $\pm$20% sampling error of the difference between upwind and downwind MiniVol PM samplers ($\pm$10% each) in Eq. 22, yields a range of error about the calculated emission rate at a single location between -46% and +140%. Averaging all the valid emission rates per sample period may reduce the potential error range to -33% to +100% by removing the sampling error of the MiniVols.

The meteorological data were carefully screened and corrected for problems prior to preprocessing for the dispersion models. It is this screening process that uncovered the incorrect wind direction averaging code for the meteorological towers discussed in section 3.1.2. As previously described, we have instead employed the horizontal, one minute averaged wind directions from sonic anemometers. The meteorological inputs for the models generated by the preprocessing programs were also screened for consistency with input measured values;

adjustments were made as necessary. The effects of the uncertainty associated with the meteorological input, however small, combined with the inherent uncertainty within the model will be most greatly impact by those receptors that are predicted to be on the edge of the plume, which in turn can greatly affect the calculated emission rates. Arya (1998) suggests that the plume edge be defined as 10% of the maximum modeled concentration to minimize these effects [55]. Therefore, emission rates calculated at locations with predicted concentrations less than 10% of the maximum predicted concentration will not be used in calculating the average emission rate.

Meteorological data were compiled as needed from the different deployed meteorological instruments. AERMET, the preprocessor of meteorological data for AERMOD, requires that the surrounding land use and land cover be categorized to quantify the Bowen ratio, surface roughness, and midday albedo. For this study, the land use on all sides of the site was classified as all cultivated land and the default monthly October values of midday albedo (0.18), Bowen ratio (0.7), and surface roughness (0.05 m) were used. During each of the sample runs the sky was clear of clouds, so the amount of cloud cover was set to 0.0 for all hours of interest. The mixing height for input into RAMMET and AERMET was set at 1000 m because all samples were started at least 2 hours after sunrise and ended at least 2 hours before sunset. In addition, all the receptor locations of interest were on the southern edge of the field so the exact depth of the mixing layer during daylight hours over such a short distance at ground level was not considered to be a significant factor. Based on the measured incoming solar radiation, vertical temperature lapse rates, and surface wind speed, stability classes for ISC during all sample periods except one were determined to be slightly unstable to very unstable. The exception to this was the sample run on 10/20/2007 that had average surface wind speeds > 6.0 m/s for two of the three sample hours, which are classified as neutral stability conditions under low to moderate incoming solar radiation [49]. The Upper Air Estimator in the AERMET View software was used to calculate required upper air parameters based on observed surface conditions.

Digital elevation map files with a 7.5 minute resolution were used to calculate receptor and source elevations [56]. The terrain was not considered to be a significant factor in the modeled concentrations as the change in elevation over the entire modeled domain (~2km x 2km) was gradual and no greater than 2 meters. The areas tilled during the sample periods were represented in the dispersion models by ground level area sources that varied in size and shape. The readings of the handheld GPS tracking device located on Tractor 1 for each tillage operation, mentioned in section 2.2, were used to develop the source areas and shapes. The GPS readings of sample locations were used to specify discrete receptors for comparison between modeled and measured concentrations at specific locations. In addition, a receptor grid with 10mx10m spacing and a flagpole height of 2.0 m above ground level was set up slightly upwind of, over, and downwind of the area source to provide a visualization of the modeled particulate matter concentrations resulting from the area source emissions. Elevations for receptors and source areas were calculated and assigned by AERMAP. Table A 1 in Appendix A provides more details about the settings used in each model. All concentrations used for emission rate calculations and presented in this report are averages over the modeled periods.

3.2.2   Plume Movement Prediction

The crossing point along the lidar beam path of the plume from the tractor with the hand-held GPS onboard was estimated using the tractor position with time information given by the GPS

unit and the minute averaged wind speed and direction. Tractor position was interpolated to the nearest minute for each GPS data point, in Universal Transverse Mercator (UTM) coordinates, to match the time of the wind data set. In actuality the tractor(s) emitted particulate plumes constantly as it (they) moved across the field, but for movement modeling purposes only, it was assumed that the tractor emitted a discrete puff of particles at this location and time. The calculated wind speed and direction at 5 meters above ground level were used to calculate where the puff would be at the end of that minute, and the wind data from the following minute were then used to calculate the plume position at the end of that minute based on the ending coordinates of the previous minute. Using a series of such calculations, the coordinates and time at which the plume crossed the lidar beam path was calculated for each minute of operation time for each day. If the calculations showed it took longer than 20 minutes to cross the lidar beam path the calculations were truncated. For those puffs whose calculations showed them crossing the beam, the crossing time and location, in both UTM coordinates and distance downbeam from the lidar, were calculated.

Predicted downwind beam-plane distances and crossing times were used as one of the quality checks for the downwind lidar scans, especially when part or all of the plume was predicted to cross the beam path closer than 500 meters to the lidar trailer.

It should be noted that GPS position with time was only available for one tractor. Therefore, the plume movement predictions for the plumes from the second tractor were not made. It should also be mentioned that no attempt to predict plume concentration or plume dispersion was made in this model.

3.3   STATISTICAL ANALYSIS OF DATA

The overall goal of the statistical analyses is to provide confidence about the observed differences between the conventional and conservation management practices and whether the differences are detectable. For highly variable discrete events, such as agricultural tillage operations, each tractor/implement pass can (and does) vary considerably from the previous tractor pass. In this way, it is the variability of the tillage process which dominates the calculation of the error bars for any given tillage operation for a particular field. Said another way, the reproducibility of the measurement devices (e.g. OPC, MiniVol, lidar) is typically much higher – often by a more than a factor of 10 – than the reproducibility of any two tractor passes. When it makes mathematical sense to use conventional statistical definitions, we make use of them. However the highly non-statistical (either Gaussian or Poisson) nature of the agricultural tillage process challenges the applicability of these methods.

Therefore, statistical analysis will depend upon the parameter being evaluated. For all parameters, a simple mean and variance will be computed over selected time intervals. For example, data from the OPC will be compiled over time and a mean and standard deviation calculated for each unit for each tillage operation. These means can be compared among locations using a simple T-test for those intervals and between tillage implements to determine if there are differences. The null hypothesis is "there are no differences in the particulate emissions between conventional and conservation management practices."

The aggregation of the particulate data with the wind profile and sonic anemometer data will provide an estimate of the particulate flux within a field. This data will be expressed as cumulative particulate emission for a specific portion of the tillage operation and then differences between systems compared using mean comparison methods. Regression analysis using multivariate methods will allow for the incorporation of different soil moisture conditions or meteorological conditions.

4.   RESULTS AND DISCUSSION

4.1   GENERAL OBSERVATIONS

4.1.1   Soil Characteristics

The average bulk density and soil moisture values, with 1σ and the number of samples collected (*n*), are presented in Table 12. Figure 15 provides a map of soil sample locations. The average bulk densities ($\pm 1\sigma$) for Field B were 1.47 ± 0.02 g/cm^3 for the furrow and 1.37 ± 0.03 g/cm^3 for the ridge. The average bulk densities for Field A were 1.52 ± 0.06 g/cm^3 and 1.34 ± 0.05 g/cm^3. It is expected that the furrow would have a higher bulk density because that is the path of the tires of the tractors, implements, and other equipment, which are known to cause soil compaction. That is also the point that has the highest pressure from water during flood irrigation. Drivers of the machinery avoid impacting the ridges because that may cause a loss of profitable growing area.

Soil moisture levels were also different between the furrow and the ridge. The furrows had the higher moisture level in both fields at 10.3 ± 0.49 % for Field B and $11.34 \pm 0.61\%$ for Field A, while the ridges were dryer at $9.45 \pm 0.06\%$ and $8.08 \pm 0.08\%$. One would expect the furrows to have more water in the soil due to shading from the sun by the ridges, exposure to slower wind speeds due to the surface friction at the level of the ridges, and the greater tendency for fallen biomass accumulation, as was observed in the fields under study (see Table 12). Figure 16 presents a timeline of measured soil moisture levels, along with tillage operations and precipitation events. Three precipitation events were observed and are discussed in Section 4.1.2. Soil moisture tended to decrease with successive disturbances caused by the tillage operations.

Analysis performed on a composite of all the samples collected yielded an average of 46% stable aggregates and soil composition of 47% sand, 36% silt, and 17% clay. Since the soil bulk density values from fields A and B are identical within the error of the measurement we expect these fields to have similar characteristics that contribute to aerosol/dust generation. Similarly, as has been shown in the literature [11][12][3][4], we expect the soil moisture content to strongly influence the amount of aerosol/dust production from any given tillage operation.

Table 12. Statistics of soil characteristics measured for both fields.

Bulk Density Data Summary	Mean (g/cm^3)	Std Dev (g/cm^3)	n	95% CI
Bulk Density for Field B Furrow	1.47	0.02	15	0.01
Bulk Density for Field B Ridge	1.37	0.03	15	0.02
Bulk Density for Field A Furrow	1.52	0.06	5	0.05
Bulk Density for Field A Ridge	1.34	0.05	5	0.04
Soil Moisture (%M) Data Summary	**Mean (%)**	**Std Dev (%)**	n	**95% CI**
%M for Field B Furrow	10.3	0.49	24	0.20
%M for Field B Ridge	9.45	0.06	24	0.02
%M for Field A Furrow	11.34	0.61	12	0.35
%M for Field A Ridge	8.08	0.08	12	0.05
%M for October 13	10.49	0.34	30	0.12
%M for October 19 (Chisel, Combined)	9.14	0.58	24	0.23
%M for October 20 (Optimizer, Combined)	6.66	0.43	10	0.27
%M for October 22	11.44	0.70	10	0.43
%M for October 23 (Disc 1, Conventional)	8.47	0.75	14	0.39
%M for October 25 (Chisel, Conventional)	6.04	0.29	17	0.14
%M for October 27 (Disc 2B, Conventional)	7.26	0.99	10	0.61
%M for October 29 (Land Plane, Conventional)	6.74	0.36	10	0.22
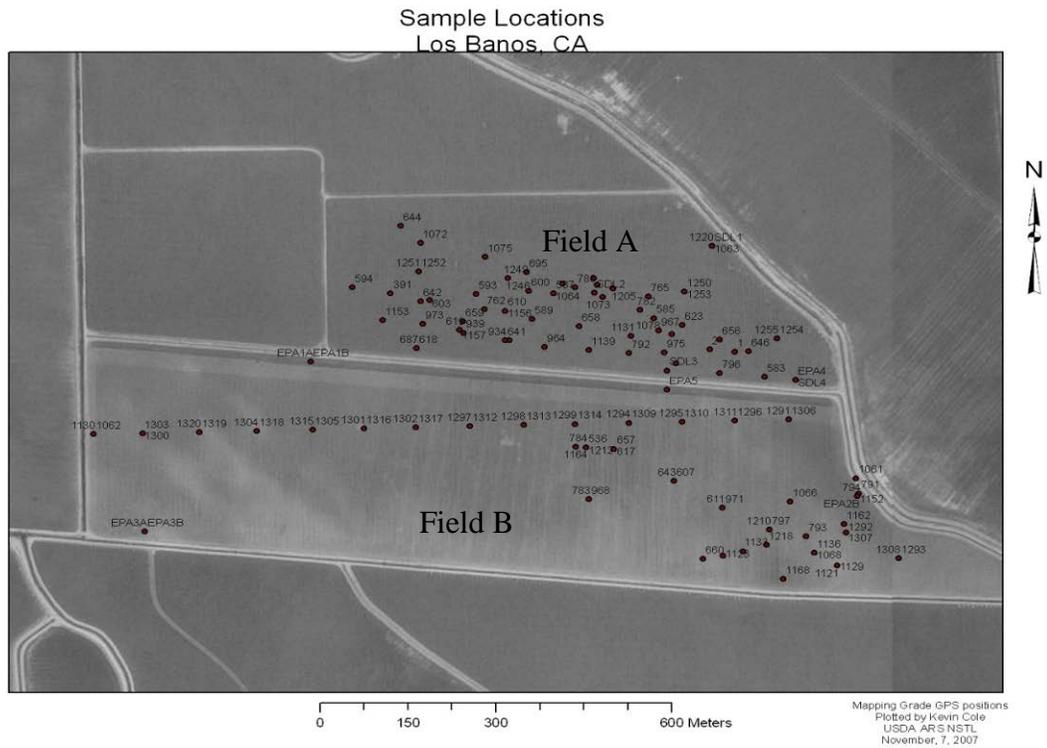
Figure 15. Soil sample collection locations in fields under study.
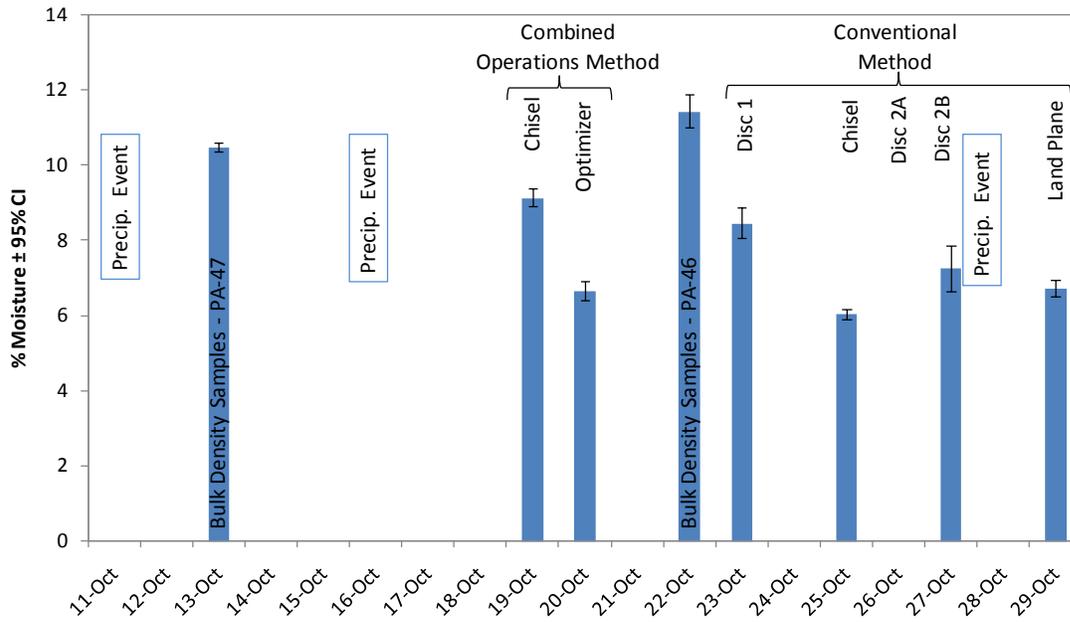
Figure 16. Timeline of soil moisture levels, tillage activities, and precipitation events.

4.1.2   Precipitation Data

Three precipitation events occurred at the study location immediately prior to and during the study. The first precipitation event occurred on October 11th, the first day of equipment deployment prior to deployment of the Davis weather station with a rain collector. This weather station later recorded two precipitation events. The second event occurred on October 16th in the evening, totaling 1.6 mm of precipitation, and the third occurred on October 27th in the late evening hours, totaling 1.2 mm. In summation, two precipitation events occurred prior to any sampling and a third event on October 27th occurred between the disc 2 pass and the land plane pass in the conventional tillage. Using the precipitation rates and totals collected and the calculated flux of water vapor representing losses due to evaporation, the depth of precipitation water in the soil over time was estimated as explained in Section 3.1.1.1 [57]. The results suggest that the accumulated water depth from the event on 10/16 had already been evaporated at the commencement of tillage activities on 10/19, as shown in Figure 17, while there was still 0.2-0.4 mm of water left in the soil from the 10/27 precipitation event during the land plane pass of the conventional tillage method on 10/29. This remaining moisture in the soil likely affected PM emissions from the land plane operation. Holmen et al. [12] and Flocchini et al. [3] found that soil moisture is an environmental variable that can have very significant effects on PM emissions.
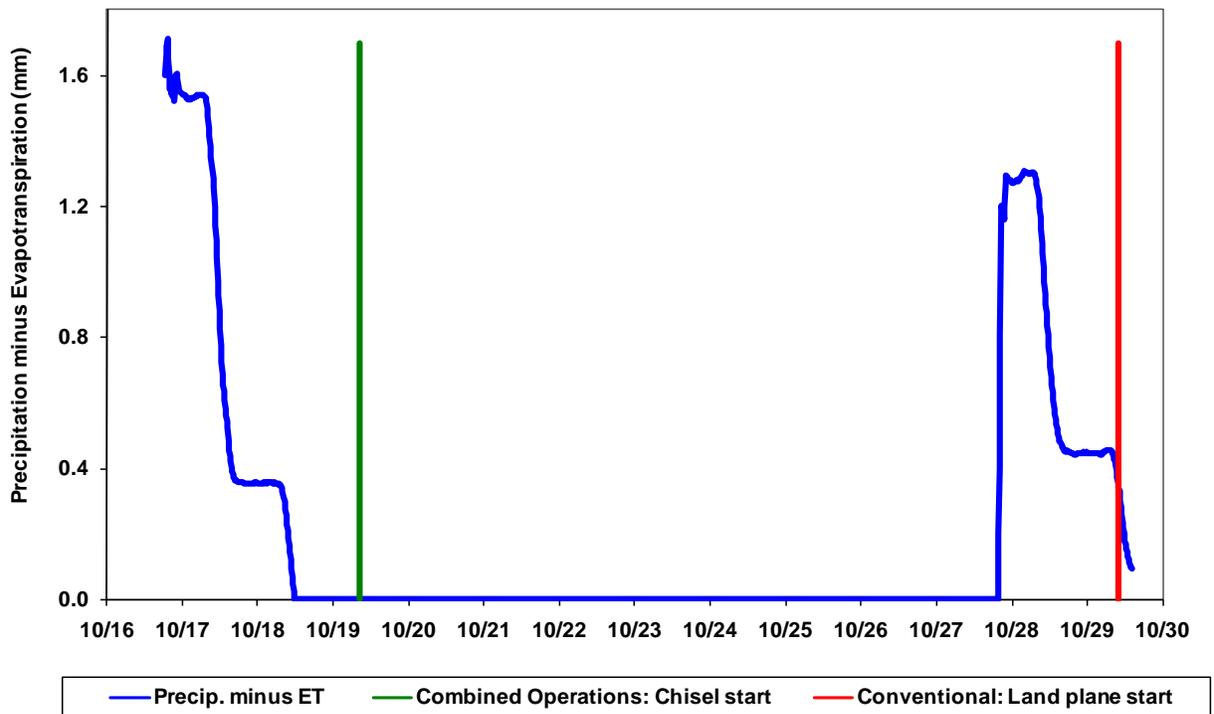
Figure 17. Expected soil moisture levels over time due to addition by precipitation and losses through evapotranspiration, with potentially affected tillage operations shown.

4.1.3 Eddy Covariance Calculations

Eddies containing heat, water vapor, and carbon dioxide occur in a spatially and temporally large range of scales. These scales can range from mm to km spatially and temporally from seconds to hours. Typically EC results are presented as 30-minute averages. This is done so as to ensure that an appropriate number of eddies have been measured and recorded that represent appropriate fluxes for heat, water, carbon dioxide exchange for a surface in question. In the case of particulates, this is a very different scale both spatially and temporally. First the particulate emissions are in effect artificially induced by agricultural production activities, in this case fall tillage practices. The variety of scale operations can vary widely in terms of the size of fields, the type and number of tillage operations, soil type, soil water content, wind speed, wind direction, surface stability conditions (meteorological condition, hot surface versus cool surface). These types of conditions render 30-minute averages as inappropriate for estimating particulate emission fluxes. Rather shorter averaging periods need to be incorporated as these periods will contain more representative information relating the particulate emissions to location, boundary layer conditions and turbulence characteristics which is a function of the surface and boundary layer conditions. Two examples are presented in Figure 18 and Figure 19. In Figure 18 three different averaging periods of 1, 15 and 30 minute averages are shown for the fiction velocity (u_*) which is good surrogate representation of the turbulence intensity at the surface. There are several critical points to note that are both obvious and subtle. First shorter averaging periods reveal increased detail in the changes of turbulence intensity. The variability clearly decreases as the averaging periods increase thus in effect smoothing much of the effect of the turbulence. For fluxes of heat, water vapor and carbon dioxide this is not such a critical issue if the appropriate conditions for eddy covariance measurements are in effect, i.e. relatively extensive homogeneous upwind surface of scalars (q, c, and T) and surface conditions (soil or vegetated surface). However particulate emission is an altogether different problem because these emissions are more or less from a relatively slow moving point source (i.e. the velocity of a tractor) and thus represents a spatially confined footprint influenced by very local conditions of turbulence and surface stability. The same issues exist for the temporal component. Thus averaging periods typically used with EC for water and carbon dioxide exchanges may very well be inappropriate for particulate emissions.

In Figure 19, one minute averages of mean wind speed, standard deviation of the vertical wind (σ_w) and u_* are presented for Site 3 on Oct. 23, 2007 for the period between 08:00 and 19:00 hours. In effect σ_w and u_* represent similar properties of boundary layer turbulence and so display similar features over the course of the day light hours for Oct. 23. Clearly the intensity of turbulent transfer responds to the diurnal inputs of solar radiation, mean wind speed and surface stability conditions. Note how as the surface stability conditions begin to move toward a more neutral case (sunset, surface heating is diminished) beginning approximately 17:00 hours, the variability observed in the mean wind, σ_w, and u_* during the midday is rapidly collapsing. Thus particulate emission transport from tillage operations are going to be influenced during specific surface boundary layer conditions. Reliable estimates of particulate emissions require accurate measurements of particulate concentrations to be integrated with accurate measurements of the surface layer boundary conditions (wind speed, direction, temperature, and u_*).
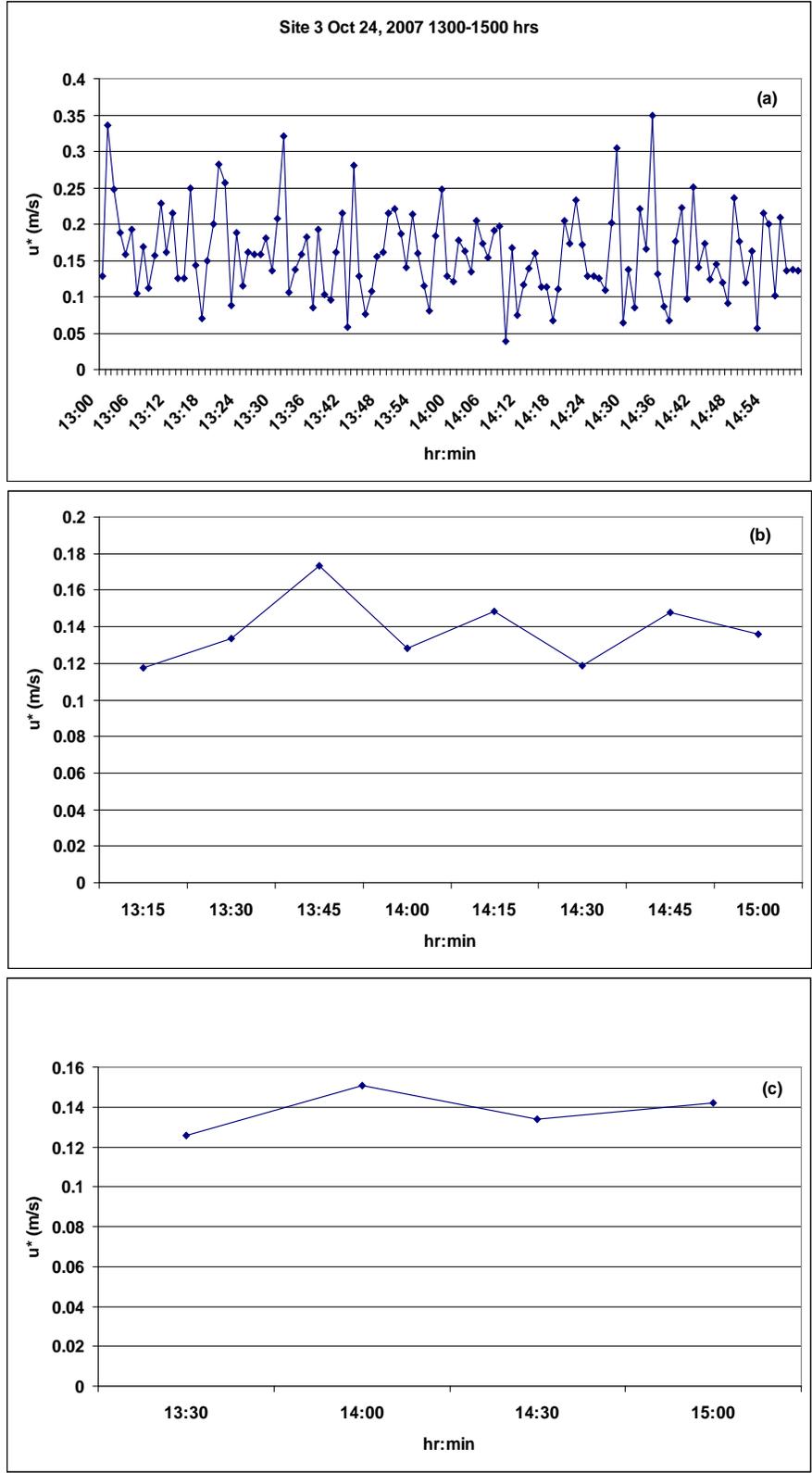
Figure 18. Friction velocity for 10/24/2007, 13:00-15:00 hours at N Met computed as (a) 1, (b) 15 and (c) 30-minute averages.
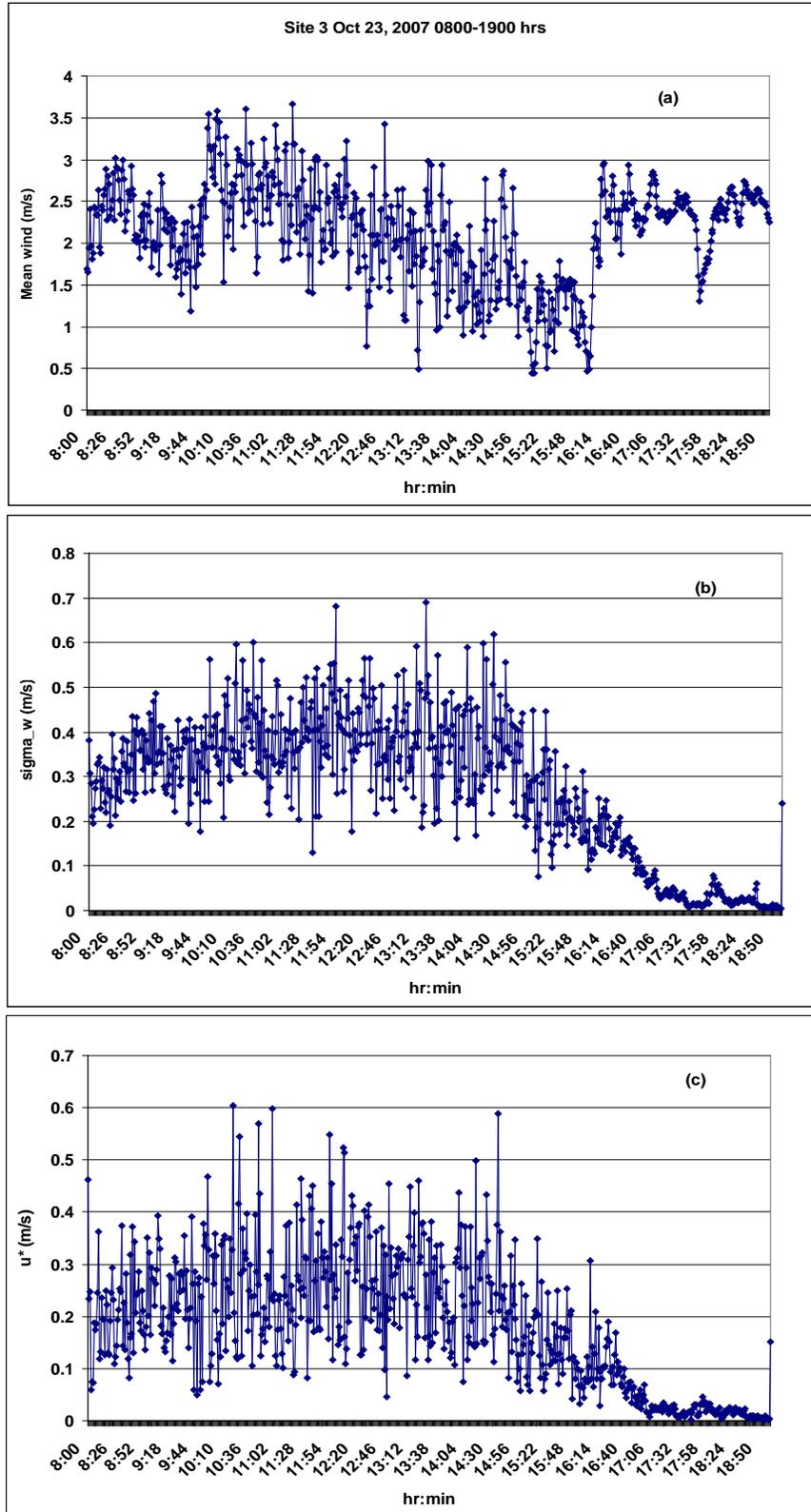
Figure 19. One minute average wind speed (a), σ_w (b), and u_* (c) for Site 3 on 10/23/2007.

4.1.4 Plume Movement Prediction

The predicted movement of puff plumes based on GPS coordinates for one tractor and wind data demonstrate well the variability of the winds. On some days, such as 10/20 the winds were very consistent and the predicted plume paths all follow the same general direction (Figure 19). When light and variable wind conditions existed for a significant portion of the sample period, as on 10/25 shown in Figure 20, plotting the predicted movements of plumes results in an unorganized and seemingly random connection of points. This was also the case for the chisel pass of the Combined Operations Method (10/19), which had the lowest predicted lidar beam-plane plume crossings at just 18.4%. This is also reflected in the relatively small percentage of valid lidar samples for the 10/19 sample period (33.6%) when compared to other sample periods (Table 11). Table 13 below gives the percent of puffs that were calculated to cross the lidar beam-plane on the downwind side of the fields under study.
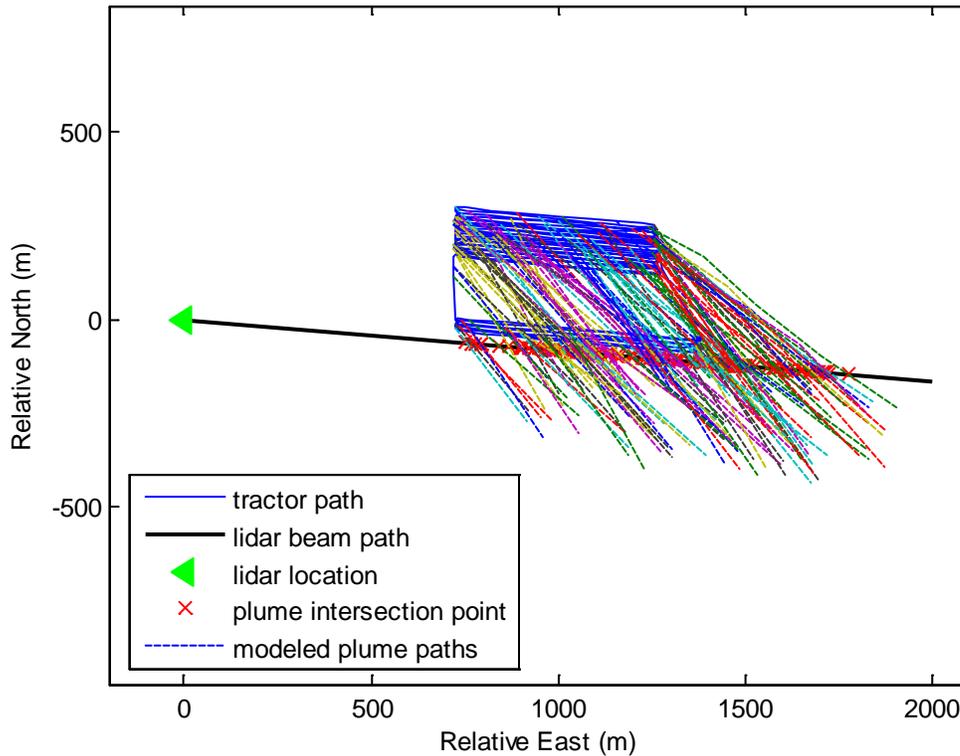
Figure 19. Predicted puff movements during the Optimizer pass in the Combined Operations Method (10/20).
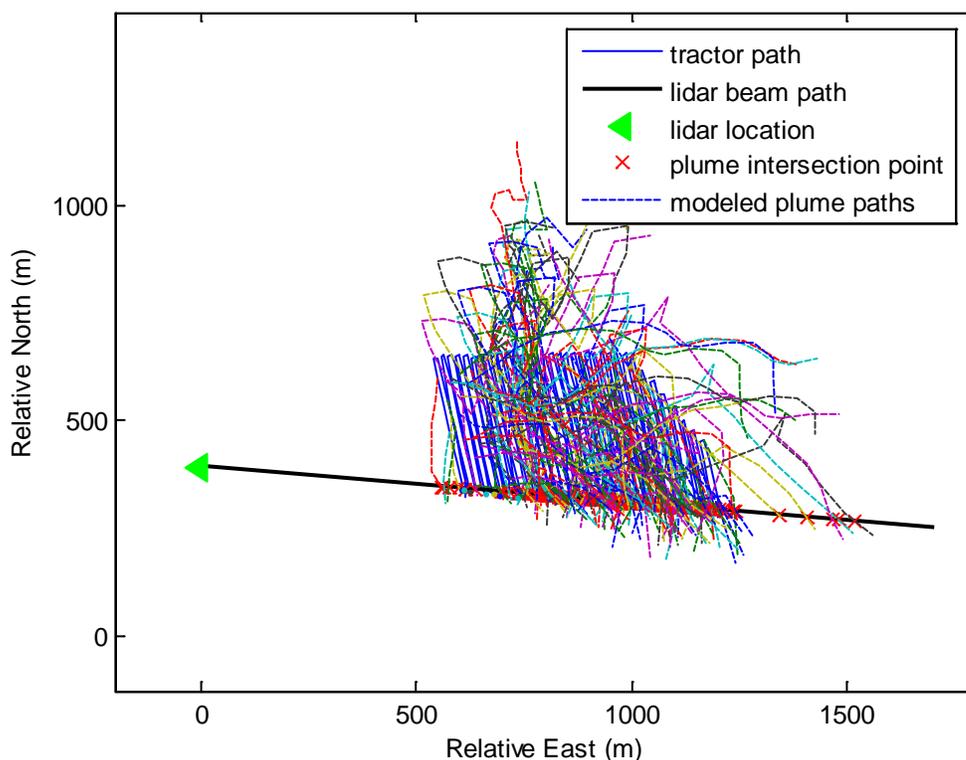
Figure 20. Predicted puff movements during the chisel pass of the Conventional Method (10/25).

Table 13. Percent of puffs predicted to cross the lidar beam plane.

Date	Operation	Beam-plane crossings (%)
10/19/2007	Combined: Chisel	18.4
10/20/2007	Combined: Optimizer	98.0
10/23/2007	Conventional: Disc 1	72.2
10/25/2007	Conventional: Chisel	54.3
10/26/2007	Conventional: Disc 2A	90.5
10/27/2007	Conventional: Disc 2B	58.5
10/29/2007	Conventional: Land Plane	74.3

4.2   AEROSOL CHARACTERIZATION DATA

The following section contains the aerosol data collected using both the filter and optical sampler methods.

4.2.1   MiniVol Filter Sampler Data

Observed $PM_{2.5}$ concentrations from the Airmetrics MiniVol samplers ranged from 5.8 to 52.9 $\mu g/m^3$; PM_{10} concentrations ranged from 16.3 to 165.3 $\mu g/m^3$; TSP concentrations ranged from 60.5 to 203.3 $\mu g/m^3$. All recorded PM concentrations are presented in Table B 1 in Appendix B.

The MDL for each sample period was calculated based on the average run time of the MiniVols, the targeted flow of 5.0 L/min, and the minimum filter catch that could be measured in the difference between the pre- and post-test filter weights of 5 µg. The MDL for each run differed based on different sample durations; the average MDL value $\pm$ 1 standard deviation ($n = 7$) was $3.7 \pm 0.9\,\mu g/m^3$, with a range of 2.3 to $4.8\,\mu g/m^3$.

All collected MiniVol samples and corresponding documents were examined for potential sampling errors (incomplete sample time, sampler malfunction, human error, etc.) and identified problem samples were removed from further calculations. Average MiniVol measured upwind/background and downwind/operation-impacted concentrations by operation are shown in Table 14. Upwind and downwind locations were separated based on wind direction and source area. In order to determine if the differences between mean upwind and downwind $PM_{2.5}$ and PM_{10} concentrations were significant, the 67% confidence intervals (CI) were calculated and are shown with the averages. Confidence intervals for TSP were not calculated because only one upwind and one downwind measurement were made each day. Mean downwind concentrations of $PM_{2.5}$, PM_{10} and TSP averaged 96%, 134% and 160%, respectively, of those upwind.

Table 14. Mean measured PM concentrations for each operation upwind and downwind of the tillage site. Error is the 67% CI about the mean for $n \geq 3$.

Date		$PM_{2.5}$ µg/m^3	PM_{10} µg/m^3	TSP µg/m^3	Wind Speed m/s	Wind Direction °	Tillage Operation
10/19/2007	Upwind	34.4 ± 3.4	41.6 ± 4.4	157.2	1.1	76	Chisel
	Downwind	24.3 ± 2.1	60.6 ± 10.3	122.5			
10/20/2007	Upwind	17.9 ± 1.8	28.2 ± 2.0	87.0	6.7	305	Optimizer
	Downwind	27.8 ± 5.3	42.1 ± 6.4	174.1			
10/23/2007	Upwind	16.1 ± 0.6	39.6	60.5	1.6	316	Disc 1
	Downwind	11.8 ± 1.2	59.7 ± 4.2	203.3			
10/25/2007	Upwind	38.6 ± 3.5	70.5 ± 10.0	123.6	1.5	2	Chisel
	Downwind	41.4 ± 2.1	78.4 ± 7.8	196.0			
10/26/2007	Upwind	26.7 ± 2.6	37.2 ± 2.5	84.0	2.9	302	Disc 2A
	Downwind	24.9 ± 1.8	52.2 ± 6.1	-			
10/27/2007	Upwind	22.1 ± 1.2	37.4 ± 7.1	70.2	3.1	30	Disc 2B
	Downwind	16.5 ± 2.0	52.5 ± 8.5	84.3			
10/29/2007	Upwind	34.8 ± 2.1	50.1 ± 2.5	89.1	1.7	49	Land Plane
	Downwind	32.3 ± 2.4	51.0 ± 4.3	62.4			

In theory downwind samplers would always measure higher concentrations than upwind, with the largest differences correlating with operations producing the most PM. During this field campaign, however, the average upwind $PM_{2.5}$ concentrations for some operations were higher

than the average measured downwind concentrations. This could be explained by the background locations being impacted by nearby sources, such as traffic on dirt roads or nearby tillage operations, or upwind sampler locations not having sufficient standoff distance from the operations. The movement of air around a tractor or other vehicle passing a sampler location will cause turbulence; at relatively low wind speeds, this may cause plumes of PM entrained in the turbulence structure to be sampled if the upwind instruments are not located at a sufficient distance upwind from the vehicle. Due to the cumulative nature of the MiniVols' PM collection, even a single exposure at these potentially high concentrations can significantly bias the final measured concentrations. Due to spatial constraints at this site, all the background sample locations were located along dirt access roads. Traffic on the access roads was observed during several sample runs, likely contributing to measured concentrations above the true background level. This phenomenon can be verified by inspecting the OPC time series data, which, due to the short sample time of 20 seconds, can track changes in background levels as well as identify the duration and quantity of contamination plumes. A discussion of the method used for determining background PM concentrations for upwind contamination scenarios is presented in section 4.2.2.

The mean mass fraction of PM_{10} and $PM_{2.5}$ with respect to the measured TSP values for both upwind and downwind samplers for each operation are presented in Table 15 and shown in Figure 20. Upwind TSP was comprised of $28.8 \pm 7.2\%$ $PM_{2.5}$ and $49.6 \pm 16.4\%$ PM_{10}. Downwind TSP was comprised of $22.8 \pm 15.7\%$ $PM_{2.5}$ and $50.0 \pm 27.4\%$ PM_{10}. Overall, $PM_{2.5}$ comprised $24.9 \pm 13.5\%$ of TSP and PM_{10} comprised $49.8 \pm 23.9\%$ of TSP for the tillage experiment. The TSP compositions along with mass concentrations are shown in Figure 20.

Table 15. Average (± 1σ) fraction of TSP that was PM$_{2.5}$ and PM$_{10}$ for each operation upwind and downwind of tillage site, and campaign averages for upwind and downwind.

Date	Upwind		Downwind		Operation
	PM$_{2.5}$/TSP	PM$_{10}$/TSP	PM$_{2.5}$/TSP	PM$_{10}$/TSP	
10/19/2007	0.22 ± 0.05	0.28 ± 0.04	0.24 ± 0.06	0.55 ± 0.20	Chisel
10/20/2007	0.21 ± 0.04	0.34 ± 0.03	0.17 ± 0.06	0.33 ± 0.24	Optimizer
10/23/2007	0.28 ± 0.01	0.68 ± 0.08	0.06 ± 0.02	0.29 ± .0.5	Disc 1
10/25/2007	0.31 ± 0.06	0.57 ± 0.14	0.21 ± 0.03	0.38 ± 0.13	Chisel
10/26/2007	0.32 ± 0.08	0.47 ± 0.05			Disc 2A
10/27/2007	0.31 ± 0.04	0.53 ± 0.21	0.20 ± 0.07	0.60 ± 0.31	Disc 2B
10/29/2007	0.39 ± 0.05	0.60 ± 0.08	0.52 ± 0.11	0.84 ± 0.21	Land Plane
	Average Upwind		**Average Downwind**		
	0.29 ± 0.07	0.50 ± 0.16	0.23 ± 0.16	0.50 ± 0.27	
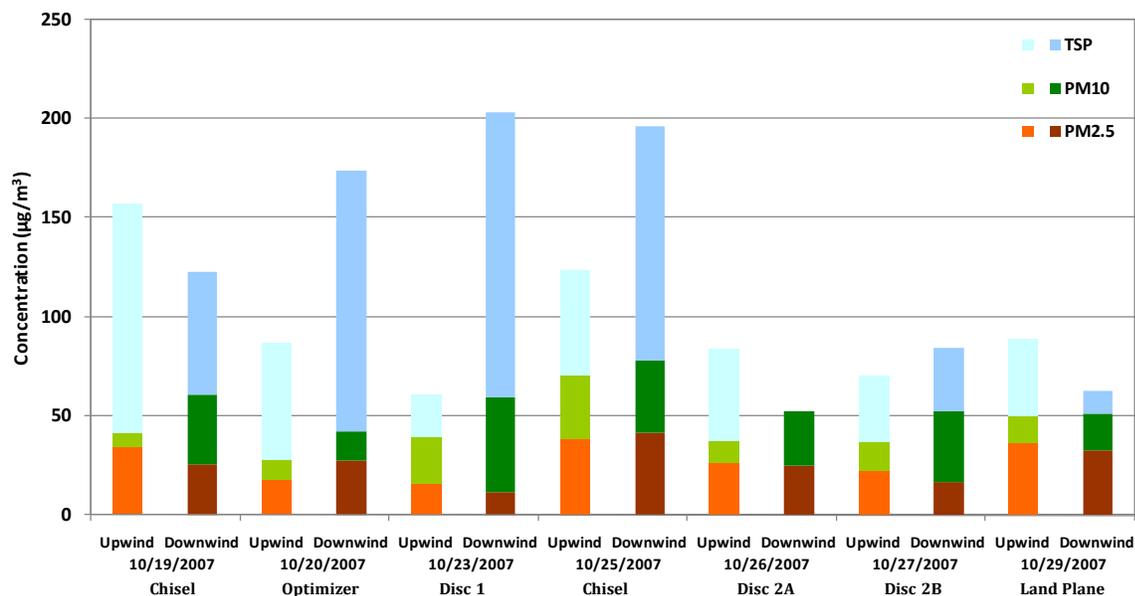
Figure 20. Average measured PM concentrations, upwind and downwind, with the particle size contributions to the total PM.

PM produced by agricultural tillage operations tends toward larger diameter particles. According to the U. S. EPA (1985), TSP emissions from agricultural tillage should be typically 21% PM_{10} and 4.2% $PM_{2.5}$ [52]. This being the case, concentrations of $PM_{2.5}$ should not vary greatly between the upwind and downwind sampling locations, whereas concentrations of PM_{10} and TSP should be more variable, as seen in this study. As previously stated, the campaign averaged $PM_{2.5}$ downwind concentrations were 93% of those measured upwind. The average downwind concentrations of PM_{10} and TSP were generally significantly larger than upwind, at 131% and 137%, respectively, of averaged upwind levels. Figure 20 illustrates both the lack of significant difference in upwind and downwind $PM_{2.5}$ concentrations and the generally significant differences between upwind and downwind PM_{10} and TSP levels.

In order to calculate an emission rate from these concentration measurements, the mass concentration observed at each sample location in the three size fractions that resulted from the source activity must be known. The difference between the upwind (background) and downwind concentrations is the result of the tillage emissions. Therefore, the downwind concentrations were compared with the sample average upwind concentration on a location-by-location basis; a location was included in the emission rate calculations only if the downwind concentration was greater than the average upwind concentration plus the 67% confidence interval. However, measured upwind concentrations were sometimes higher than downwind concentrations. This is potentially a result of contaminated samples as discussed earlier. Ideally, the background PM concentration for each operation was measured by an upwind tower distanced from the operations so as not to be affected by varying wind direction, turbulent eddies created by the operations during light and variable wind conditions, or traffic on the surrounding dirt roads. While the impacts of such contamination events on filter-based, sample period-average MiniVol data cannot directly be calculated, examination of time series data from a collocated OPC (based

on 20 second sample times) provides a method to detect such contamination and estimate the amount of contributed mass on the filter. We use a simple proportional correction to estimate the background PM levels using the OPC time series data. These proportionally scaled PM values can then be used for emission rate calculations. An OPC background concentration (OPC_{back}) may be found by taking an average of the OPC measured concentrations with any plume events omitted. Then, the ratio of OPC_{back} and the average OPC measured concentration for the sample period (OPC_{ave}) can be used to scale the MiniVol concentration (C_{ave}), which is the period average PM concentration, to provide a background mass concentration (C_{back}), as in Eq. 24.

$$C_{back} = C_{ave} \left(\frac{OPC_{back}}{OPC_{ave}} \right)$$

(24)

Due to the expected error of ±10% on the reported MiniVol concentrations, the calculated C_{back} values were used in place of C_{ave} for average upwind calculations only if the difference between the PM_{10} and TSP OPC_{back} and OPC_{ave} concentrations were greater than 10%. In such cases, the calculated $PM_{2.5}$ C_{back} values were also used in place of C_{ave}. It should be noted that data which use the proportional scaling to estimate the upwind MiniVol concentrations are based entirely upon OPC data.

The OPC-based proportional scaling method was applied to upwind locations for the chisel pass of the combined operations tillage method and disc pass 1 and disc pass 2B of the conventional tillage method. The proportionally calculated C_{back} values (feasibility was based on the ability to identify and separate plume events) were then used as background PM concentrations in determining facility produced concentrations. For these three sample periods, the statistical significance of the differences between average upwind and downwind concentrations was determined using the C_{back} values. In instances where the upwind TSP concentration was greater than the downwind concentration (10/19 and 10/29), the method for determining PM background levels using a collocated OPC was applied to the downwind measurement location. The derived TSP C_{back} concentration was then used as the background value for TSP emission rate calculations.

Table 16 presents the average upwind and downwind measured PM concentrations used for comparison to determine which downwind locations could be used to calculate emission rates via inverse modeling. Upwind averages that include background PM concentrations calculated using OPC data are designated using an asterisk (*) and the background TSP concentrations calculated using a collocated downwind OPC and MiniVol monitoring TSP are marked with a double asterisk (**). Some of the downwind averages in Table 16 are slightly different than those presented in Table 15 as those locations that were only slightly impacted by the operation under study were removed from emission rate calculations. Such locations for removal were identified through examination of reported MiniVol concentrations, OPC time series data, and model-predicted impacts (i.e. the dispersion models predicted a concentration less than 10% of the maximum weighted average for the sample period). Mean downwind concentrations of $PM_{2.5}$, PM_{10} and TSP used for emission rate calculations were 101%, 152% and 183%, respectively, of upwind levels. Comparisons of upwind average concentrations plus the calculated 67% confidence interval versus location-by-location downwind locations determined that emission

rates could be calculated for PM_{10} during each sample period, TSP for all but 10/26 which is a result of a sampling problem, and four of the seven sample periods for $PM_{2.5}$.

Table 16. Upwind and downwind average concentrations ± 67% CI (for *n*≥3) used in emission rate calculations.

Date		$PM_{2.5}$ µg/m^3	PM_{10} µg/m^3	TSP µg/m^3	Tillage Operation
10/19/2007	Upwind	32.9* ± 3.0	39.8* ± 3.6	81.0**	Chisel
	Downwind	25.7 ± 1.8	65.1 ± 11.3	122.5	
10/20/2007	Upwind	17.9 ± 1.8	28.2 ± 2.0	87.0	Optimizer
	Downwind	27.8 ± 5.3	42.1 ± 6.4	174.1	
10/23/2007	Upwind	15.4* ± 0.8	41.8* ± 3.0	60.5	Disc 1
	Downwind	11.8 ± 1.2	63.1 ± 3.1	203.3	
10/25/2007	Upwind	38.6 ± 3.5	70.5 ± 10.0	123.6	Chisel
	Downwind	41.4 ± 2.1	78.4 ± 7.8	196.0	
10/26/2007	Upwind	24.6 ± 2.1	41.3 ± 2.2	84.0	Disc 2A
	Downwind	26.7 ± 2.0	54.7 ± 7.4	-	
10/27/2007	Upwind	21.7* ± 1.0	26.1* ± 4.5	63.5*	Disc 2B
	Downwind	18.3 ± 2.0	62.5 ± 9.6	84.3	
10/29/2007	Upwind	35.2 ± 1.5	49.2 ± 1.6	53.5**	Land Plane
	Downwind	34.0 ± 1.6	57.3 ± 3.3	62.4	

* Adjusted PM concentration using OPC data
** Background level calculated using OPC and MiniVol data from the downwind location

4.2.2   ISC/AERMOD dispersion models

To better understand the emission locations and local rates, it is useful to apply dispersion models to the filter data. The model settings and seed emission rate of 50 µg/s-m^2 as explained in section 3.2.1 were used in both air dispersion models and often produced estimated concentrations higher than those measured, but generally within an order of magnitude. However, the modeled concentrations represent only facility produced pollutant and do not include background aerosol levels. Thus, to compare the modeled concentrations to field measurements, the measured background PM concentrations must be subtracted from the measured downwind concentrations.

4.2.2.1   ISCST3

Modeled average concentrations by ISCST3 ranged from 0.0 to 683.0 μg/m^3 with the highest concentrations typically modeled at a height of 2 m on the southern edge of the tillage sites, although this varied slightly with shifting wind directions. Figure 21 shows an example of ISCST3 modeled concentrations at 2m above ground level for the Disc 1 pass as part of the conventional tillage operations with 1.6 m/s average north winds.
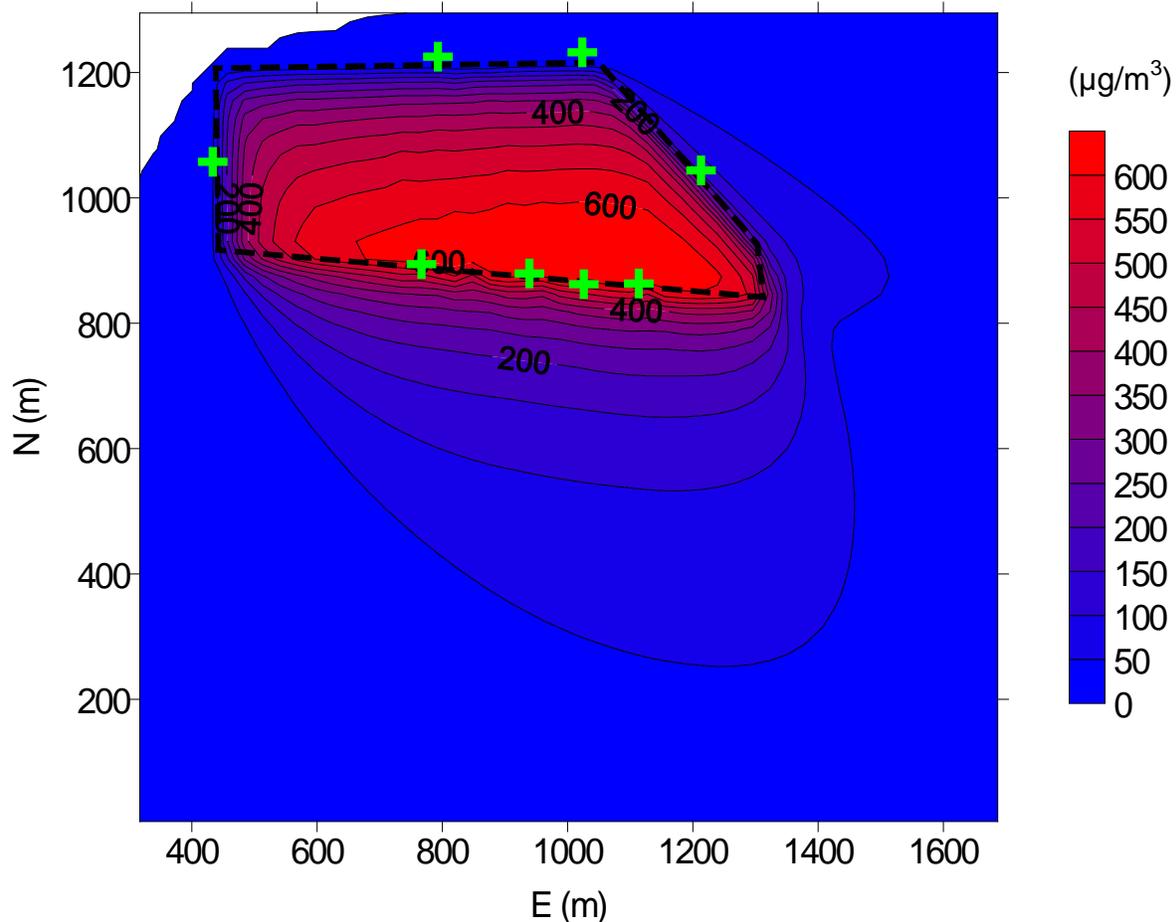
Figure 21. Modeled period average ISCST3 results (modeled hours = 8, sample time = 7.27 hrs) at 2m above ground level for the Disc 1 pass of the conventional tillage operations on October 23, 2007 with light north winds. The field area is outlined by the thick dashed line and sampler locations are shown in green; contour line numerical values are in μg/m^3.

4.2.2.2   AERMOD

Modeled average concentrations by AERMOD ranged from 0.0 to 438.3 μg/m^3 with the highest concentrations typically modeled at a height of 2 m on the southern edge of the tillage sites, although this varied slightly with shifting wind directions. Concentrations predicted by AERMOD were generally lower than those predicted by ISCST3 at the same emission rate, meaning that AERMOD predicts greater dispersion of the particles under most conditions found in this study. Figure 22 shows an example of AERMOD modeled concentrations at 2m above ground level for the same Disc 1 pass shown in Figure 21.
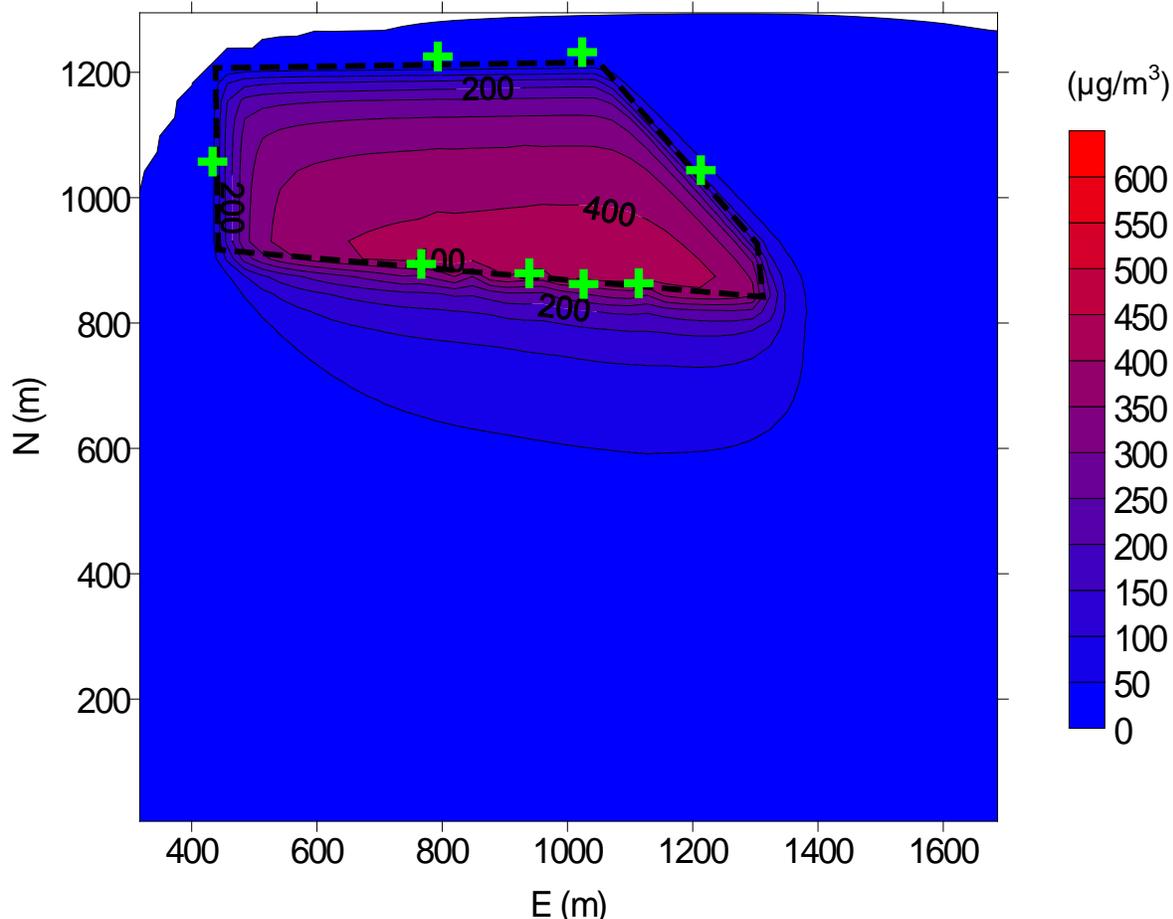
Figure 22. Modeled period average AERMOD results (modeled hours = 8, sample time = 7.27 hrs) at 2m above ground level for Disc 1 pass of the conventional tillage operations on October 23, 2007 with light north winds. The area of operations is outlined by the thick dashed line and sampler locations are shown in green; contour line numerical values are in μg/m³.

4.2.3   PM Chemical Analysis

4.2.3.1   Organic Carbon/Elemental Carbon Analyzer

The $PM_{2.5}$ OC/EC time series data collected at the downwind Air Quality trailer (AQT) is shown in Figure 23. As can be seen the $PM_{2.5}$-associated elemental carbon was typically quite low, averaging 0.5 μg/m³ ± 0.04 μg/m³ (at the 95% confidence interval) and showed relatively little variability. This would suggest that the site was not significantly impacted by typical EC sources such as biomass or diesel combustion and is more of a regional phenomenon. The observed organic matter concentrations, derived by multiplication of the raw OC concentrations by 1.7 (refer back to section 3.1.4.3), were seven-to-eight times the EC concentrations averaging 3.8 μg/m³ ± 0.23 μg/m³. Although the $PM_{2.5}$ organic component seemed to vary more and occasionally show greater concentration spikes, these episodes generally occurred during non-test events. During observational periods of the agricultural testing, those time periods when co-located filter-based PM samples were also collected, the elemental carbon $PM_{2.5}$ concentrations varied from 0.1 to 0.9 μg/m³, while the organic matter $PM_{2.5}$ concentrations varied from 1.4 to 6.1 μg/m³. On average, the carbon-related material accounted for 28.4 percent of the observed (downwind) $PM_{2.5}$ mass (see Figure 24).
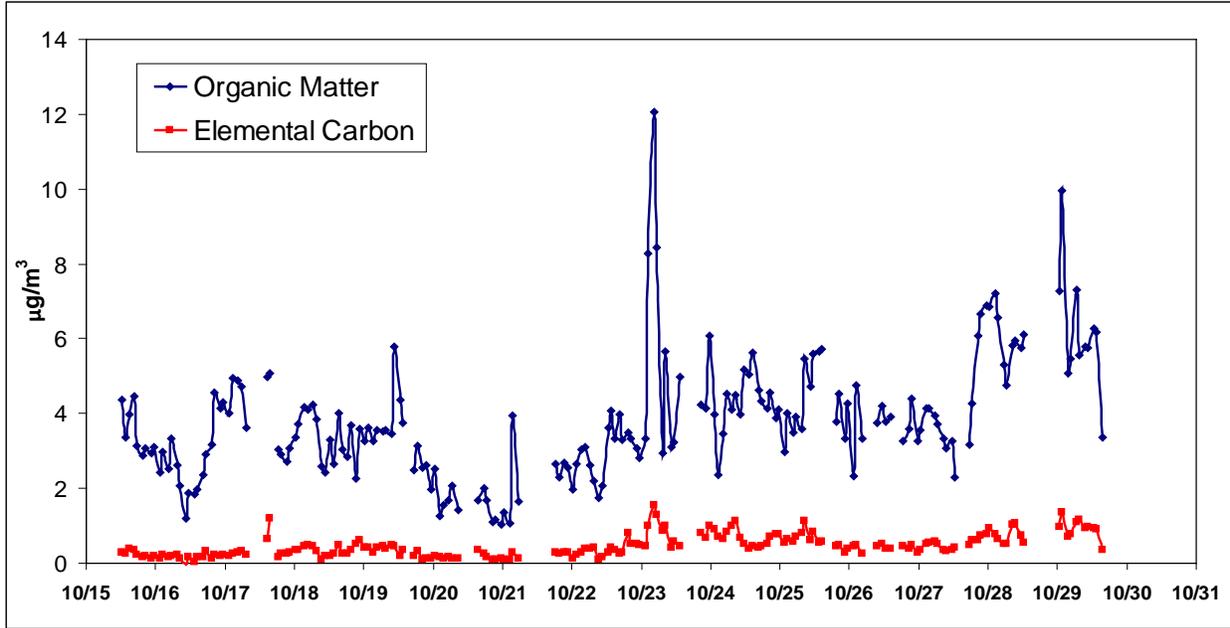
Figure 23. PM$_{2.5}$ OC/EC time series concentrations as collected at the downwind AQ trailer location. It should be noted that the raw instrument OC concentrations have been multiplied by 1.7 to account for potential non-carbon functional groups.
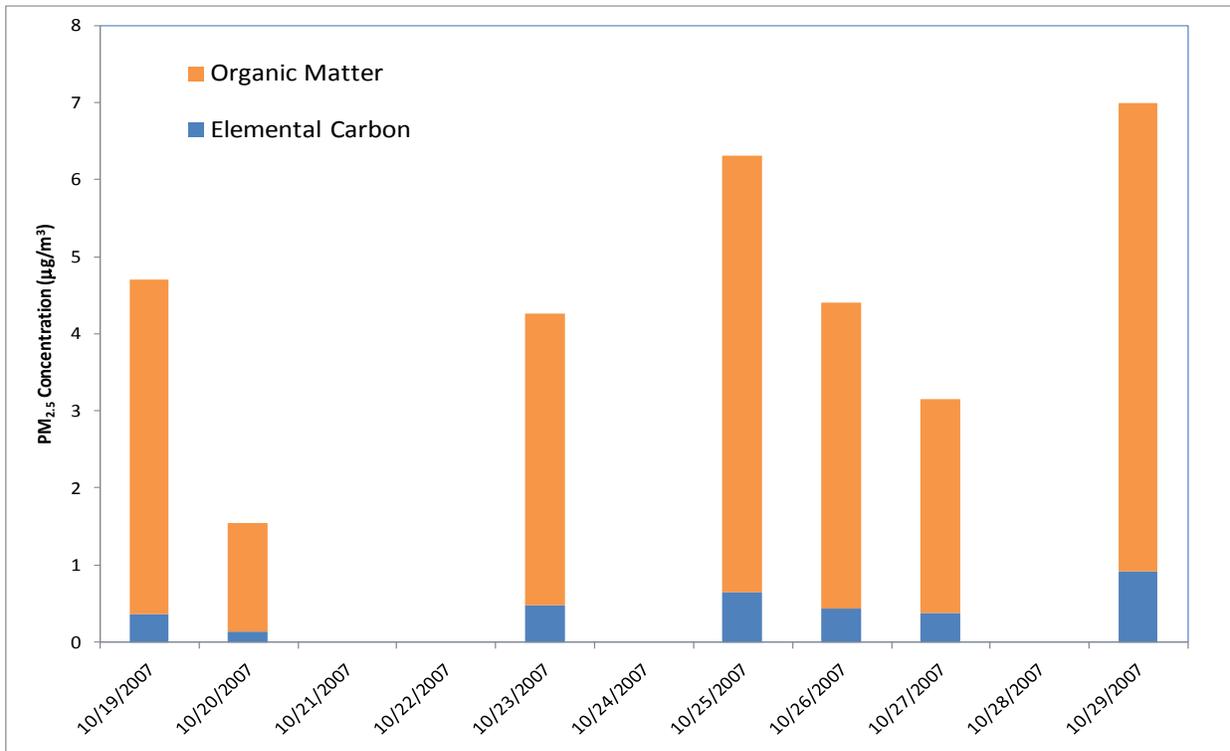
Figure 24. PM$_{2.5}$ organic matter and elemental carbon concentrations during specific sampling periods (parallel to filter-based sampling).

4.2.3.2   Ion Chromatographic (IC) Analysis

In addition to the near-real time carbon compositional analysis, water soluble ionic analysis was performed on selected $PM_{2.5}$, PM_{10}, and TSP filters collected at the AQ trailer, as well as one upwind (N1) and downwind location (S2), to more completely account for the near source particle chemical composition. It should be kept in mind that due to the availability of only one real-time PM carbon system, ambient PM carbon content was only determined for one site (AQT) and one size fractionation ($PM_{2.5}$). However, since the total (EC/OC) carbon fraction was relatively consistent across the field tests, the assumption can be made the EC and OC concentrations are conserved across the sampling fields, or in other words, the observed PM carbon component may be more related to regional sources as opposed to the local tillage operations.

All of the predicted ions where observed except nitrite which was not detected (n.d.) in any of the samples. As might be expected if the presumed sources are more regional in nature, the ionic species showed very little mass concentration differences between the upwind (N1) and downwind (AQT and S2) sample locations (see Table 17). On average, chloride, sulfate, and nitrate were the most dominant anions, while sodium, ammonium, and potassium were the dominant cations.

Table 17. Averaged filter ionic analysis for upwind and downwind samples for Oct. 23rd, 25th, and 26th, 2007.

	F^- ($\mu g/m^3$)	Cl^- ($\mu g/m^3$)	NO_2^- ($\mu g/m^3$)	SO_4^{-2} ($\mu g/m^3$)	NO_3^- ($\mu g/m^3$)	Na^+ ($\mu g/m^3$)	NH_4^+ ($\mu g/m^3$)	K^+ ($\mu g/m^3$)	Mg^{+2} ($\mu g/m^3$)	Ca^{+2} ($\mu g/m^3$)
Upwind (N1) $PM_{2.5}$	0.3	1.6	n.d.	0.3	0.4	1.4	0.4	0.6	0.0	0.3
Upwind (N1) PM_{10}	0.4	1.6	n.d.	1.6	0.7	1.6	0.8	0.7	0.9	1.0
Upwind (N1) TSP	0.3	1.2	n.d.	0.3	0.8	1.6	1.0	0.6	0.3	1.0
Downwind (S2, AQT) $PM_{2.5}$	0.3	0.9	n.d.	0.2	0.4	1.1	0.5	0.4	0.1	0.4
Downwind (S2, AQT) PM_{10}	0.2	1.0	n.d.	0.2	0.6	1.0	1.0	0.5	0.1	0.6
Downwind (S2, AQT) TSP	0.6	1.2	n.d.	0.7	1.2	2.0	1.4	0.9	0.2	1.4

Nationwide fine PM composition has been shown by Malm (2000) to be dominated by five aerosol classes: sulfates, nitrates, organic carbon, light-absorbing (elemental) carbon, and crustal elements [58]. Through the IC analysis of filter samples and the direct EC/OC measurements, four of the five dominant PM types have been quantified; these four known PM types combine to form only a few $\mu g/m^3$. By mass balance, the remainder of the PM mass (on the order of tens of $\mu g/m^3$) is composed of unanalyzed, and therefore unknown, constituents and is most likely composed of insoluble crustal elements. Therefore, it can be assumed that the remaining fine particle collected mass was likely dominated by soil-based particles. The bar chart in Figure 25 graphically demonstrates this crustal element dominance, shown as the "unknown" component in the summation bars, at both the upwind and downwind sampling locations and across all size ranges, with the relative contribution also increasing with particle size. The unknown, or crustal portions, may have a combination of local and regional sources, which cannot be separated based on the nature of the data collection and analysis. Magliano et al. (1999) found crustal/geological elements comprised 49% to 66% of fall PM_{10} measurements during the 1995 Integrated Monitoring Study (IMS95) in the San Joaquin Valley around Corcoran, CA, a small town also in a highly agricultural area about 100 miles southeast of Los Banos, CA [59]. Results from the IMS95 showed a factor of 2 variability in the mass contributed by geological sources, which were assumed to be dominated by dirt road traffic and agricultural operations, between monitoring sites that suggests strong site-specific, local geological influences. Over the three specified days analyzed, on average, the upwind $PM_{2.5}$, PM_{10}, and TSP filter samples contained 59.4%, 69.2%, and 86.1% "unknown" species, respectively. Similarly, the downwind "unknown" fractions were 69.4%, 77.9%, and 86.6% for $PM_{2.5}$, PM_{10}, and TSP, respectively.
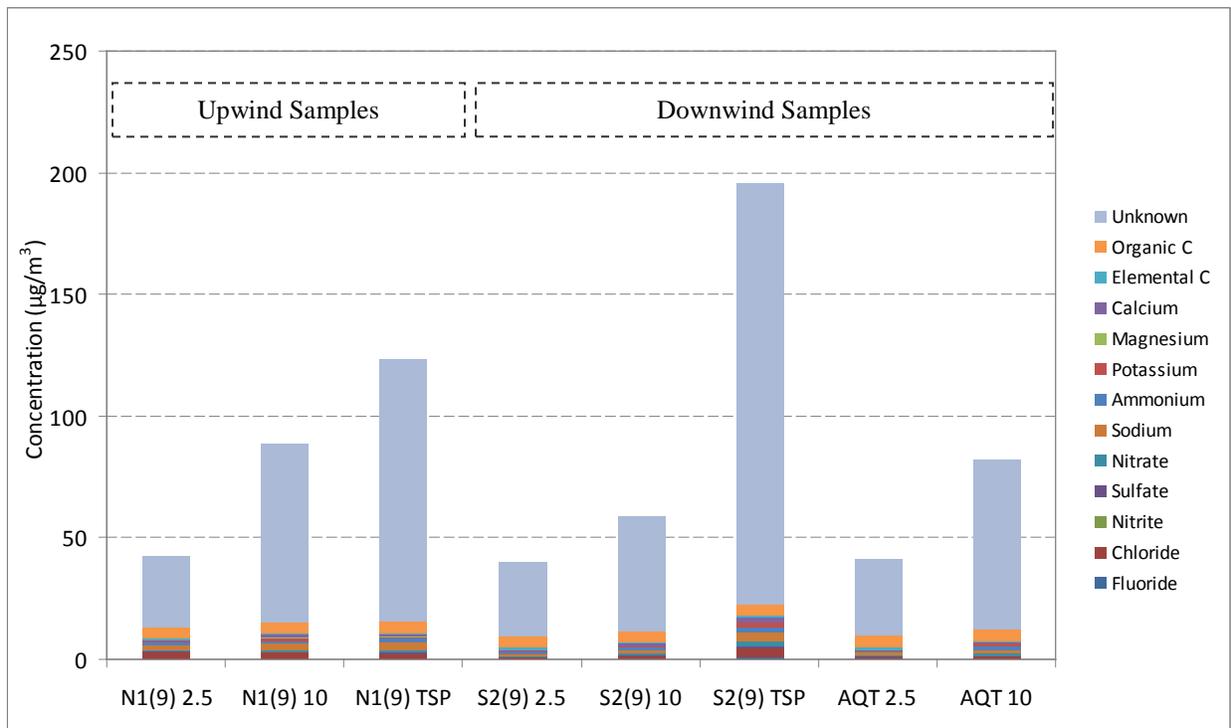
Figure 25. Chemical composition of downwind $PM_{2.5}$, PM_{10} and TSP filters from the chisel pass in the conventional tillage method, 10/25.

4.2.4   Aerosol Mass Spectrometer

The aerosol mass spectrometer sampled at the Los Banos site from October 15, 2007 through October 26, 2007. However, due to instrument malfunctions, data was only successfully collected from 10/15-10/18/2007, prior to all the tillage operations and measurements. The mass calibration of the instrument was drifting with time even within a saving period. This makes the spectra difficult to interpret and very problematic to quantify, as it was necessary to go through each spectrum by hand to verify the resolution of the ion peaks. The data may be able to yield information from the period of 10/18-10/21/2007, but the data acquired after that appear impossible to interpret. During the three days for which data meeting quality assurance tests was obtained, overall mass concentrations ranged from ~3-15 $\mu g\ m^{-3}$. The chemical composition of PM_1 particles as measured by the AMS during that time was dominated by ammonium nitrate and organic matter. Ammonium nitrate made up ~49.5% of the particulate mass, organic matter made up 39%, and ammonium sulfate ~9% (see Figure 26 and Figure 27). A calculation of mole ratio shows complete neutralization between the basic species (ammonium ion) when compared to acidic ones (nitrate, sulfate, and chloride ions). The chemical composition of the organic material as measured in the mass spectra appears to be a mix of oxygenated species (likely regional secondary oxidation products) and hydrocarbon-like compounds (probably a primary aerosol source such as combustion emissions.) The oxygenated species are dominant as would be expected in an environment dominated by secondary reaction chemistry.
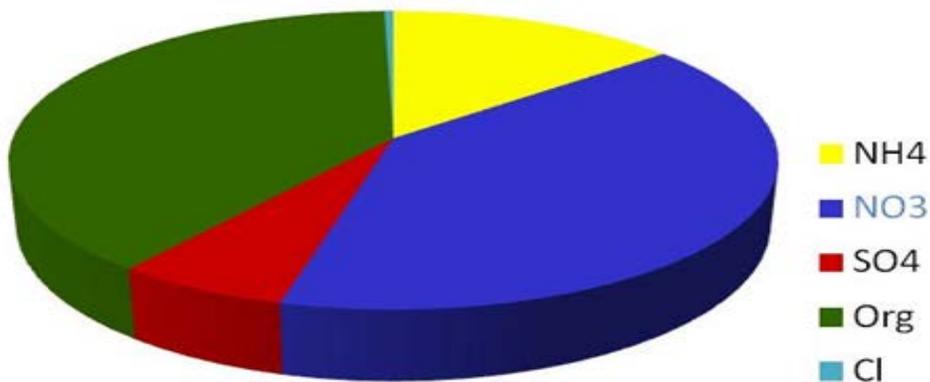
Figure 26. Average chemical composition of particles measured by AMS (~PM$_1$) in Los Banos, 10/15/2007 – 10/17/2007.
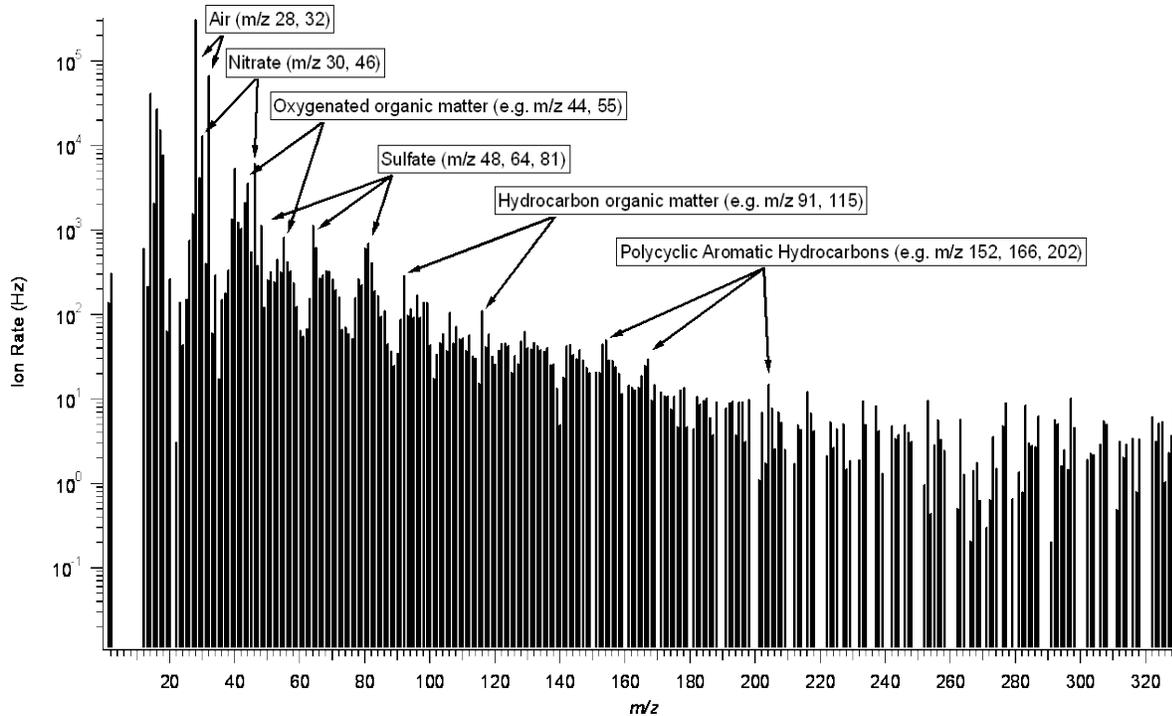
Figure 27. Typical mass-to-charge (m/z) data collected at Los Banos, with significantly contributing ions and their source particles identified.

4.3   OPTICAL CHARACTERIZATION DATA

4.3.1   Optical Particle Counter

The distribution of optical particle counters surrounding the fields of interest at two heights provided the ability to examine particle emissions by number and size, as well as to see the time series of PM concentrations through application of the MCF.

Examples of particle volume size distributions measured during tillage operations (dV/dd is the change in aerosol volume concentration normalized by the change in particle diameter), in units of $\mu m^3/cm^3/\mu m$, are presented in bar graph form in Figure 28. Each graph shows the background particle volume distribution, a volume distribution of aerosols downwind of the source, and the difference between the two that is the volume distribution of the emitted particles. It should be mentioned that by examining these data based on volume concentration, the large particles have a more visible effect than if number concentrations were examined. However, viewing the data in this way is advantageous because it is analogous to mass – the shape of and difference between the curves remains the same and only the scale changes as the transition to mass concentration is made. Therefore, the given bar graphs show that the greatest volume (and mass) of emitted aerosols is in the large particle range above a diameter greater than about 2.5 µm. As seen in the reported PM sampler levels, the greatest contribution by tillage activities was in the PM_{10} and TSP measurements.
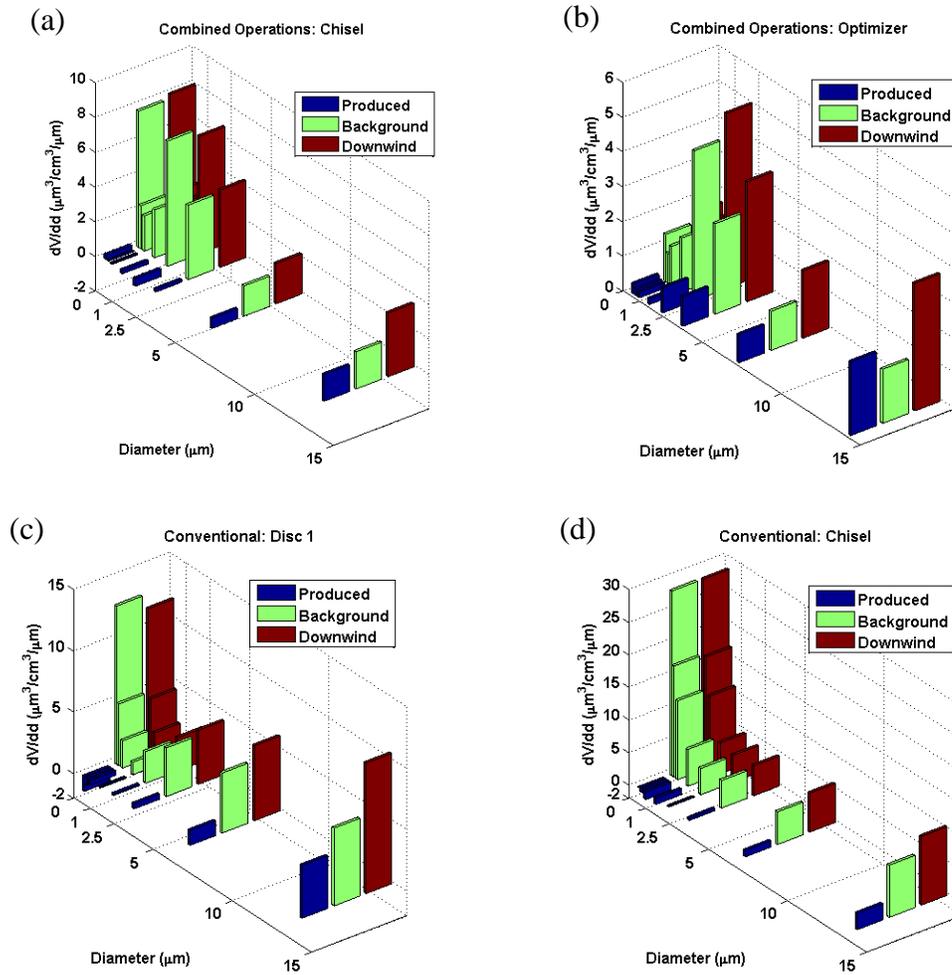
Figure 28. Sample period average particle volume size distributions ($\mu m^3/cm^3$-μm) measured from upwind (background) and downwind (background plus emissions) locations, with the difference being the aerosol emitted by the tillage activity. (a) is the chisel operation of the combined operations tillage method, (b) is the optimizer operation of the combined operations tillage method, (c) is the disc 1 operation of the conventional tillage method, and (d) is the chisel operation of the conventional tillage method.

4.3.2 Optical to PM Mass Concentration Conversion

A critical factor in converting the lidar data from number density (volume) data to mass concentration fields is the derivation of the Mass Conversion Factor (MCF). This step was described in Eq. 14. The daily average MCF calculated from the distribution parameters measured by OPCs, from both the upwind and downwind sides combined, are shown in Figure 28. Sample period average particle volume size distributions ($\mu m3/cm3$-μm) measured from upwind (background) and downwind (background plus emissions) locations, with the difference being the aerosol emitted by the tillage activity. (a) is the chisel operation of the combined operations tillage method, (b) is the optimizer operation of the combined operations tillage method, (c) is the disc 1 operation of the conventional tillage method, and (d) is the chisel operation of the conventional tillage method.

The particle size distributions measured by OPCs upwind and downwind of the source were used in lidar retrievals to estimate the range dependent V_k (see Eq. 17). Collocated OPC and PM sampler data were used to estimate the MCF as described in section 3.1.4.2. This in turn was used to convert lidar-measured particle concentration to mass concentration units, which can be compared with the PM sampler measurements.

MCF values estimated as a mean value for each day and for the whole campaign are presented in Table 18, with the daily means ± the corresponding 95% confidence interval (CI) as in Figure 29. Day to day variation in the MCF is not fully understood, but is likely due to changes in background aerosol sources and composition, as the point samplers collected ambient aerosol for a much larger fraction of the time than the tillage plume. The relatively high $PM_{2.5}$ MCF values calculated for 10/20 is due to a drop in small particle (< 1.0 µm) counts by all the OPCs that day, with respect to other days, while $PM_{2.5}$ concentrations measured by PM samplers did not show a similar drop. The reason for this phenomenon is unknown at this time.

Table 18. Mass conversion factors estimated for each day of the tillage operations and averaged for the whole campaign. Error values represent the 95% confidence interval.

	Date	Daily MCF (g/cm³)							Overall MCF (g/cm³)
		19-Oct	20-Oct	23-Oct	25-Oct	26-Oct	27-Oct	29-Oct	
$PM_{2.5}$	Average ± 95% CI	3.40 ± 0.63	4.90 ± 1.89	2.38 ± 0.39	2.16 ± 0.24	2.92 ± 0.42	2.57 ± 0.57	2.73 ± 0.24	2.95 ± 0.35
	n	7	6	7	8	6	8	7	49
PM_{10}	Average ± 95% CI	1.42 ± 0.14	1.71 ± 0.50	1.34 ± 0.16	1.29 ± 0.20	1.40 ± 0.18	1.37 ± 0.59	1.61 ± 0.10	1.44 ± 0.13
	n	7	7	6	7	7	8	6	48
TSP	Average ± 95% CI	2.51	2. 77	0.63	1.09	1.03	0.84	1.16	1.53 ± 0.51
	n	2	2	1	2	1	2	2	12
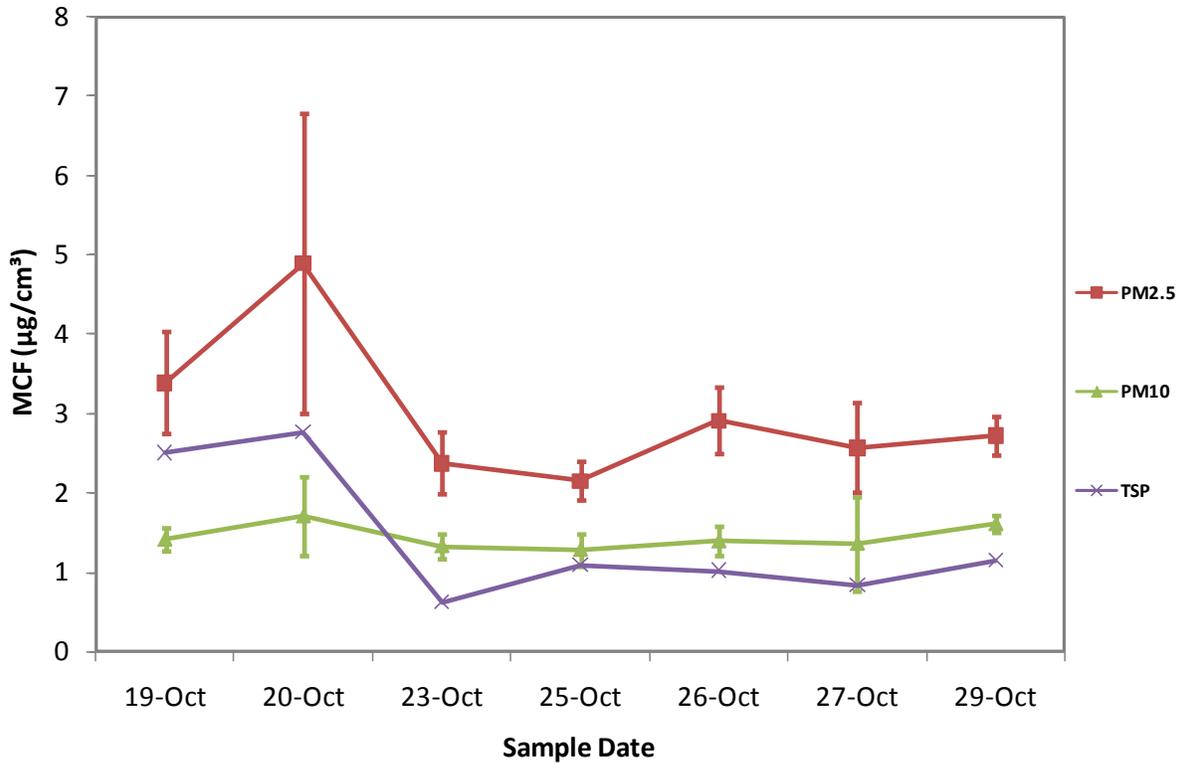
Figure 29. Average daily MCF with error bars representing the 95% confidence interval.

After lidar measurements were converted to PM concentrations, a quality assurance step of comparing collocated PM sampler, OPC, and lidar concentrations during 'stare' modes was performed. The time series of routine lidar stares were plotted with the time series data from the calibration OPC to ensure that trends and concentrations are the same in both data sets (Figure 30). It should be noted that lidar measurements were taken every 0.5 seconds while the OPCs recorded 20 second samples. Therefore, the 40 lidar measurements are presented for every OPC measurement.
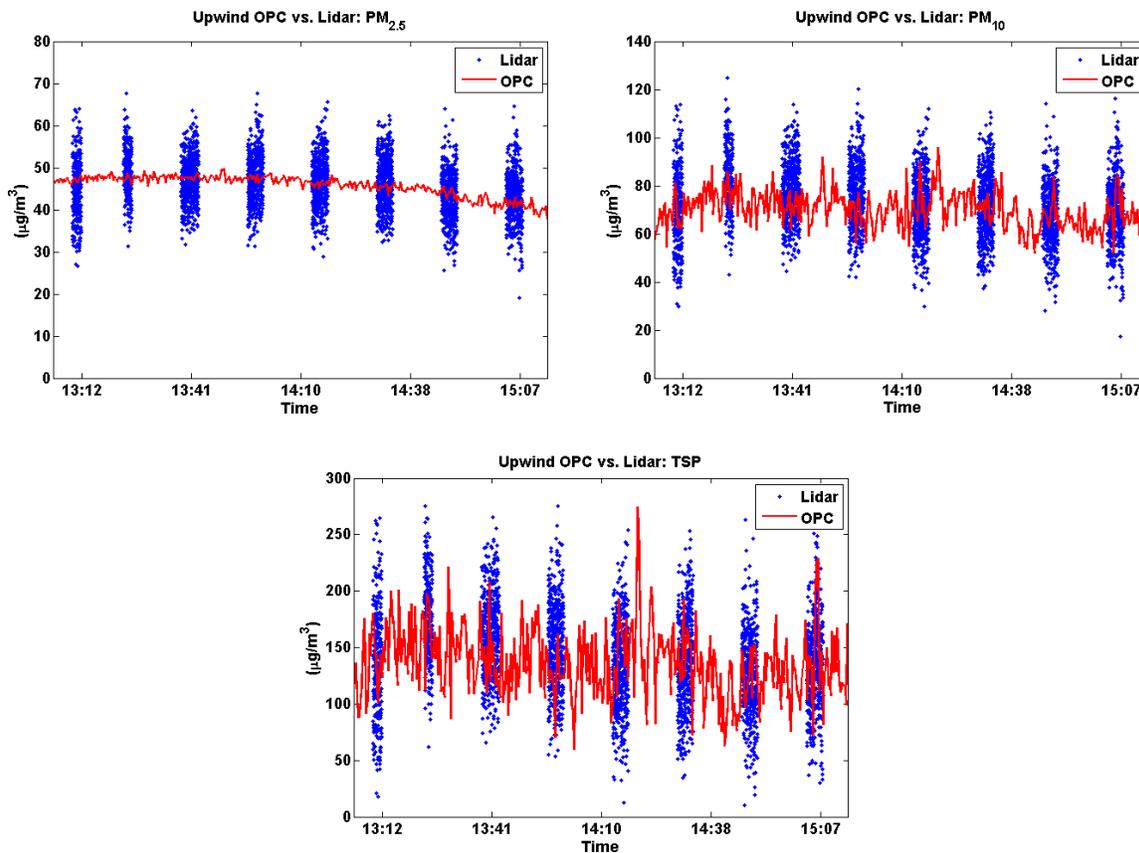
Figure 30. PM$_{2.5}$, PM$_{10}$, and TSP mass concentrations retrieved from collocated lidar and OPC during the 'stare' time series for 10/25. Data acquisition time of the lidar data is 0.5 sec while OPCs were set to 20 sec accumulation time. Measurements were done on the upwind side of facility (location N1 – "Pig" OPC).

To compare lidar and OPC retrievals with collocated PM sampler measurements, the lidar and OPC time series were averaged and a 95% confidence interval was calculated over the corresponding MiniVol sampling time. Results from these calculations for 10/23 are presented in Table 19. The OPC (20 sec) and lidar (0.5 sec) collect data at a much higher rate than the MiniVols (7.25 hrs for this sample run) and are able to capture the temporal variability of the background aerosol concentration. On many days during this field trial the measured background variability exceeded the uncertainty of lidar retrievals [46].

Table 19. Comparison of PM mass concentrations (µg/m³) as reported by MiniVol samplers and mean values measured by collocated OPCs and lidar at N1 (upwind) and S5 (downwind) for 10/23/2007.

Upwind	$PM_{2.5}$ (µg/m³)	PM_{10} (µg/m³)	TSP (µg/m³)
PM sampler (N1)	17.0	35.9	60.5
Upwind PM sampler average ± 67% CI	15.5 ± 0.8	40.0 ± 3.0	60.5
OPC (N1) ± 95% CI	13.9 ± 0.2	54.5 ± 3.9	65.6 ± 6.3
Lidar ± 95% CI	13.8 ± 0.2	45.9 ± 0.9	60.1 ± 1.4
Downwind			
PM sampler (S5)	9.9	74.5	203.3
Downwind PM sampler average ± 67% CI	11.7 ± 1.2	62.9 ± 3.0	203.3
OPC (S5) ± 95% CI	12.8 ± 0.2	63.5 ± 3.1	97.0 ± 13.0
Lidar ± 95% CI	41.7 ± 9.0	193.7 ± 47.7	297.7 ± 76.6

A similar comparison of OPC and lidar time series data measured from downwind of the tillage field is shown in Figure 30. The spikes of the concentrations (especially of PM_{10} and TSP) are due to the dust plume generated by tillage operations crossing this OPC. Spikes are rarely observed on the upwind side of the field (upwind spikes are associated with road traffic).

As a quality check, comparison analysis of collocated lidar, OPC, and MiniVol data was done for all days of campaign. An example of the lidar retrieved PM concentration vs. one of the OPCs (Horse) is shown in Figure 31. In general, the OPC and lidar data averaged for the PM sampler acquisition time are in good agreement with mass concentrations measured by the collocated PM samplers. Discrepancies between point source instruments (PM samplers and OPC) and lidar are due to inherently different measurement techniques. Point instruments capture particle concentration at a single point (a few cm³) with a small volumetric flow (1.6×10^{-5} to 8.3×10^{-5} m³/s). The lidar acquires information in a volume of ~3 m³ for each bin along the laser beam for each sample (2 samples per second in this experiment), and thus can capture a spatially variable plume while the plume may miss the point sensors. The best agreement is observed when the lidar is compared with PM sampler data averaged over several locations along the up- or down-wind side of the tillage field. For similar reasons, using MCF values averaged over the whole campaign yields larger discrepancies between collocated lidar and OPC/PM sampler PM concentration data than daily averaged MCF values. Based on these observations, a daily averaged MCF is used for conversion of lidar 'staple' data used for flux and emission rate calculations.
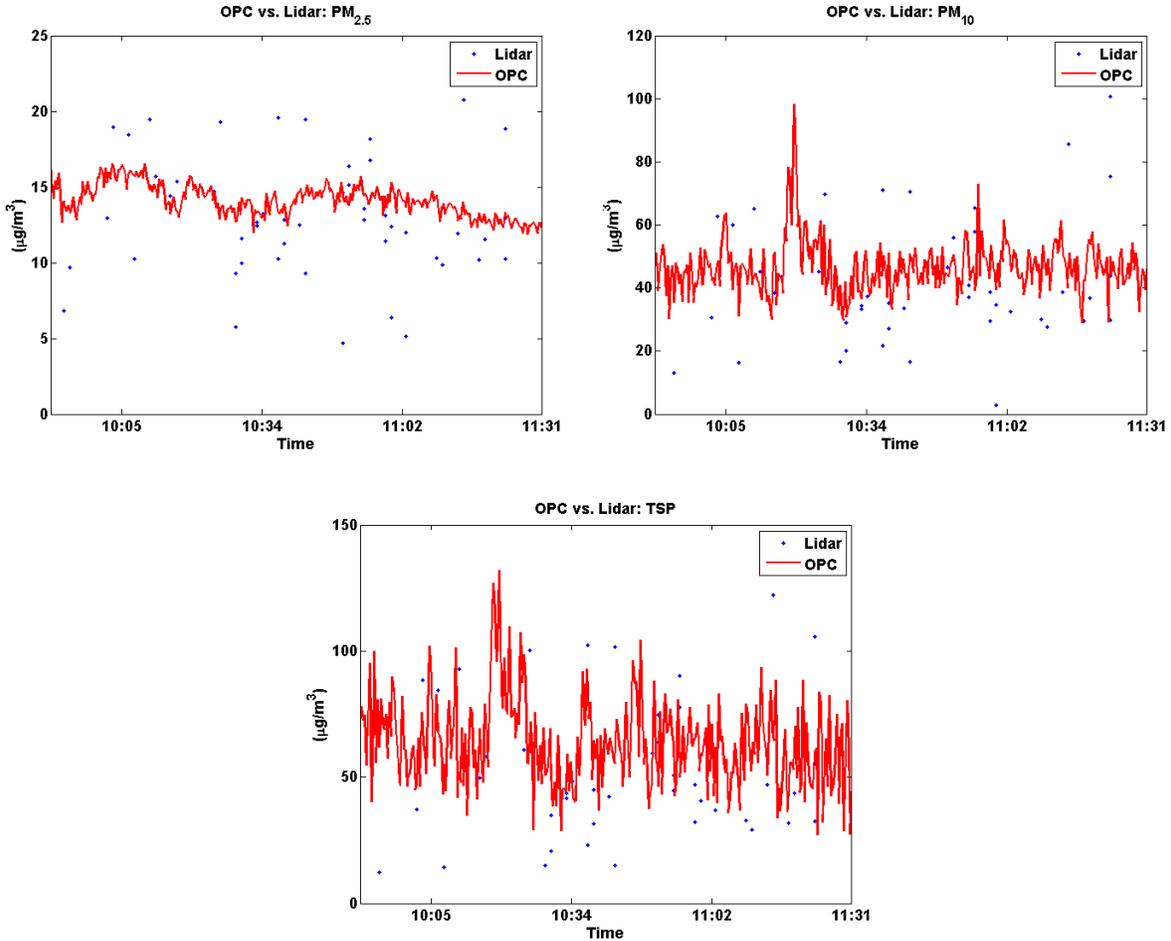
Figure 31. PM$_{2.5}$, PM$_{10}$, and TSP mass concentrations retrieved from collocated lidar and OPC during 'staple' scanning (bottom point for the range bin of the OPC, collected from each staple shown). Data acquisition time of the lidar data point is 0.5 sec while OPCs were set to 20 sec accumulation time. Measurements were done on the downwind side of facility (location S5 – 'Horse' OPC) on 10/23/2007.

4.3.3 Lidar Aerosol Concentration Measurements

Examples of the lidar-derived upwind and downwind plume area average volume concentrations used in the flux calculations shown below, are shown in Figure 32 and Figure 33. The two top panels show the profile averaged wind speed and direction values used in the flux calculation, with the third and fourth panels showing the area averaged volume concentrations measured upwind (C$_U$) and downwind (C$_D$) in $\mu g^3/cm^3$ (see Eq. 17). Wind speeds and directions for some of the days that measurements were made were light and variable, a wind condition that is known to challenge our flux measurement method. The concentrations derived from the lidar scans to be used in flux calculations were carefully quality controlled to assure that the upwind and downwind measurements were not contaminated by road traffic or mixed air flows that did not represent the operation under test. Quality controlled data are presented in these plots and in the table summaries. The quality control rejects experimental data on the basis of three conditions that violate the process flux measurement assumptions:

a. Wind direction $> \pm 80°$ at the time of the scan from the optimal wind direction of 360° based on the lidar location

b. External fugitive dust entering from the upwind side of the field due to traffic or other non-stationary anomaly (e.g. dust devil).

c. Contamination of the reference OPC from the upwind side of the field.

Wind directions used to screen the lidar derived aerosol concentrations to be included in the flux and emission measurements were limited to +/-80° of magnetic North. It was assumed that the upwind concentration measurements would be more uniform than the downwind measurements and more downwind scans were made than those of the upwind conditions. In Figure 32 and Figure 33, the gaps in the upwind concentration are due to this sampling plan.
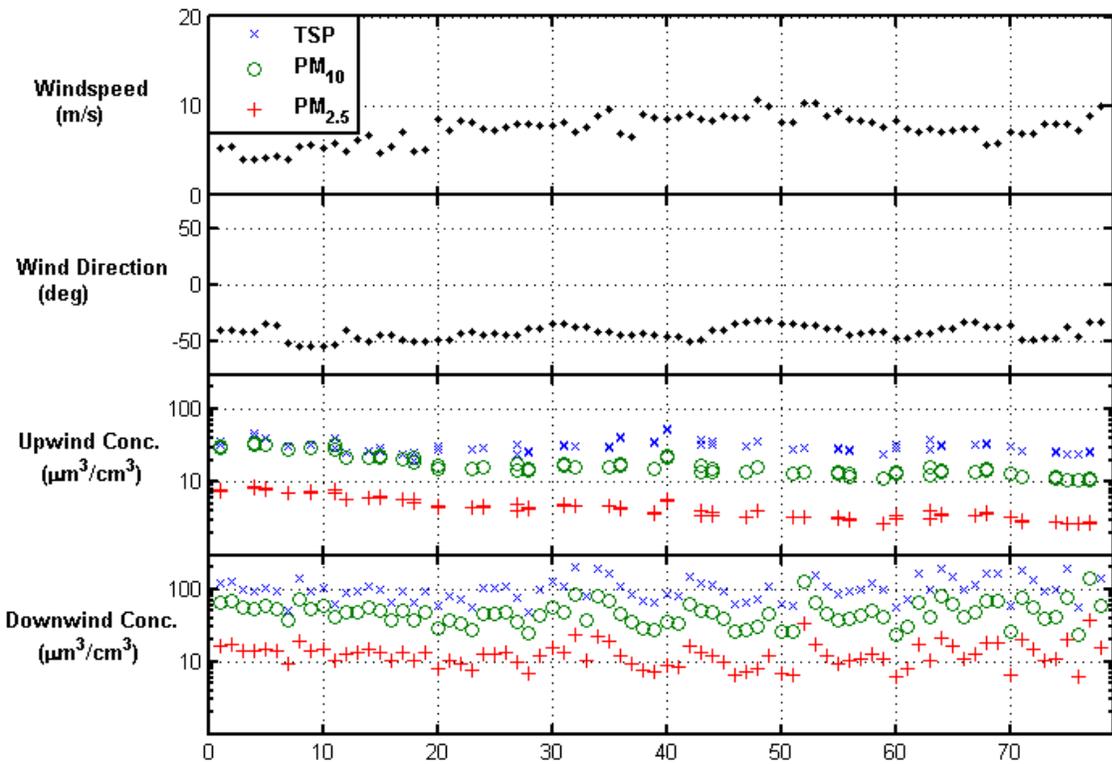
Figure 32. Wind speed, wind direction, upwind and downwind plume area average particulate volume concentrations, for the October 20, 2007 Optimizer pass of the combined operation tillage.
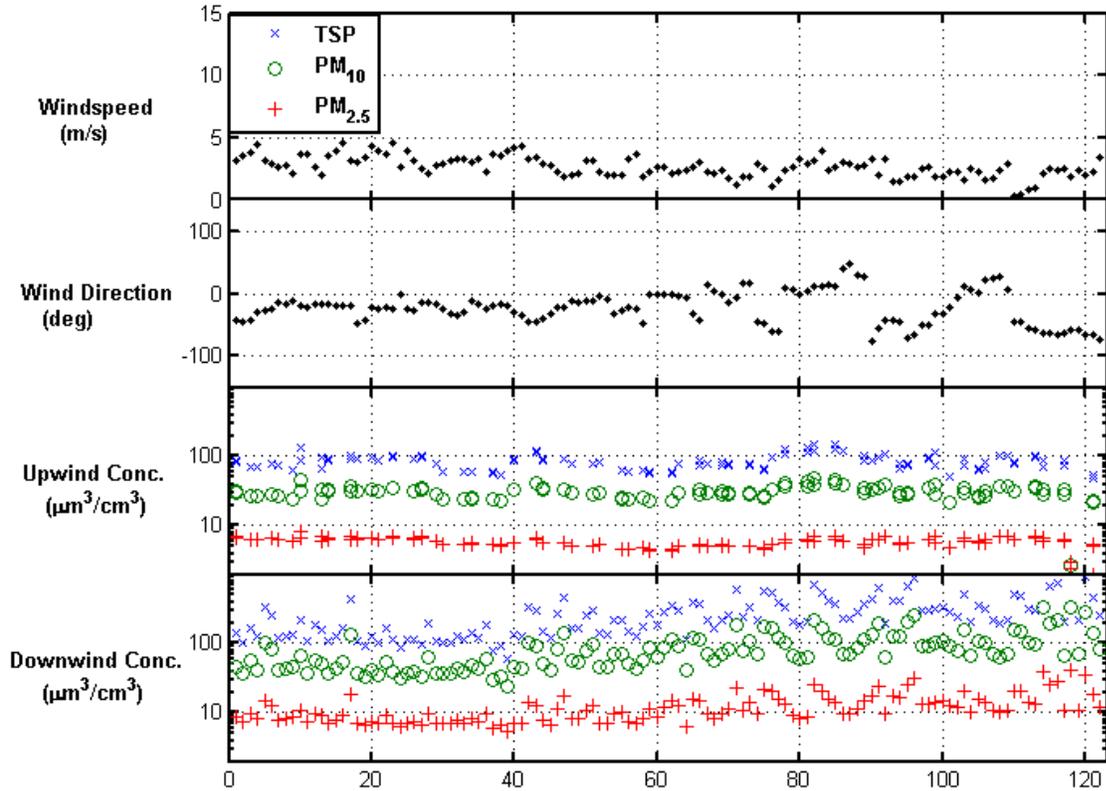
Figure 33. Wind speed, wind direction, upwind and downwind plume area averaged particulate volume concentrations for the October 23, 2007 first disc pass of the conventional tillage operation.

4.4   FLUXES AND EMISSION RATES

Emission rates were calculated using the lidar measurements, and compared with the model results for comparison to previous studies.

4.4.1   Lidar based Fluxes and Emission Rates

The combination of 'staple' and 'stare' measurements, as described in Section 3.1.5, of the mass concentration distribution measurements from the upwind and downwind sides of the field were performed continuously during the each tillage operation of the field campaign. Figure 34 and Figure 35 show calculated net flux measurements for sequential lidar measurements taken during the Optimizer pass in the combined operation tillage method on 10/20/2007 and the initial discing pass of the conventional tillage operation on 10/23/2007, respectively. The net flux is the product of the plume area averaged volume concentration (C_D-C_U) difference multiplied by the daily average MCF (see Table 18) and the component of the wind velocity that is perpendicular to the lidar beam. This quantifies the mass passing through the lidar's vertical scan per unit time.
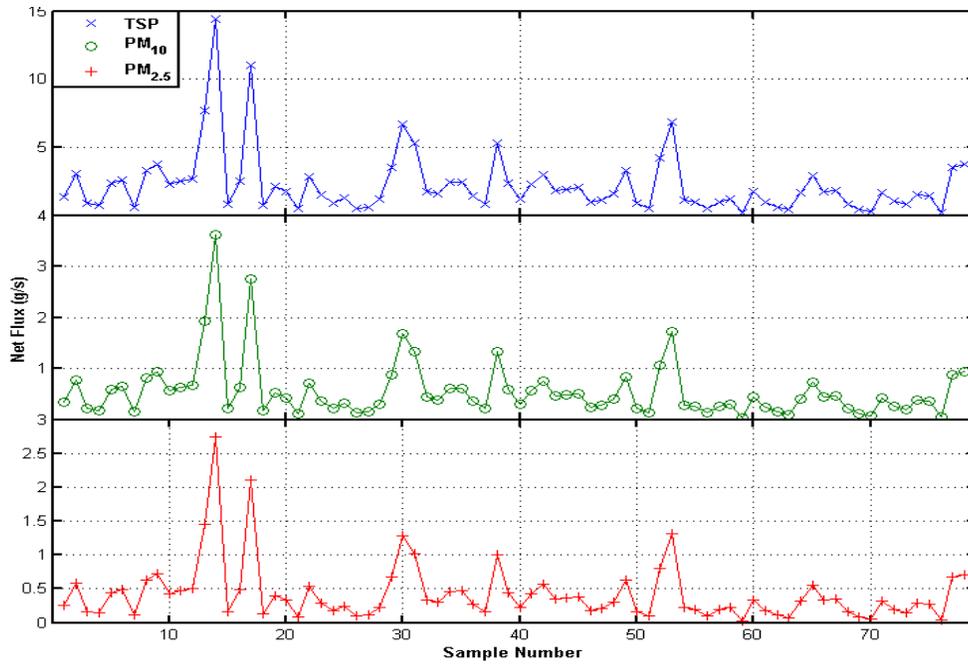
Figure 34. Lidar derived fluxes (g/s) of PM$_{2.5}$, PM$_{10}$, and TSP for the October 20, 2007 Optimizer pass of the combined operation tillage over the operation sample time of 2.85 hrs.
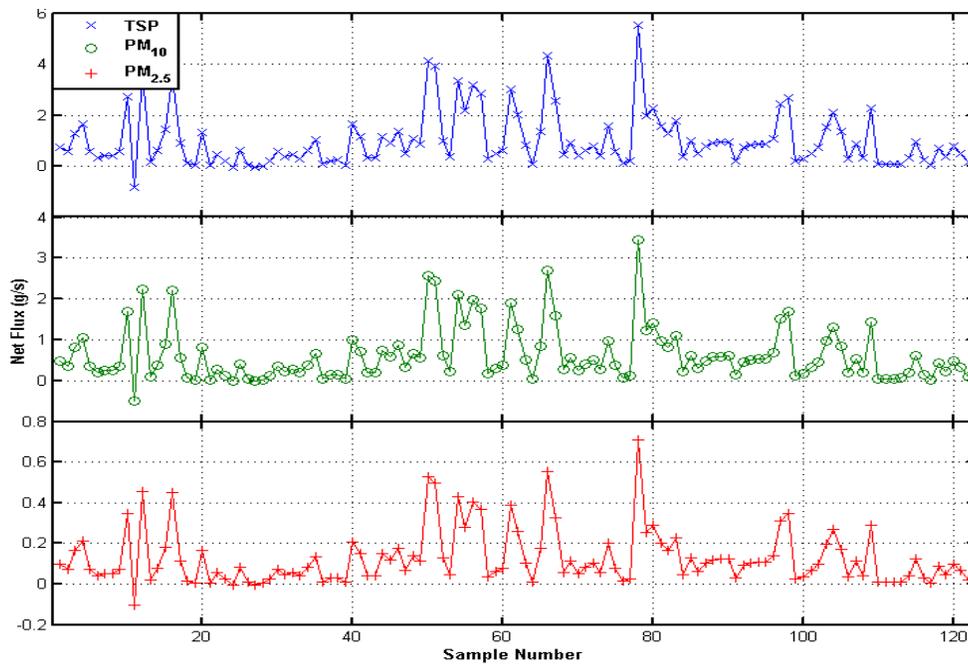
Figure 35. Lidar derived fluxes (g/s) of PM$_{2.5}$, PM$_{10}$, and TSP for the October 23, 2007 first disc pass of the conventional tillage operation over the operation sample time of 7.27 hrs.

Net fluxes were calculated using up- and downwind concentration measurements averaged over each vertical scan and using average wind information for the time of the individual scan. Single scan differences, of course, do not account for accumulation or depletion in the measurement box due to wind speed variation during a scan, for input background variation, or for storage in or flushing of the flux box due to the existing large scale wind eddy structure (i.e. we do not attempt to measure the same air mass at the upwind and downwind scans). The process is assumed to be a continuous emission source and several scans are required to achieve a meaningful mean estimate of the facility emission. For calculation efficiency, the flux was calculated through the downwind surface first and then the upwind flux, differencing the flux rather than concentration. The plume area was chosen manually by observing each downwind scan and highlighting the area to be included in the calculation. Choosing an area that fully includes the source plume but not a lot of extra area eliminates the need to spend resources calculating for pixels which do not contribute significant flux.

Using the series of flux measurements collected during each tillage operation, similar to those in Figure 34 and Figure 35, the mean fluxes were calculated for all days and are shown in Table 20 with respective 95% confidence intervals. The error bars used here for the lidar data denote our confidence in the mean due to the scan to scan variability due to the wind transport process occurring on that day, and not to the precision of the accuracy of the individual measurements. Measurement precision, as reported by Bingham et al. [60] show measurement accuracy on the order of 0.1g/s. This is evident in the initial scans shown in Figure 35, where transport across the downwind plane was at or below the lidar system detection limit. Standard deviations of the measurement sequences can be of the same magnitude as the fluxes under light and variable wind conditions, with some scans showing very light, diffuse plumes crossing the lidar plane followed by very dense ones.

Table 20. Mean fluxes (g/s) ± 95% confidence interval from quality controlled samples for each tillage operation.

Operation	$PM_{2.5}$ (g/s)	PM_{10} (g/s)	TSP (g/s)
Combined : Chisel (10/19/07)	0.33 ± 0.15	0.49 ± 0.23	1.91 ± 0.88
Combined: Optimizer (10/20/07)	0.43 ± 0.10	0.56 ± 0.13	2.23 ± 0.51
Conventional: Disc1 (10/23/07)	0.13 ± 0.02	0.62 ± 0.12	1.00 ± 0.19
Conventional: Chisel (10/25/07)	0.30 ± 0.08	0.66 ± 0.17	1.96 ± 0.50
Conventional: Disc 2A (10/26/07)	0.41 ± 0.12	0.72 ± 0.21	1.45 ± 0.43
Conventional: Disc 2B (10/27/07)	0.22 ± 0.05	0.53 ± 0.13	0.90 ± 0.22
Conventional: Land Plane (10/29/07)	0.09 ± 0.02	0.15 ± 0.04	0.22 ± 0.06

The relatively high uncertainty in the flux data of 10/19 is due to the relatively small number of valid samples and the high variability of those samples due to the light and variable wind conditions that were present on that day. This higher uncertainty is evident in the summary calculations of the chisel operation for that day. The flux data presented in Table 20 were multiplied by the total tractor operation time to yield a total mass emitted, and then normalized by area tilled to calculate emission rates presented in Table 21. While the lidar-measured fluxes for the Optimizer pass in Table 20 are higher than the chisel pass of the same treatment, the emission rates reported in Table 21 for the Optimizer are lower due to the fact that the Optimizer pass treats about two times as much area in the same amount of time as the chisel pass.

The 95% confidence interval of the total mass emitted per day was calculated by using the sample statistics (standard deviation and number count) for each day. The 95% confidence interval for the total emission, on the other hand, was derived using the assumption that the average emission rate of each day can be treated as a random variable. The variance of the average emission rate of each day was assumed to equal the variance of the sample set divided by the number of samples for that day. The 95% confidence interval for the daily mean was calculated by assuming a Gaussian distribution and calculating the interval in which the daily mean falls with a 95% probability. The variance of the total emission for each technique was calculated as the sum of the variances of each operation. The 95% confidence interval was then calculated again assuming a Gaussian distribution.

The lowest emission rate for each PM size fraction among the investigated operations was derived for the land plane operation in the conventional tillage method. It should be noted that emission rates and factors available in literature for land planning are much higher than all other activities; in the CARB document listing emission factors for agricultural tillage land planning has an emission factor ten times that of discing, tilling, and chiseling. This relationship between the emission rates for land planing and discing/tilling/chiseling was not seen in this study, which is likely due to the remaining water in the surface soil from the precipitation event that occurred the evening of October 27th. The summed $PM_{2.5}$, PM_{10}, and TSP emission rates for the Combined Operation and Conventional methods all have a statistically significant difference at the 95% confidence interval calculated as described in the previous paragraph.

In summary, Aglite – in combination with OPC and PM samplers – indicates that the Optimizer makes more concentrated plumes than does a conventional tillage rig, this is largely because the Optimizer moves twice as much soil per tractor pass than a conventional implement. However, since the Optimizer requires fewer tractor passes to till a field, the total amount of dust generated is smaller. Therefore <u>the emission rate for a field tilled by the Optimizer is smaller than for conventional tillage</u>.

Table 21. Aerosol mass transfer (± 95% confidence interval) from each field (flux normalized by operation duration and area tilled) as calculated from lidar data for all tillage operations.

Operation	$PM_{2.5}$ (mg/m^2)	PM_{10} (mg/m^2)	TSP (mg/m^2)
Combined: Chisel	45.3 ± 13.1	69.0 ± 19.9	265.9 ± 76.6
Combined: Optimizer	32.5 ± 5.0	42.7 ± 6.6	169.9 ± 26.2
Sum for Combined Operation Method	77.8 ± 14.0	111.6 ± 20.9	435.8 ± 80.9
Conventional: Disc 1	20.4 ± 2.6	99.7 ± 12.5	159.8 ± 20.0
Conventional: Chisel	35.8 ± 5.9	79.5 ± 13.1	235.1 ± 38.8
Conventional: Disc 2	39.5 ± 11.2	80.7 ± 20.5	149.3 ± 40.3
Conventional: Land plane	13.8 ± 3.9	21.9 ± 6.2	33.4 ± 9.4
Sum for Conventional Method	109.5 ± 13.5	281.9 ± 28.0	577.6 ± 60.1

4.4.2   ISCST3 Model Emission Rates

The individual downwind measured concentrations were evaluated to determine if they were greater than the average upwind concentration plus the 67% confidence interval for each operation. In locations where the downwind concentration was higher and the model predicted concentration was greater than 10% of the maximum modeled concentration, emission rates were calculated using the source-produced concentrations (downwind minus upwind), modeled concentrations and the seed emission rate as shown in Eq. 22. The resulting emission rates are shown in Table 22. To compare combined and conventional operations, the emission rates of individual operations were normalized by the sample time. The mass per unit area of PM emitted by the individual operations could then be summed to provide total mass emitted from the combined and conventional tillage operations. The 95 percent confidence intervals reported in Table 22 were calculated the same way as those for the lidar emission rates (see Section 4.4.1).

On two of seven days there were not any measured $PM_{2.5}$ concentrations greater than the average upwind concentration plus the 67% confidence interval. Therefore, no $PM_{2.5}$ emission rates were calculated for these sample periods. The second disc pass was carried out over two sample periods, October 26th and 27th, due to farm equipment malfunctions on the 26th, as stated previously. Single emission rate values for $PM_{2.5}$ and PM_{10} for the disc 2 pass were calculated by averaging the emission rates on a mass per unit area basis across these two sample periods. Due to the absence of a valid downwind TSP sample for October 26th and the model predicted concentration at the downwind TSP sample location being about 5% of the maximum predicted concentration on October 27th, the TSP emission rate for the disc 2 pass was calculated by assuming that the PM_{10}/TSP emission rate ratio observed during the disc 1 pass of 0.18 was representative of disc passes under similar conditions and then dividing the disc 2 PM_{10} emission rate of 204.2 mg/m^2 by 0.18 to yield a TSP emission rate of 1130.5 mg/m^2 for the operation. For the land plane operation on 10/29, attempts to calculate the source impacts on the downwind TSP sampler using a collocated OPC as described in Section 4.2.1 yielded a TSP emission rate slightly less than the PM_{10} emission rate for the same operation. Since PM_{10} is a subset of TSP and the PM_{10} emission rate cannot physically be greater than the TSP emission rate, the TSP emission rate was assigned the same value as the PM_{10} emission rate as a conservative estimate of actual TSP emissions. As seen in the lidar-based emission rates, the land plane operation emission rates were lower than those for all the other operations, which is likely due to the residual soil moisture from the precipitation event that occurred on October 27th.

The PM_{10} emission rate for the chisel pass of the conventional tillage method is based on calculations at two points, and therefore does not have a reported 95% confidence interval. The difference between the summed PM_{10} emission rates for the Combined Operations Method and the Conventional Method are not significant at the 95% confidence interval. The Combined Operations summed TSP emission rate was less than 25% of the Conventional Method, but the statistical significance could not be determined. For $PM_{2.5}$ emission rates were not summed because one data point for each method was not calculated.

Table 22. Mean emission rates (± 95% CI for *n*≥3) for each operation as determined by inverse modeling using ISCST3.

Operation	PM$_{2.5}$ (mg/m^2)	PM$_{10}$ (mg/m^2)	TSP (mg/m^2)
Combined: Chisel	-	103.6 ± 83.4	180.1
Combined: Optimizer	54.6 ± 86.0	79.0 ± 94.9	321.3
Sum for Combined Operation Method	**-**	**182.5 ± 126.4**	**501.3**
Conventional: Disc 1	-	99.5 ± 64.0	550.8
Conventional: Chisel	63.7 ± 81.0	122.5	296.7
Conventional: Disc 2	18.2 ± 5.7	204.2 ± 240.8	1130.5
Conventional: Land plane	36.3 ± 32.4	45.4 ± 32.3	45.4*
Sum for Conventional Method	**-**	**472.0 ± 289.5**	**2023.3**

* Set equal to PM$_{10}$ emission rate as a conservative estimate of actual TSP emissions

4.4.3   AERMOD Model Emission Rates

The inverse modeling technique was also applied to predicted concentrations from the AERMOD air dispersion model; the calculated emission rates are shown in Table 23, with the reported 95% confidence intervals calculated in the same manner as those for the lidar emission rates (see Section 4.4.1). AERMOD emission rates were determined using the same techniques described for the calculations of emission rates from ISCST3, including the calculation of the TSP emission rate for the disc 2 pass based on the PM$_{10}$/TSP emission rate ratio for the disc 1 pass. However, with respect to the TSP emission rate for the land plane operation, a calculated TSP emission rate greater than the PM$_{10}$ emission rate was achieved using the OPC based background calculations and was used as the TSP emission rate instead of setting the TSP value equal to the PM$_{10}$ value as was done in the ISCST3 emission rate calculations.

As in the ISCST3 data set, the PM$_{10}$ emission rate for the chisel pass of the conventional tillage method is based on calculations at two points, and therefore does not have a reported 95% confidence interval. As seen in the lidar- and ISCST3-based emission rates, the land plane operation emission rates were lower than those of all the other operations, which is likely due to the residual soil moisture from the precipitation event that occurred on October 27th. The difference between the summed PM$_{10}$ emission rates for the Combined Operations Method and the Conventional Method are not significant at the 95% confidence interval. The Combined Operations summed TSP emission rate was about 25% of the Conventional Method, but the statistical significance could not be determined. PM$_{2.5}$ emission rates were not summed because one of the data points for each method was not calculated.

Table 23. Mean emission rates (± 95% CI for *n*≥3) for each operation as calculated by inverse modeling using AERMOD.

Operation	$PM_{2.5}$ (mg/m^2)	PM_{10} (mg/m^2)	TSP (mg/m^2)
Combined: Chisel	-	185.3 ± 159.2	322.6
Combined: Optimizer	62.3 ± 96.4	90.9 ± 106.3	367.9
Sum for Combined Operations Method	**-**	**276.2 ± 191.4**	**690.5**
Conventional: Disc 1	-	119.2 ± 57.2	981.0
Conventional: Chisel	33.3 ± 113.9	160.4	411.2
Conventional: Disc 2	23.4 ± 6.6	147.8 ± 90.9	1216.6
Conventional: Land plane	38.6 ± 45.5	44.8 ± 10.8	58.4
Sum for Conventional Method	**-**	**472.2 ± 109.7**	**2666.9**

4.5   DERIVED EMISSION RATE COMPARISON

Two emission rate determination approaches were employed in this study to calculate three different sets of emission rates in order to quantify differences between conventional tillage methods and a combined operations tillage method using the Optimizer. Emission rates calculated by the two models and the lidar, with their respective error estimates, are shown in Figure 36 for $PM_{2.5}$, PM_{10} and TSP. Due to the measured downwind $PM_{2.5}$ concentrations not being statistically different from the upwind average for two of the seven sample periods, total emissions were not calculated using ISCST3 and AERMOD models. Error estimates were unable to be calculated for the model-derived TSP emission rates due to the number of upwind and downwind TSP concentrations measurements limited to 1 each per day. The limited number of points available to calculate model-derived emission rates, while carefully collected and analyzed, show conclusively the limitations of trying to use even large arrays of point samples to measure the emissions associated with weak fugitive dust sources having spatial and temporal variations. The upwind and downwind concentration differences due to plume impact on the scattered samplers on some days were simply below the detection limit of the sampling system, especially for the $PM_{2.5}$ size fraction. The lidar system, however, effectively sampled the vertical downwind plane and measured time-resolved plume characteristics for each operation at each particulate size fraction.

The advantage that lidar brings to these measurements is that lidar samples far more of the air volume over the field than does an array of point samplers. Point samplers are stationary and depend on the plume to pass over their specific location, and even then they only sample the few cm3 near their inlet. Lidar, on the other hand, interrogates an entire "curtain" of air from ground level up to 1000 m in height. In this way, there is no part of the plume that can exit the field without the lidar seeing it. Lidar also addresses artifacts due to plume inhomogeneity. For example, if a particularly concentrated portion of an otherwise very diffuse plume passes over a OPC/MiniVol station, the ISCST3/AERMOD models will set the concentration of the entire plume according to a smooth Gaussian function. On the other hand, what lidar will see the small "hot spot" as a discontinuity in an otherwise very diffuse cloud. What lidar does that models cannot is perform a physical integration of the actual plume.
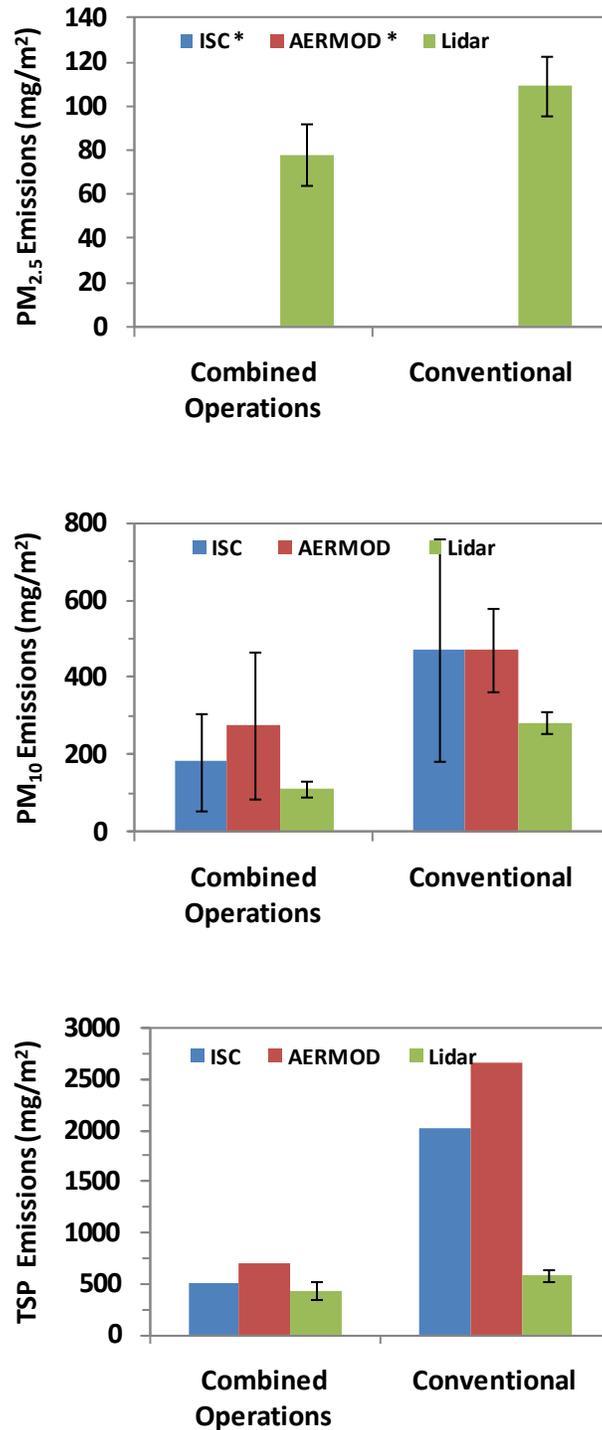
Figure 36. Summed PM$_{2.5}$, PM$_{10}$, and TSP emission rates ± 95% confidence intervals for both tillage methods derived from lidar flux measurements and inverse modeling using ISCST3 and AERMOD. (* One PM$_{2.5}$ emission rate missing per tillage method, therefore no total emissions were calculated.)

While plume modeling is an invaluable tool for investigating different dispersion and transport phenomena, it is no substitute for experimental data – especially data that provides full field coverage and is highly spatially resolved. Models take as input a few sparse point measurements, assign a plume shape, propagate the plume and then integrate the result. ISCST3 and AERMOD do not yet account for microturbulence or plume discontinuities, features that lidar excels at identifying. In the tillage operations discussed in this report, the emission source is (1) moving and (2) is small in comparison to the size of the field. It is not surprising then, that emission modeling based on an array of few point samplers will yield different, and predictably larger, emission rates than lidar-based emission measurements. By the same reasoning the error associated with emission estimates should be smaller for lidar than for modeled emissions.

A summary table of the PM_{10} emission rates calculated from each approach is given in Table 24 for comparison. The calculated PM_{10} emission rates demonstrate that for total mass of PM_{10} per unit area the Combined Operations method produced between 40% and 60% as much as the conventional method based on all employed measurement systems. The emission rate in mg/m^2 of the Optimizer pass is less than the emission rate of the chisel pass in the same treatment for all three emission rate calculations, despite the fact it resulted in higher downwind concentrations, as measured by the lidar and point samplers. One reason for this is that the tillage rate (hectares/hr) of the chisel pass was about half that of the Optimizer pass. As seen in Figure 36 and Table 21, the lidar calculated $PM_{2.5}$, PM_{10}, and TSP emissions were statistically different between tillage treatments at the 95% confidence interval.

Table 24. Calculated PM_{10} emission rates (± 95% confidence interval) from the lidar and inverse modeling using two dispersion models.

Date	Operation	Emission Rates (mg/m^2)		
		Lidar	ISCST3	AERMOD
10/19/2007	Combined: Chisel	69.0 ± 19.9	103.6 ± 83.4	185.3 ± 159.2
10/20/2007	Combined: Optimizer	42.7 ± 6.6	79.0 ± 94.9	90.9 ± 106.3
Sum	**Combined Operations**	**111.6 ± 20.9**	**182.5 ± 126.4**	**276.2 ± 191.4**
10/23/2007	Disc 1	99.7 ± 12.5	99.5 ± 64.0	119.2 ± 57.2
10/25/2007	Chisel	79.5 ± 13.1	122.5	160.4
10/26-27/2007	Disc 2	80.7 ± 20.5	204.2 ± 240.8	147.8 ± 90.9
10/29/2007	Land Plane	21.9 ± 6.2	45.4 ± 32.3	44.8 ± 10.8
Sum	**Conventional**	**281.9 ± 28.0**	**472.0 ± 289.5**	**472.2 ± 109.7**

In general, the largest difference between the three sets of calculated emission rates is between the two models and the lidar. This is likely due to the difference in techniques – inverse modeling using air dispersion models versus a mass balance approach to lidar flux measurements. The models are limited to time steps and meteorological averages of 1 hour and the types of sources that can be used (point source, volume source, area source, or line source), which means that a compromise must be made when dealing with a small, moving area source such as is the case in agricultural tillage. Also, the temporal and spatial resolution of the lidar allows it to see micro-scale variations in plume characteristics and movement such as plume strength, frequency, lofting and detachment from the surface, wind direction effects and wind speed effects. The models must assume a constant emission from a ground level area source, while the lidar sees the plume movement as the tractor moves across the field. This kind of microstructure cannot be captured by the long term sampling required for implementation of

ISCST3 and AERMOD, consequently ISCST3 and AERMOD are incapable of generating fine levels of spatial and temporal detail. Examples of such differences in technique are evident when comparing single scan and sample period average PM concentrations measured by the lidar with average modeled concentrations at a vertical plane corresponding to the lidar scan area. Figure 37 presents the average modeled concentrations in $\mu g/m^3$ for the chisel pass of the conventional tillage method as determined by (a) ISCST3 and (b) AERMOD. It should be noted that AERMOD better accounts for actual turbulence characteristics, which is the cause of the slight differences between the two graphs. In both cases, the highest concentrations are modeled at just above ground level with an exponential drop-off in concentration with increasing height above ground level. Figure 38(a) presents the average lidar measured concentrations contributed by the source (downwind concentrations minus the average upwind concentrations) for the same operating period, while Figure 38(b) shows a single scan in which a significantly dense plume has lofted above and is nearly detached from the surface. The plumes measured by the lidar were detected much higher than the model predicts, as evident by the higher than background concentrations measured at heights up to and exceeding 100 m in the average lidar measured concentrations. As the point sensors were deployed near the surface (at 2 and 9 meters) downwind of the source, these higher plumes were not sampled.

Another potentially important factor to consider is the exhaust emissions from the tractor engines. Exhaust PM_{10} emissions from the tractors were estimated in order to determine if their contribution to total emissions could be significant. Using the fuel consumption information provided by the cooperating farming company and the PM_{10} emission rate as a function of fuel used given by Kean et al. [27], the tractor exhaust contribution was calculated to be between 4.6% and 18.5% as shown in Table 25 when compared to the lidar-derived total PM_{10} emissions. We have chosen to use the lidar-derived emission values in Table 25 because they are the smallest of the three emission values and will therefore be most sensitive to the effect of tractor exhaust; tractor exhaust would be an even smaller fraction of the emission rates derived from modeling. The calculated tractor exhaust contribution was greater than 10 percent of the overall emission rates on only the land plane pass of the conventional tillage method. (Note: this day had unusually low tillage associated emissions due to residual surface moisture from the precipitation event on 10/27, as shown in Section 4.1.2.) Referring to the list of tractors used by operation found in Table 3 and field notes recorded by personnel, the tractor used for the land plane pass was the smallest and oldest of those used, while the other tractors were manufactured within the last several years. The emission rate given by Kean et al. was calculated as an average for the entire agricultural off-road fleet in 1996. Since that time, reductions in exhaust emissions have been implemented, which is evident in the assigned emission rates that decrease with increasing model year in the U.S. EPA's NONROAD emissions model [25], that would result in actual PM emissions being overestimated. The estimated PM_{10} exhaust emission data indicate that tractor exhaust emissions should be a measurable contributor to total process particulate emission, but the actual contribution may be too small to measure. Since the estimated tractor exhaust emission amounts are smaller than the corresponding lidar measurement uncertainties for each operation, the contribution of engine exhaust emissions to the total measured emissions is swamped by the high intrinsic variability of tillage operation emissions. These data show that the tractor emissions were only a small part of the total aerosol emissions from all operations, and that the combined operations tillage produced 55% less tractor emissions.
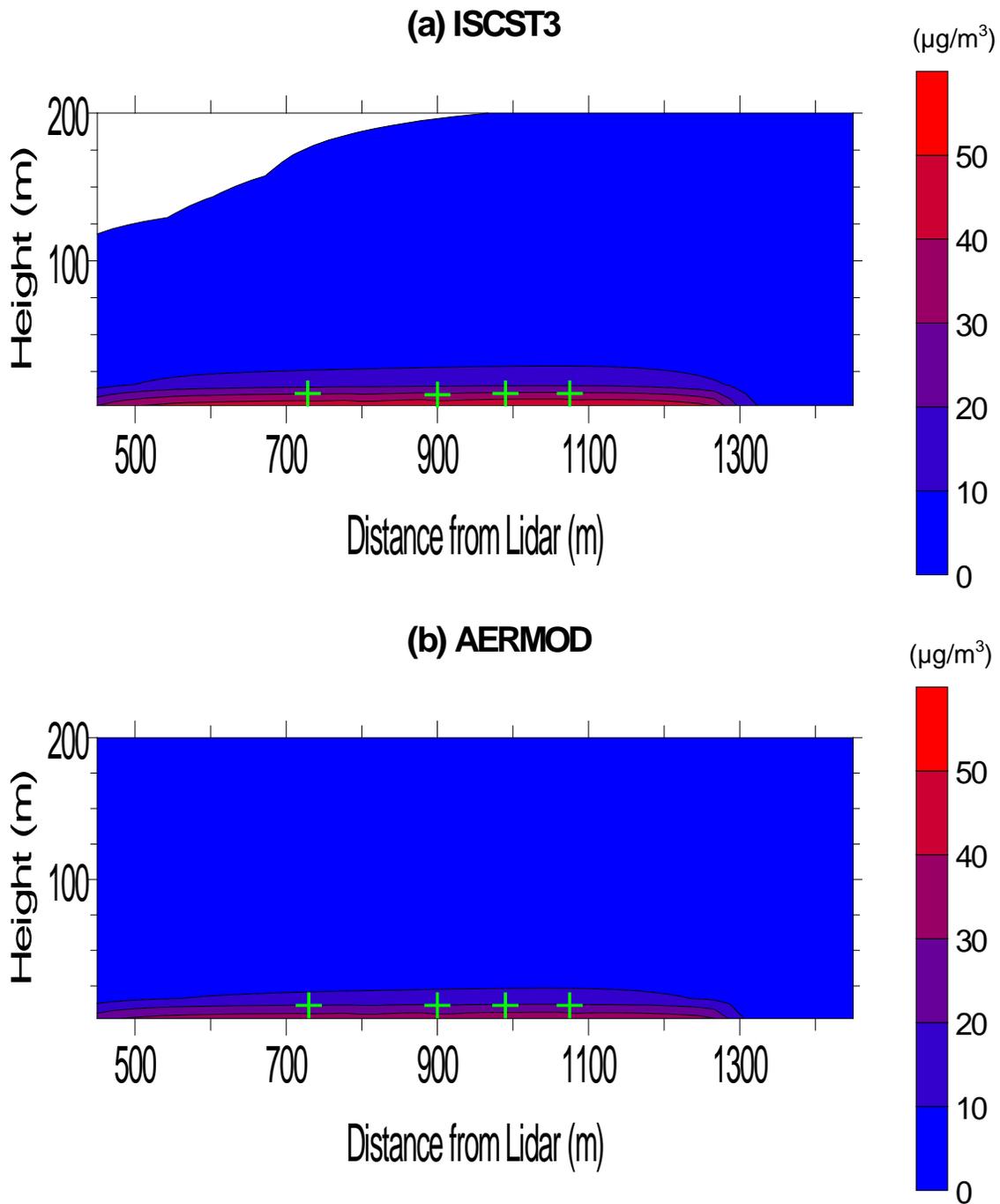
(a) ISCST3

(b) AERMOD

Figure 37. Weighted average PM$_{10}$ concentrations (μg/m^3) modeled by (a) ISCST3 and (b) AERMOD using derived emission rates for 10/23 (modeled hours = 5, sample time = 4.24 hrs) along the downwind vertical plane that corresponds to the lidar scanning plane. The green markers show point sampler locations on the downwind side of the field. Maximum predicted concentrations for ISCST3 and AERMOD were 49.9 and 37.7 μg/m^3, respectively, at 2 m above ground level.
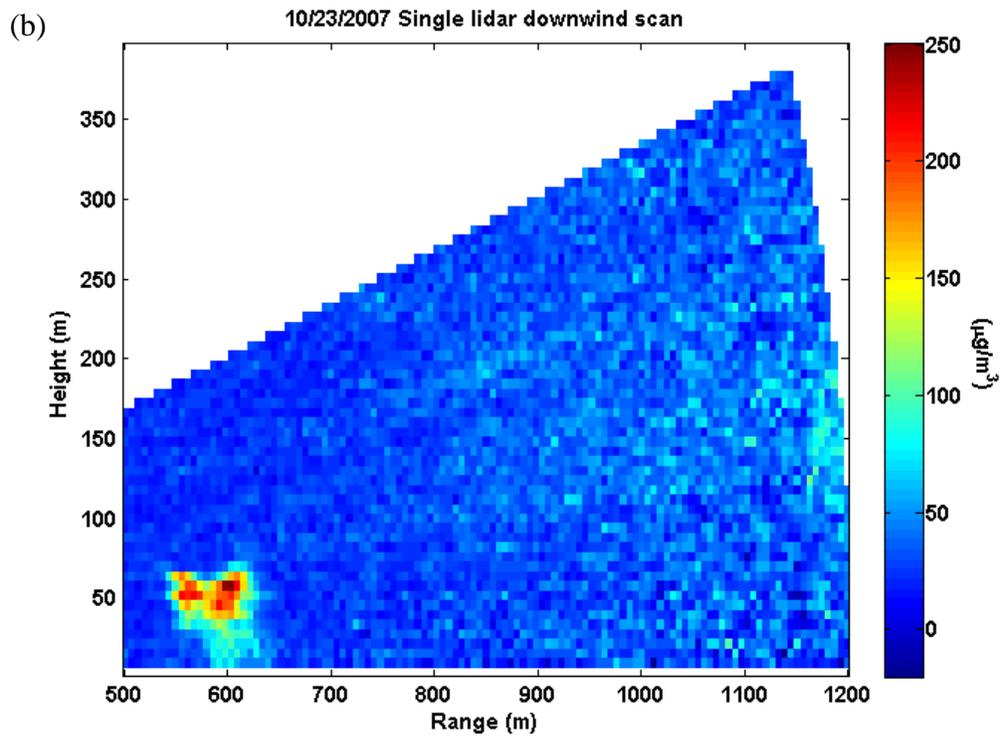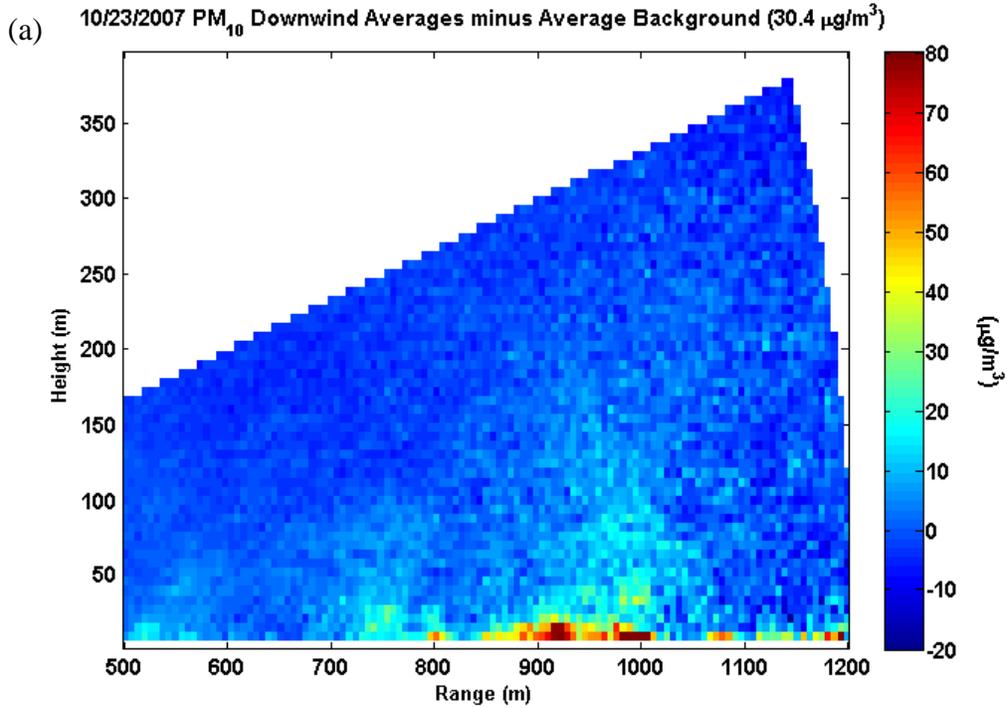
Figure 38. Lidar-measured downwind PM$_{10}$ concentrations (a) averaged over all valid scans over the 4.24 hr long sample period for 10/23 (*n*=122) and (b) for a single vertical scan, which demonstrates observed plume lofting.

Table 25. A comparison of lidar-based total calculated PM$_{10}$ emissions from the tillage activities and estimated tractor exhaust, calculated based on fuel usage and an emission factor of 3.23 g PM$_{10}$/L fuel (Kean et al. [26]).

Operation	Fuel Usage (liters) (Bowles Farming Co., 2008 [32])	Estimated PM$_{10}$ Exhaust Emissions (kg)		Lidar-derived PM$_{10}$ Emissions (mg/m^2)	Exhaust % of Lidar-derived PM$_{10}$ Emissions (%)
		(g)	(mg/m^2)		
Combined: Chisel	340.7	1100.4	5.0	68.4 ± 19.7	7.3
Combined: Optimizer	174.9	564.9	2.9	43.2 ± 6.6	6.7
Sum for Combined Operation Method	**515.6**	**1665.3**	**7.8**	**111.5 ± 20.8**	**7.0**
Conventional: Disc 1	396.0	1278.9	5.0	95.9 ± 12.0	5.2
Conventional: Chisel	221.4	715.3	3.7	80.7 ± 13.3	4.6
Conventional: Disc 2	312.3	1008.7	4.0	79.6 ± 20.8	5.0
Conventional: Land plane	100.7	325.2	4.1	22.2 ± 6.3	18.5
Sum for Conventional Method	**1030.4**	**3328.1**	**16.8**	**278.4 ± 28.1**	**6.0**

5. SUMMARY AND CONCLUSIONS

A Regional Applied Research Effort (RARE) project to determine the control effectiveness of Conservation Management Practices (CMPs) for agricultural tillage was awarded to the U.S. EPA Environmental Sciences Division, National Exposure Research Laboratory. A study was conducted to quantify particulate emissions (PM$_{2.5}$, PM$_{10}$, and TSP) from conventional agricultural tillage methods and a CMP tillage method utilizing the Optimizer during after-harvest land preparation. The Optimizer is a tillage implement that incorporates functions from multiple conventional tillage implements into one piece of equipment. The objective of this study was to address three fundamental research questions:

1) What are the magnitude, flux, and transport of PM emissions produced by agricultural practices for row crops where tillage CMPs are being implemented vs. the magnitude, flux, and transport of PM emissions produced by agricultural practices where CMPs are not being implemented?

2) What are the control efficiencies of equipment being used to implement the "combined operations" CMP? If resources allow assessing additional CMPs, what are the control efficiencies of the "equipment change/technological improvements" and "conservation tillage" CMPs?

3) Can these CMPs for a specific crop be quantitatively compared, controlling for soil type, soil moisture, and meteorological conditions?

The study was carried out October 19-29, 2007 in the San Joaquin Valley of California on a commercial production farm. Two adjacent fields with the same crop and similar soil properties

were selected for observation. The CMP tillage treatment involved two passes over the field: 1) a chisel pass, and 2) an Optimizer pass. The conventional tillage treatment comprised four passes: 1) a disc 1 pass, 2) a chisel pass, 3) a disc 2 pass, and 4) a land plane pass. Tractor malfunctions required the disc 2 pass to be measured over 2 consecutive days, while all other measurements were made on a single day for each pass. Particulate emissions were determined using arrayed, filter-based sampling coupled with inverse modeling, using both ISCST3 and AERMOD, as well as mass balance using advanced scanning lidar techniques. Supporting operation characteristics (operation time, number of tractors in operation, potential contamination issues, etc.) were recorded and meteorological, soil characteristic, and particle count and chemical composition measurements were made and are reported in this document. The cooperating farming company recorded tractor operation time and fuel usage for comparison.

Differences not statistically significant (based on the upwind 67% confidence interval) between average upwind concentrations and individual downwind values prevented $PM_{2.5}$ emission rate determination using the models for three of the seven measurement periods. However, the scanning lidar technology employed was able to calculate emissions for all measurement periods. Table 26 summarizes important PM_{10} aerosol emission values found during this study along with results from previous studies found in literature. Emission factors in units of mg/m^2-pass were converted to emission rates with units of mg/m^2 by assuming a single pass for comparison. The values herein reported are in occasional agreement with those reported by Flocchini et al. (2001) and Madden et al. (2008), as well as the emission factors used by CARB to calculate area source PM_{10} contributions from agricultural tilling [3][4][13]. While the values from all three published studies are generally not in close agreement, they are well within the range of the variability expected from measurements made under different meteorological and soil conditions, as demonstrated by the wide range of values from Flocchini et al. (2001) [3] summarized in Table 1. Both models and the lidar used to derive emission rates in this study report low emission rates for the land plane pass of the conventional tillage method, which is likely due to water in the soil surface layer from the precipitation event on 10/27 that had not yet evaporated. This finding is consistent with the influence of soil moisture and other meteorological variables found by Flocchini et al (2001) [3].

The many differences between how to extract lidar-derived and point sampler derived emission rates have been detailed in previous section of this report. The critical distinction between lidar and point sampler emission rates is primarily that of a paradigm shift. Lidar functions as a broad array of volume point samplers, essentially covering an entire field with thousands of OPCs. The analysis of the emission rate between the two methods differs in that a point-sampler based model uses a mathematical function to draw a picture of a plume based on a handful of data points whereas the lidar directly sums the results from all of its virtual OPCs to determine the extent and concentration of the plume. Derivation of emission rates using modeling techniques is an invaluable tool for investigating different dispersion and transport phenomena, this report shows that it is no substitute for experimental data – especially data that provides full field coverage and is highly spatially resolved. By their nature, models smooth point sampler data and routinely overestimate the extent of the plume, therefore yielding different, and predictably larger, emission rates when compared to lidar-based measurements.

Table 26. A comparison of PM$_{10}$ emission rates herein derived and found in literature.

Operation	Flocchini et al. (2001) [3] *	Madden et al. (2008) [4] *	CARB (2003a) [13]	This study		
				Lidar	ISCST3	AERMOD
	(mg/m^2)	(mg/m^2)	(mg/m^2)	(mg/m^2)	(mg/m^2)	(mg/m^2)
Disc 1	166.1	161.8	134.5	99.7 ± 12.5	99.5 ± 64.0	119.2 ± 57.2
Chisel	512.2		134.5	79.5 ± 13.1	122.5	160.4
Disc 2	58.5	612.5	134.5	80.7 ± 20.5	204.2 ± 240.8	147.8 ± 90.9
Land Plane			1401.0	21.9 ± 6.2	45.4 ± 32.3	44.8 ± 10.8
Conventional Method Sum			**1804.5**	**281.9 ± 28.0**	**472.0 ± 289.5**	**472.2 ± 109.7**
Chisel	512.2		134.5	69.0 ± 19.9	103.6 ± 83.4	185.3 ± 159.2
Optimizer				42.7 ± 6.6	79.0 ± 94.9	90.9 ± 106.3
Combined Operations Method Sum				**111.6 ± 20.9**	**182.5 ± 126.4**	**276.2 ± 191.4**

* Average of available data per operation

Lidar-derived emission rates for PM$_{2.5}$, PM$_{10}$, and TSP by operation are presented in Table 27, along with the average tillage rate in hours per hectare, where the hour represents total tractor operation time, and fuel use rate. In the case where two tractors were operating at the same time, the total tractor operation time would be twice that of the elapsed time of the operation. Comparisons were made between the conventional and CMP tillage practices based on these same variables and are shown in the same table. The unitless control efficiency (η) was calculated according to Eq. 25, which was based on a collection efficiency equation found in Cooper and Alley (2002).

$$\eta = \frac{E_{CT} - E_{COT}}{E_{CT}} \tag{25}$$

where E_{CT} is the calculated emission rate for the conventional tillage method and E_{COT} is the calculated emission rate for the combined operations tillage method [61]. Therefore, the control efficiency of the CMP for particulate emissions was 0.29 ± 0.02, 0.60 ± 0.01, and 0.25 ± 0.01 for PM$_{2.5}$, PM$_{10}$, and TSP, respectively.

The tillage rate was a significant factor resulting in the Optimizer pass emission rates being lower than the chisel pass for the Combined Operation tillage method despite higher concentrations measured during the Optimizer pass sample. The tractor time and fuel per hectare required to perform the CMP work were 37.8% and 48.6% of the conventional method, respectively. A similar reduction in tractor exhaust emissions is expected to have taken place, as well as the supporting vehicle exhaust and PM emissions from driving on dirt access roads.

Table 27. Lidar-derived particulate emissions, tillage rate, and fuel usage comparison between conventional and combined operations tillage.

	Average Emission Rates ± 95% CI (mg/m^2)			Average Tillage Rate (hr$_{tractor}$/hectare)	Average Fuel Usage (L/hectare)
	PM$_{2.5}$	PM$_{10}$	TSP		
Combined Operations Method					
Chisel	45.3 ± 13.1	69.0 ± 19.9	265.9 ± 76.6	0.38	15.5
Optimizer	32.5 ± 5.1	42.7 ± 6.6	169.9 ± 26.2	0.21	8.7
Sum	**77.8 ± 14.0**	**111.6 ± 20.9**	**435.8 ± 80.9**	**0.59**	**24.2**
Conventional Method					
Disc 1	20.4 ± 2.6	99.7 ± 12.5	159.8 ± 20.0	0.44	16.0
Chisel	35.8 ± 5.9	79.5 ± 13.1	235.1 ± 38.8	0.33	9.7
Disc 2	39.5 ± 11.2	80.7 ± 20.5	149.3 ± 40.3	0.37	10.7
Land plane	13.8 ± 3.9	21.9 ± 6.2	33.4 ± 9.4	0.42	10.7
Sum	**109.5 ± 13.5**	**281.9 ± 28.0**	**577.6 ± 60.1**	**1.56**	**47.1**
Comparison of Tillage Methods					
Combined Operations / Conventional (%)	**71.1**	**39.6**	**75.5**	**37.8**	**48.6**
Statistically Significant Difference at 95% CI	**Yes**	**Yes**	**Yes**	**Unknown**	**Unknown**
Control Efficiency, η, ± Std Dev	**0.289 ± 0.016**	**0.604 ± 0.007**	**0.246 ± 0.013**	**---**	**---**

While not directly addressing the efficacy of CMP measures, an important component of this investigation is to assess the utility of lidar for measuring particulate emissions in an agricultural setting. Our lidar measurements clearly indicate that lidar is an effective tool for visualizing plumes from tillage operations. Specifically, the lidar captures far more particulate matter suspended at heights above 20 meters than either of the two models predict. This is a critical observation for two reasons, (1) the emission characteristics from these tillage studies cannot be accurately represented with either ISCST3 or AERMOD analyses because these models are being used at the limit of their designed performance and do tend to <u>overestimate process emissions,</u> and (2) there is substantially more vertical transport than previously thought, which poses larger questions about the role of PM entrainment and transport away from the tillage site Lidar, on the other hand, is capable of sensitively interrogating aerosol concentrations at elevations up to several thousand meters. It is clear that the incorporation of lidar measurements is an important complement to ground based sensors because ground based sensors cannot measure elevated plumes. ISCST3 and AERMOD would realize significant benefits if lidar-derived information could be incorporated into their calculations.

6.   ACKNOWLEDGMENTS

7.   PUBLICATIONS

G. E. Bingham, C. C. Marchant, V. V. Zavyalov, D. J. Ahlstrom, K. D. Moore, D. S. Jones, T. D. Wilkerson, L. E. Hipps, R. S. Martin, J. L. Hatfield, J. H. Prueger, R. L. Pfeiffer. 2009. Lidar based emissions measurement at the whole facility scale: Method and error analysis. Journal of Applied Remote Sensing, 3(1), 033510 [doi: 10.1117/12.829411].

C. C. Marchant, T. D. Wilkerson, G. E. Bingham, V. V. Zavyalov, J. M. Andersen, C. B. Wright, S. S. Cornelsen, R. S. Martin, P. J. Silva, J. L. Hatfield. 2009. Aglite lidar: A portable elastic lidar system for investigating aerosol and wind motions at or around agricultural production facilities. Journal of Applied Remote Sensing, 3(1), 033511 [doi: 10.1117/12.829412].

M. D. Wojcik, G. E. Bingham, C. C. Marchant, V. V. Zavyalov, D. J. Ahlstrom, K. D. Moore, T. D. Wilkerson, L. E. Hipps, R. S. Martin, J. L. Hatfield, J. H. Prueger. "Lidar Based Particulate Flux Measurements of Agricultural Field Operations" IGARSS 2008, Boston, Massachusetts, July 2008.

M. D. Wojcik, K. D. Moore, "Laboratory for Atmospheric and Remote Sensing (LARS)", Wind Erosion Workshop organized by the Agriculture Research Service – Wind Erosion Research Unit, Manhattan, Kansas, April 2008.

V. V. Zavyalov, C. C. Marchant, G. E. Bingham, T. D. Wilkerson, J. L. Hatfield, R. S. Martin, P. J. Silva, K. D. Moore, J. Swasey, D. J. Ahlstrom, T. L. Jones. 2009. Aglite lidar: Calibration and retrievals of well characterized aerosols from agricultural operations using a three-wavelength elastic lidar. Journal of Applied Remote Sensing, 3(1), 033522 [doi: 10.1117/12.833365].

8. REFERENCES

[1]   U.S. EPA. 1995. User's guide for the Industrial Source Complex (ISC3) Dispersion Models. Research Triangle Park, NC: U.S. Environmental Protection Agency, Office of Air Quality Planning and Standards Emissions. Monitoring, Analysis Division. January, 2008. http://www.epa.gov/scram001/userg/regmod/isc3v2.pdf.

[2]   U.S. EPA. 2005. Revision to the Guideline on Air Quality Models: Adoption of a Preferred General Purpose (Flat and Complex Terrain) Dispersion Model and Other Revisions; Final Rule. 40 CFR Part 51. Washington, D.C., U.S. Environmental Protection Agency. January 2008. http://www.epa.gov/ttn/scram/guidance/guide/appw_05.pdf.

[3]   Flocchini, R.G., James, T.A., Ashbaugh, L.L., Brown, M.S., Carvacho, O.F., Holmen, B.A., Matsumura, R.T., Trezpla-Nabalgo, K., Tsubamoto, C. 2001. Interim Report: Sources and sinks of PM_{10} in the San Joaquin Valley. Crocker Nuclear Laboratory, UC-Davis, CA.

[4]   Madden, N.M., Southard, R.J., Mitchell, J.P. 2008. Conservation tillage reduces PM10 emissions in dairy forage rotations. Atmospheric Environment 42:3795-3808.

[5]   Pope, C.A. 1991. Respiratory hospital admissions associated with PM10 pollution in Utah, Salt Lake, and Cache Valleys. Archives of Environmental Health 46(2):90-97.

[6]   Hinds, W. C. 1999. Aerosol Technology: Properties, Behavior, and Measurement of Airborne Particles, 2nd Edition. John Wiley & Sons, New York.

[7]   40 Code of Federal Regulations (CFR) 50.6. National primary and secondary ambient air quality standards for PM_{10}.

[8]   40 CFR 50.7. National primary and secondary ambient air quality standards for $PM_{2.5}$.

[9]   Holmen, B.A., Eichinger, W.E., Flocchini, R.G. 1998. Application of elastic LIDAR to PM_{10} emissions from agricultural nonpoint sources. Environmental Science and Technology 32:3068-3076.

[10]   Conservation Management Practices Program Report. January 2006. San Joaquin Valley Air Pollution Control District for 2005.

[11]   Holmen, B.A., James, T.A., Ashbaugh, J.L., Flocchini, R.G. 2001a. LIDAR-assisted measurement of PM_{10} emissions from agricultural tilling in California's San Joaquin Valley—Part I. LIDAR. Atmospheric Environment 35:3251-2364.

[12]   Holmen, B.A., James, T.A., Ashbaugh, J.L., Flocchini, R.G. 2001b. LIDAR-assisted measurement of PM10 emissions from agricultural tilling in California's San Joaquin Valley—Part II: Emission factors. Atmospheric Environment 35:3265-3277.

[13]   California Air Resources Board (CARB). 2003a. Area Source Methods Manual, Section 7.4: Agricultural Land Preparation.

[14]   CARB. 2003b. Area Source Methods Manual, Section 7.5: Agricultural Harvest Operations.

[15]   U.S. Environmental Protection Agency (EPA). 2001. Procedures document for national emission inventory. Criteria Air Pollutants 1985-1999. EPA-454/R-01-006.

[16]   Clausnitzer, H., Singer, M.J. 1996. Respirable-dust production from agricultural operations in the Sacramento Valley, California. Journal of Environmental Quality 25:877-884.

[17]   Clausnitzer, H., Singer, M.J. 2000. Environmental influences on respirable dust production from agricultural operations in California. Atmospheric Environment 34:1739-1745.

[18]   Baker, J.B., Southard, R.J., Mitchell, J.P. 2005. Agricultural dust production in standard and conservation tillage systems in the San Joaquin Valley. Journal of Environmental Quality 34:1260-1269.

[19]   Mitchell, J.P., Southard, R.J., Madden, N.M., Klonsky, K.M., Baker, J.B., De Moura, R.L., Horwath, W.R., Munk, D.S., Wroble, J.F., Hembree, K.J., Wallender, W.W. 2008. Transition to conservation tillage evaluated in San Joaquin Valley cotton and tomato rotations. Journal of California Agriculture 62(2):74-79.

[20]   Veenstra, J.J., Horwath, W.R., Mitchell, J.P., Munk, D.S. Conservation tillage and cover cropping influence soil properties in San Joaquin Valley cotton-tomato crop. Journal of California Agriculture 60(3):146-153.

[21]   Upadhyaya, S.K., Lancas, K.P., Santos-Filno, A.G., Raghuwanshi, N.S. 2001. One-pass tillage equipment outstrips conventional tillage method. Journal of California Agriculture 55(5):44-47.

[22]   Mitchell, J.P., Munk, D.S., Prys, B., Klonsky, K.K., Wroble, J.F., De Moura, R.L. 2006. Conservation tillage production systems compared in San Joaquin Valley cotton. Journal of California Agriculture 60(3):140-145.

[23]   U.S. EPA. March 17, 2008. NONROAD Model (nonroad engines, equipment, and vehicles). Accessed: August 21, 2008. Available: http://www.epa.gov/otaq/nonrdmdl.htm#techrept.

[24]   U.S. EPA. 2004. Exhaust and Crankcase Emission Factors for Nonroad Engine Modeling – Compression-Ignition. EPA420-P-04-009. April 2004.

[25]   U.S. EPA. 1991. Nonroad Engine and Vehicle Emission Study – Report. EPA 460/3-91-02. November 1991.

[26] CARB. 1999. Emissions inventory of off-road large compression-ignited engines (≥25hp) using the new OFFROAD Emissions Model. Mail-Out #MSC99-32. December 1999.

[27] Kean, A.J., Sawyer, R.F., Harley, R.A. 2000. A fuel-based assessment of off-road diesel engine emissions. Journal of the Air and Waste Management Association 50:1929-1939.

[28] National Resource Conservation Service (NRCS). 2009. Web Soil Survey 2.1. 13 May 2009. http://websoilsurvey.nrcs.usda.gov/app/.

[29] Geology.com. May 2009. http://geology.com/state-map/california.shtml.

[30] Cooperating producer. September 2007. Personal communication.

[31] Tillage International, Inc. August 2008. Personal communication.

[32] Cooperating producer. October 2008. Personal communication.

[33] California Irrigation Management Information System (CIMIS). 2007. Data for Station #56 (Los Banos) for September and October of 2004 through 2006. September 2007. http://wwwcimis.water.ca.gov/cimis/frontStationDetailInfo.do?stationId=56&urlPicDirection=W.

[34] Tanner, C. B., and G.W. Thurtell. 1969. Anemoclinometer measurements of Reynolds stress and heat transport in the atmospheric surface layer, Final Report, United States Army Electronics Command, Atmospheric Science Laboratory, Fort Huachuca, Arizona.

[35] Lee, X., Finnigan, J. and K.T. Paw U. 2004. Coordinate Systems and Flux Bias Error. In: *Handbook of Micrometeorology: A Guide for Flux Measurement and Analysis*. Lee, X. Massman, W. and B. Law Eds. Kluwer Academic Publishers, Boston/Dordrecht/London

[36] Webb, E. K., Pearman, G. I., Leuning, R., 1980. Correction of flux measurement for density effects due to heat and water vapor transfer. Quarterly Journal of the Royal Meteorological Society 106:85-100.

[37] Doran, J.W., Jones, A. 1996. Methods for assessing soil quality. SSSA Special Publication Number 49. Soil Science Society of America. Madison, Wisconsin.

[38] Soil Sampling and Methods of Analysis, ed by M.R. Carter, Canadian Society of Soil Science. Lewis Publishers, 1993:508-509.

[39] *Ibid.* 659-662.

[40] Chen, F.-L., Williams, R., Svendsen, E., Yeatts, K., Creason, J., Scott, J., Terrell, D., Case, M. 2007. Coarse particulate matter concentrations from residential outdoor sites associated with the North Carolina Asthma and Children's Environment Studies (NC-ACES). Atmospheric Environment 41:1200-1208.

[41] Chow, J. C., Watson, J. G., Lowenthal, D. H., Chen, L.-W A., Tropp, R. J., Park, K., Magliano, K. A. 2006. PM2.5 and PM10 Mass Measurements in California's San Joaquin Valley. Aerosol Science and Technology 40(10):796–810.

[42] Airmetrics MiniVol Portable Air Sampler Operation Manual v. 5.

[43] Rupprecht & Patashnick, n.d. Series 5400 Elemental Carbon/Organic Carbon Analyzer Instrument Manual.

[44] Malm, W.C. and J.L. Hand. 2007. An examination of the physical and optical properties of aerosols collected in the IMPROVE program. Atmospheric Environment 41:3407-3427.

[45] Marchant, C. 2008. Algorithm Development of the AGLITE-LIDAR Instrument, MS Thesis, Utah State University.

[46] Zavyalov, V. V., Marchant, C. C., Bingham, G. E., Wilkerson, T. D., Hatfield, J. L., Martin, R. S., Silva, P. J., Moore, K. D., Swasey, J., Ahlstrom, D. J., Jones, T. L. 2009. Aglite lidar: Calibration and retrievals of well characterized aerosols from agricultural operations using a three-wavelength elastic lidar. Journal of Applied Remote Sensing, 3(1), 033522 [doi: 10.1117/12.833365].

[47] Klett, J.D. 1985. LIDAR inversion with variable backscatter/extinction ratio. Appl. Opt. 24: 1638-83.

[48] U.S. EPA. 2009. Guideline on Air Quality Models. Appendix W. U.S. Code of Fed. Regulations, 40 CFR Part 51. May 2009. http://www.epa.gov/scram001/guidance/guide/appw_05.pdf.

[49] Cooper, D.C., Alley, F.C. 2002. Air pollution control: A design approach. Waveland Press Inc. Prospect Heights, Illinois. 611-626.

[50] Turner, D.B. 1970. Workbook of Atmospheric Dispersion Estimates. Washington, D.C., U.S. Environmental Protection Agency.

[51] Paine, R.J., Lee, R.F., Brode, R., Wilson, R.B., Cimorelli, A.J., Perry, S.G., Weil, J.C., Venkatram, A., Peters, W.D. 1998. Model evaluation results for AERMOD. Research Triangle Park, NC:U.S. Environmental Protection Agency, Office of Air Quality Planning and Standards Emissions, Monitoring, Analysis Division. March 2008. http://www.epa.gov/scram001/7thconf/aermod/evalrep.pdf.

[52] U.S. EPA. 1985. Compilation of air pollutant emission factors (AP-42), Fourth Edition: Chapter 9. Research Triangle Park, N.C. U.S Environmental Protection Agency.

[53] U.S. EPA. 1995. Compilation of air pollutant emission factors (AP-42), Fifth Edition: Chapter 9. Research Triangle Park, N.C. U.S Environmental Protection Agency.

[54]   National Research Council, National Academies of Science. 2003. Air emissions from animal feeding operations: Current knowledge, future needs. The National Academies Press. Washington, D.C. 95.

[55]   Arya, S.P. 1998. Air Pollution Meteorology and Dispersion. Oxford University Press.

[56]   Lakes Environmental. 2009. Terrain Data: 7.5-Min DEM Native Format – United States. June 2009. http://www.webgis.com/terr_us75m.html.

[57]   Massman, W.J., Lee, X. 2002. Eddy covariance flux corrections and uncertainties in long-term studies of carbon and energy exchanges. Agricultural and Forest Meteorology 113:121-144.

[58]   Malm, W. 2000. Spatial and seasonal patterns and temporal variability of haze and its constituents in the United States: Report III, Interagency Monitoring of Protected Visual Environments (IMPROVE) Report, May 2000.

[59]   Magliano, K.L., Hughes, V.M., Chinkin, L.R., Coe, D.L., Haste, T.L., Kumar, N., Lurmann, F.W. 1999. Spatial and temporal variations in PM_{10} and $PM_{2.5}$ source contributions and comparison to emissions during the 1995 integrated monitoring study. Atmospheric Environment 33:4757-4773.

[60]   Bingham, G.E., Marchant, C. C., Zavyalov, V. V., Ahlstrom, D. J., Moore, K. D., Jones, D. S., Wilkerson, T. D., Hipps, L. E., Martin, R. S., Hatfield, J. L., Prueger, J. H., Pfeiffer, R. L. 2009. Lidar based emissions measurement at the whole facility scale: Method and error analysis. Journal of Applied Remote Sensing, 3(1), 033510 [doi: 10.1117/12.829411].

[61]   Cooper, D.C., Alley, F.C. 2002. Air pollution control: A design approach. Waveland Press Inc. Prospect Heights, Illinois. 100.

9. APPENDICES

9.1 APPENDIX A

Table A 1. Settings for the ISCST3 and AERMOD dispersion models for the tillage study in the ISC-AERMOD View software by Lakes Environmental, Inc. All settings were held constant across the sample periods except the source area size and shape, which changed each day, and the downwind receptor locations, which were specific to each field studied. (--- = not applicable)

Setting	ISCST3	AERMOD
Control Pathway		
Dispersion Options	Regulatory Default	Regulatory Default
Output type	Concentration	Concentration
Plume Deposition	None	---
Pollutant	Other – PM	Other – PM
Averaging Time	Period, 1-Hr	Period, 1-Hr
Dispersion Coefficient	Rural	Rural
Terrain Height Options	Elevated	Elevated
Terrain Calculation Algorithms (ISC), Receptor Elev./Hill Hghts (AERMOD)	Simple terrain only	Run using the AERMAP Receptor Output file
Source Pathway		
Source type	Area Poly	Area Poly
Base Elevation	Imported from AERMAP	Imported from AERMAP
Release height	0.0 m AGL	0.0 m AGL
Emission rate	5.0 E-5 g/(s-m^2)	5.0 E-5 g/(s-m^2)
Initial Vertical Dim. of the plume	Blank	Blank
Building downwash	None	None
Receptor Pathway		
Uniform Cartesian Grid (# Receptors: 17940)	138x130, 10x10m spacing, flagpole height z = 2.0 m AGL	138x130, 10x10m spacing, flagpole height z = 2.0 m AGL
Discrete Cartesian Receptors (# Receptors: 17)	Placed at sample locations, z = 2, 5, and 9 m AGL	Placed at sample locations, z = 2, 5, and 9 m AGL
AERMET View Settings		
Hourly Surface Data	---	Source: on-site data, mixing height = 1000 m AGL
Adjustment to Local Time	---	8 hr (Pacific)
Application Station Elevation MSL	---	29.2 m

Setting	ISCST3	AERMOD
Upper Air Data	---	Source: calculated based on on-site data, mixing height = 1000 m AGL
Mode	---	Upper Air Estimator
Sectors Parameters	---	
Time Zone	---	8 (Pacific)
Randomize NWS Wind Directions	---	Yes
Anemometer Height	---	6.2 m AGL
Wind direction sectors	---	1: Start = 0°, End = 360°
Land Use Type	---	Cultivated Land
Surface parameters per sector	---	Monthly, October default values for Midday Albedo = 0.18, Bowen Ratio = 0.7, and Surface Roughness = 0.05 m
Meteorology Pathway		
Surface Met Data	Source: on-site data, mixing height = 1000 m AGL	Source: calculated from on-site data and default values
Profile Met Data	---	Source: estimated from on-site data
Anemometer Height	6.2 m AGL	---
Primary Met Tower Base Elevation above MSL	---	29.2 m
Read Entire Met Data File	Yes (only provided data for sample period times)	No
Specify Data Periods to Process	---	Set to sample period times, varied by sample
Wind Speed Categories	Default	Default
Output Pathway		
Tabular Outputs		
All	Highest values table: 1st	Highest values table: 1st
Buildings	None	None
Terrain	Calculated values from AERMAP using 7.5 Min DEM	Calculated values from AERMAP using 7.5 Min DEM

9.2   APPENDIX B

Table B 1. Particulate matter concentrations measured by the Airmetrics MiniVol samplers shown by date, location, and PM size fractionation.

Location (height in m)	Size	19-Oct	20-Oct	Location (height in m)	Size	23-Oct	25-Oct	26-Oct	27-Oct	29-Oct
Upwind – Combined Operations CMP				*Upwind – Conventional tillage practices*						
U1 (9)	PM_{10}	36.8	27.3	U2 (9)	PM_{10}	*	69.2	38.1	19.3	*
	$PM_{2.5}$	28.4	19.8		$PM_{2.5}$	16.4	43.1	22.6	20.9	32.0
N1 (2)	PM_{10}	37.3	31.4	N1 (2)	PM_{10}	43.3	53.4	43.7	40.3	55.2
	$PM_{2.5}$	38.9	21.8		$PM_{2.5}$	16.9	40.5	34.2	25.1	*
N1 (9)	TSP	157.2	87.0	N1 (9)	TSP	60.5	123.6	84.0	70.2	90.6
	PM_{10}	50.6	27.5		PM_{10}	35.9	88.9	35.8	35.5	47.1
	$PM_{2.5}$	42.0	13.4		$PM_{2.5}$	17.0	42.6	23.4	19.4	33.3
N2 (2)	PM_{10}	*	33.1	N2 (2)	PM_{10}	*	*	*	54.5	48.1
	$PM_{2.5}$	28.3	16.4		$PM_{2.5}$	14.3	28.1	26.4	23.0	39.1
Downwind – Combined Operations CMP				*Downwind – Conventional tillage practices*						
W1 (9)	PM_{10}	37.7	21.5	W2 (9)	PM_{10}	39.7	63.2	31.2	31.5	45.8
	$PM_{2.5}$	15.7	---		$PM_{2.5}$	---	---	---	---	---
E1 (9)	PM_{10}	43.9	65.0	E2 (9)	PM_{10}	58.1	75.2	49.7	---	49.9
	$PM_{2.5}$	27.5	43.3		$PM_{2.5}$	12.9	51.4	23.9	---	36.3
S1 (2)	PM_{10}	*	*	S4 (2)	PM_{10}	69.3	*	48.8	57.4	55.0
	$PM_{2.5}$	32.5	*		$PM_{2.5}$	10.2	47.1	19.6	28.2	32.8
S1 (9)	PM_{10}	48.2	23.0	S4 (9)	PM_{10}	58.2	111.0	40.3	92.4	*
	$PM_{2.5}$	26.6	*		$PM_{2.5}$	*	43.7	21.3	16.3	33.2
S2 (2)	PM_{10}	53.6	*	S5 (2)	PM_{10}	*	70.6	71.6	67.0	68.3
	$PM_{2.5}$	29.2	19.7		$PM_{2.5}$	14.0	35.0	*	18.9	35.4
S2 (9)	TSP	122.5	174.1	S5 (9)	TSP	203.3	196.0	*	84.3	63.1
	PM_{10}	**	40.9		PM_{10}	75.5	59.0	48.6	30.7	58.6
	$PM_{2.5}$	40.0	*		$PM_{2.5}$	9.9	40.4	25.4	14.4	27.1
S3 (2)	PM_{10}	57.3	37.7	S6 (2)	PM_{10}	62.3	91.3	73.9	59.5	47.1
	$PM_{2.5}$	24.5	43.8		$PM_{2.5}$	15.8	38.8	33.9	14.3	36.0
S3 (9)	PM_{10}	55.4	29.5	S6 (9)	PM_{10}	54.9	28.5	64.5	16.3	57.4
	$PM_{2.5}$	20.6	20.8		$PM_{2.5}$	13.8	33.6	28.0	7.7	39.4
AQ1 (5)	PM_{10}	111.2	56.7	AQ2 (5)	PM_{10}	*	*	20.0	*	25.5
	$PM_{2.5}$	21.1	27.5		$PM_{2.5}$	5.8	41.5	22.0	13.9	17.8
				Tripod 1	PM_{10}	---	---	---	65.0	---
					$PM_{2.5}$	---	---	---	18.1	---

--- Data point not collected

* Compromised by sampler or human error

** Removed due to reported $PM_{2.5}$ value with ±10% error bars being greater than collocated PM_{10} value ±10% (i.e., the ±10% error bars did not overlap)

EPA

United States
Environmental Protection
Agency

Please make all necessary changes on the below label, detach
or copy and return to the address in the upper left hand corner.

If you do not wish to receive these reports CHECK HERE ☐ ;
detach, or copy this cover, and return to the address in the
upper left hand corner.

PRESORTED STANDARD
POSTAGE & FEES PAID
EPA PERMIT No. G-35